CANADIAN JOURNAL OF RESEARCH

VOLUME 25 JULY, 1947 NUMBER 4

— SECTION A —

PHYSICAL SCIENCES

Contents

Page

The Effect of Wind on the Thermal Resistance of Clothing with Special Reference to the Protection Given by Coverall Fabrics of Various Permeabilities—*P. Larose* - - - 169

Permeability Studies. II. Surface Area Measurements of Inorganic Pigment Powders—*J. C. Arnell* - - - - 191

The Gamma-ray Measurement of Radium Ore Concentrates—*W. J. Hushley and W. R. Dixon* - - - - - - - 210

New Photographic Emulsions Showing Improved Tracks of Ionizing Particles—*Pierre Demers* - - - - - - 223

A Method for Computing Transformations in Radioactive Series—*W. H. Watson* - - - - - - - - - - 252

Ratio of Neutron Absorption Cross-sections of Boron and Hydrogen—*W. J. Whitehouse and G. A. R. Graham* - - 261

A Theorem on Neutron Multiplication—*G. Placzek and G. Volkoff* 276

NATIONAL RESEARCH COUNCIL
OTTAWA, CANADA

CANADIAN JOURNAL OF RESEARCH

The *Canadian Journal of Research* is issued in six sections, as follows:

A. Physical Sciences	D. Zoological Sciences
B. Chemical Sciences	E. Medical Sciences
C. Botanical Sciences	F. Technology

For the present, each of these sections is to be issued six times annually, under separate cover, with separate pagination.

The *Canadian Journal of Research* is published by the National Research Council of Canada under authority of the Chairman of the Committee of the Privy Council on Scientific and Industrial Research. The *Canadian Journal of Research* is edited by a joint Editorial Board consisting of members of the National Research Council of Canada, the Royal Society of Canada, and the Chemical Institute of Canada.

Sections B and F of the *Canadian Journal of Research* have been chosen by the Chemical Institute of Canada as its medium of publication for scientific papers.

EDITORIAL BOARD

Representing National Research Council	*Representing* Royal Society of Canada	
Dr. J. B. Collip *(Chairman)*, Director, Research Institute of Endocrinology, McGill University, Montreal.	Dr. A. Norman Shaw, Chairman, Department of Physics, McGill University, Montreal.	Section III
Dr. Paul E. Gagnon, Director of the Graduate School, Laval University, Quebec.	Dr. J. W. T. Spinks, Department of Chemistry, University of Saskatchewan, Saskatoon.	
Dr. A. R. Gordon, Head, Department of Chemistry, University of Toronto, Toronto.	Professor J. R. Dymond, Director, Royal Ontario Museum of Zoology, Toronto.	Section V
Dr. J. A. Gray, Professor of Physics, Queen's University, Kingston.	Dr. H. S. Jackson, Head, Department of Botany, University of Toronto, Toronto.	

Ex officio	*Representing* The Chemical Institute of Canada
Dr. Léo Marion, Editor-in-Chief, Department of Chemistry, National Research Laboratories, Ottawa.	Dr. R. V. V. Nicholls, Associate Professor of Chemistry, McGill University, Montreal.

Editorial Committee

Editor-in-Chief,	Dr. Léo Marion
Editor, Section A,	Dr. A. Norman Shaw
Editor, Section B,	Dr. J. W. T. Spinks Dr. R. V. V. Nicholls
Editor, Section C,	Dr. H. S. Jackson
Editor, Section D,	Professor J. R. Dymond
Editor, Section E,	Dr. J. B. Collip
Editor, Section F,	Dr. J. A. Anderson Dr. R. V. V. Nicholls Dr. A. Norman Shaw

Manuscripts should be addressed:

Editor-in-Chief,
Canadian Journal of Research,
National Research Council, Ottawa, Canada.

Canadian Journal of Research

Issued by THE NATIONAL RESEARCH COUNCIL OF CANADA

VOL. 25, SEC. A. JULY, 1947 NUMBER 4

THE EFFECT OF WIND ON THE THERMAL RESISTANCE OF CLOTHING WITH SPECIAL REFERENCE TO THE PROTECTION GIVEN BY COVERALL FABRICS OF VARIOUS PERMEABILITIES[1]

P. LAROSE[2]

Abstract

The thermal resistance of a pile fabric uncovered and covered with thin fabrics of various permeabilities was measured under different conditions of wind velocities and wind direction. Wind velocities up to 30 m.p.h. were used and tests were carried out with winds striking the surface of the material at 0°, 30°, 45°, and 90°. The permeabilities of the covers varied between 0 and 193 cu. ft. per sq. ft. per min., under a pressure difference of ½ in. of water across the fabric. The effects of varying the conditions of the thermal resistance of the boundary air layer are discussed and corrections applied to the results for the resistance of this air layer. The results show that for low wind velocities, the permeability, within wide limits, is relatively of little importance, but with higher wind velocities it is advantageous to employ a covering fabric of as low a permeability as possible.

Introduction

During the war, the thermal insulation of clothing assumed an increased importance as a result of the wide range of climatic conditions under which the fighting forces had to operate. This applied particularly to the airmen who, sometimes within a matter of minutes, had to change from a tropical atmosphere to one in which the temperature was well below freezing point. The question of warm clothing was also of great concern to mountain troops. The necessity of suitable clothing, if the greatest efficiency was to be obtained from the soldiers, was well recognized, and the problem of maintaining men in comfort in various climatic surroundings was one that occupied the attention of physiologists.

One of the climatic factors that affect the protection afforded by clothing is wind. Very little work had been done, prior to the war, on the effect of wind on thermal insulation of clothing. The work that had been carried out involved experiments with a very limited range of air velocities, and in most tests the results reported did not lend themselves to a calculation of the direct changes caused by the air movement. Moreover, in most of the experiments, a single material or fabric was tested at one time whereas in practice clothing usually consists of several layers of fabrics superposed and differing one from

[1] *Manuscript received March 12, 1947.*

Contribution from the Textile Section, National Research Laboratories, Ottawa, Canada. Issued as N.R.C. No. 1559.

[2] *Chemist.*

another. More particularly if protection against wind is desired, one usually wears an outer shell of some fabric generally designated as 'wind-proof'. It was the thermal protection given by this particular layer in which we were specially interested, and the determination of the relation between the degree of protection given by the 'coverall' fabric, the velocity of the air or wind striking the material, and the permeability of this material. Most experiments carried out previously had taken no account of the air permeability of the textile materials tested. The experiments described in this paper were therefore designed with the view to determining the effect of wind velocity, wind direction, and permeability of coverall on its thermal resistance in combination with a comparatively thick underlying fabric.

Methods

The apparatus used for measuring the heat transmission through the combination of fabrics investigated was similar, except in method of control and in size, to that described by Cleveland (1) and used at the National Bureau of Standards, Washington. It consisted of a central brass plate, 10 in. square, 3/16 in. thick, surrounded by a guard ring 2 in. wide of the same thickness as the central plate and placed in the same plane. An air space about 1/12 in. wide separated the guard ring from the central plate. Both guard ring and central plate were painted a dull black. Another brass plate, 14 in. square, was placed 3 in. below and parallel to the central plate and guard ring. A number of reflecting aluminium foil layers spaced about ½ in. apart divided the space between the bottom and top plates. The brass plates, guard ring, and foil were encased in a wooden frame 2½ in. thick and fitted with a bottom 1 in. thick. The bottom plate, central plate, and guard ring were heated independently of one another by means of electric resistances placed directly below them. The current through these various heater resistances was controlled by means of hand-manipulated rheostats. During the initial stage of an experiment, the rheostats were adjusted frequently to maintain equality of temperature of the guard ring, central plate, and bottom plate, but after some time the plates would reach a practically steady state and little adjustment was required from then on. The fabrics were placed directly on top of the plate and guard ring. The samples, 20 in. square, were sufficiently large to cover the whole top of the apparatus, including the wooden frame.

The earlier tests carried out with low air velocities were performed in a room maintained under controlled conditions of temperature and humidity. Under such conditions it was possible to bring the apparatus to an equilibrium state in a relatively short time, but later, when higher wind speeds were desired, it was found impractical to carry out the experiments in the air-conditioned room, and, under the varying conditions of the laboratory, equilibrium was reached in a more or less longer time depending on the steadiness of the ambient conditions. It was possible, however, to carry out one test per day on the average.

Conducting the tests in the ordinary laboratory with no temperature control resulted also in some uncertainty regarding the temperature of the room. This point will be dealt with in discussing the results.

Temperatures were measured by means of thermocouples but, except in some of the later experiments, temperature differences between the various points were determined and not the absolute temperatures since these were not required for the calculations in which we were interested. The temperature of the air was taken as that of a ½ in. mesh grid placed above the sample. In some of the later experiments, a copper wire ring was used but there was no significant difference between the results obtained in this way and the results obtained with the grid, other conditions being equal. The grid (or ring) was placed about 1 in. above the surface of the fabric and parallel to it. A thermometer placed on the grid, at one side, served to show at a glance, any variation in the temperature of the grid during the tests. In the earlier experiments, it was thought that the grid was at a distance from the top of the fabric sufficient to have it take up the temperature of the room and to use its temperature as that of the room, but it was found in later experiments that, apparently owing to convection currents, the grid was in fact warmer than the air in the room, and a correction based on the results of these experiments was applied to arrive at the air temperature in the earlier experiments. However, some degree of uncertainty is attached to this correction, for reasons to be explained later. The difference in temperatures between the central plate and the guard ring was measured with four sets of thermocouples connected in series, one set to each side of the plate, so that the potential difference indicated on the potentiometer corresponded to the sum total of the temperature differences across each thermocouple between plate and guard. The other measurements taken were the temperature differences between central plate and bottom plate, and between the central plate and grid (air). In some of the later experiments, the temperature differences between central plate and surface of fabric was also determined. The potentiometer and thermocouples used allowed temperature differences to be read to within 0.02° C.

In the initial experiments an ordinary 12 in. propeller type fan with axial flow was used to produce the air circulation. It was placed with its centre about 8 in. away from the outside edge of the apparatus and slightly above it for the horizontal wind, and in corresponding positions but higher up for winds of 30° and 45° to the horizontal. With it, speeds up to 11 m.p.h. could be obtained but when higher speeds were required, a centrifugal fan with a 6 in. diameter outlet giving radial flow was used. This produced winds up to 30 m.p.h. The position of the fan was such that the outlet was about 24 in. above the sample being tested. Although the outlet of the fan was only 6 in., at 24 in. distance it exerted a fairly uniform effect over the whole central plate. Since the speed of the fan motor could not readily be altered, the variation in wind velocity was obtained by placing diaphragms of different sizes in the inlet opening of the fan.

The wind velocities recorded in the initial experiments, in which the propeller fan was used, were obtained by measurement with a vane-anemometer placed over the centre of the samples. Measurements made at various points between the fan and the surface of the fabric showed quite a variation with a rapid drop as the anemometer approached the fabric, when the fan was placed above the surface of the fabric. This was to be expected in view of the change in direction of the air as it approached the flat surface of the test piece. Arbitrarily the wind velocity was taken as that 4 in. above the surface of the fabric.

It should be kept in mind that the vane-anemometer measures only streamline flow and gives no indication of eddy currents or turbulent flow, but turbulent flow would not be expected to have much bearing on the thermal resistance except in disturbing the protecting air layer above the fabric. The effect of the wind on the air going through the fabric would be expected to depend only on the vertical component. However, air current measurements were also made with a katathermometer. The results obtained in this way checked fairly well with the anemometer figures arbitrarily chosen as described above, except for one of the lower velocities. This tended to show that there was little turbulent flow. Nevertheless, it was thought desirable to measure the velocity of the wind by a third method giving directly the pressure exerted on the fabric due to the wind. It would appear that this pressure is the most important factor affecting the heat loss by penetration of air through the covering fabric. In this latter method a dummy 'hot-plate' and 'guard ring' was built of beaver board of the same dimensions as those of the metal plates used in the thermal insulating apparatus. The fan was placed directly above this in the same relative position that it had over the hot-plate. The 'central plate' was balanced on a trip scale and the force necessary to maintain it in position with the various velocities was measured. The force for the lower velocities was however very small and difficult to measure accurately with this rather crude installation. The wind velocities calculated in this way agreed closely with those obtained by the other two methods.

The permeabilities reported for the various coveralls are those obtained with the 'Frazier' apparatus described by Schiefer and Boyland (10) and refer to air flow through the fabric with a pressure gradient across it equivalent to $\frac{1}{2}$ in. of water. The permeability P will always be in cubic feet of air per square foot per minute for that pressure difference.

Materials

As coverall fabrics, light cotton materials were used where the given permeabilities are 8 to 66 cu. ft. per sq. ft. per min., parachute canopy fabrics for the higher permeabilities, and plastic coated cotton materials for those stated as having zero permeability. The colour of the cotton fabrics having permeabilities $P=8$ and $P=13$ was white and that of the others khaki.

The parachute fabrics were white, while one of the coated fabrics was khaki, the other green.

The basic material used below the coverall fabric was, for most experiments, a single mohair pile fabric with a thickness of 0.51 in. under no pressure and 0.45 in. under a pressure of 0.1 lb. per sq. in. The number of tuft ends per square inch was 50. The tufts were bound with a cotton ground fabric. The total weight of the fabric was 35½ oz. per sq. yd., of which 22½ oz. was mohair pile. The apparent density of the pile was therefore of the order of 4.0 lb. per cu. ft. The double pile fabric used in some of the later experiments was one in which the pile was 2/18's worsted yarn of 60's quality wool, woven on to a cotton ground fabric. The number of tufts per square inch was 160. Since the construction was such that the tufts were continuous from one side to the other, the number of tuft ends were the same on either side. The weight of this fabric was 23 oz. per sq. yd., of which 14 oz. was wool pile. The thickness for all practical purposes was the same as that of the mohair fabric except that the tufts were more irregular in length.

Results

Wind Velocity

In order to show how the wind velocity measured varied according to the method employed in measuring it, the following table summarizes the results of a number of tests in which the wind velocity was determined by the three

TABLE I

WIND VELOCITIES IN MILES PER HOUR OBTAINED BY DIFFERENT METHODS

Test	Vane-anemometer	Kata-thermometer	Dynamic pressure
A	3½	4	4
B	4½	4½	3½
C	9	6	6½
D	14	12½	12½
E	16	15	14
F	22	22	21
G	26	26½	23

different methods referred to previously. In reporting the wind velocity in Table IV, and others that follow, the results obtained with the katathermometer will be given because the readings obtained with the vane-anemometer varied somewhat with the position of the instrument, and it was not convenient to use the direct pressure method for the regular determination of velocity.

Initial Thermal Resistance Tests

These tests were conducted, as mentioned before, with a propeller fan so placed that it produced a wind parallel to the surface of the material in one series of tests and a wind at 30° to the surface for the next series of tests. In

the first series, several textile materials were used to obtain a rough idea of the effect of the horizontal wind on the thermal resistance, but the second series was carried out with the definite purpose of finding out the effect of covers of various permeabilities, and the underlying fabrics were limited to two double pile fabrics of similar construction but differing somewhat in the quality of the pile and in thickness.

The results of the initial tests with a horizontal wind are given in Tables II and III.

TABLE II

THERMAL RESISTANCE OF VARIOUS MATERIALS IN STILL AIR[1] AND IN A HORIZONTAL WIND

Material	Thermal resistance, clos[2]	
	In still air	With wind (velocity in parentheses)
Overcoating	1.91	1.45 (7 m.p.h.)
Loose pad of wool (thickness 1 in.+)	6.42	5.13 (7 m.p.h.)
Very loose pad of wool	5.40	2.33 (7 m.p.h.)
Same with fine cotton cover	5.68	5.43 (7 m.p.h.)
Double pile fabric *A* (½ in.)	2.83	2.47 (8 m.p.h.) 2.06 (12 m.p.h.)
Same with cotton cover	3.35	2.77 (12 m.p.h.)
Cover alone	0.53	—
Double pile fabric *B* (½ in.)	2.44	2.08 (9 m.p.h.) 2.10 (12 m.p.h.) 2.04 (13 m.p.h.)
Single pile fabric (¼ in.)	1.35	0.88 (11 m.p.h.)

[1] *Although the vane-anemometer did not register any air movement when the fan was not in motion, there was some air circulation in the room, perhaps around 0.2 m.p.h., caused by the conditioning system. The anemometer did not register at speeds lower than 0.3 m.p.h. The term 'still air' is, therefore, only relative. The same remark applies to later tests.*

[2] *As this paper deals with clothing materials, the clo unit, proposed by Gagge, Burton, and Bazett (2) has been used to express thermal resistance. This unit has been defined as the thermal resistance of the clothing necessary to maintain in comfort a sitting–resting subject in a normally ventilated room (air movement 20 ft. per min.) at a temperature of 70° F. and a humidity of the air that is less than 50%. It is equivalent to 0.18* $\frac{^\circ C.}{Cal./hr./sq.\ m.}$ *or 0.88* $\frac{^\circ F.}{B.t.u./hr./sq.\ ft.}$.

The use of thermal resistance as a measure of the thermal insulation given by fabrics offers many advantages over that of thermal conductance, which has been most widely used by those concerned with the heat transmission through insulating materials.

Tests with Higher Wind Velocities and Various Angles of Incidence

Although the initial results indicated an appreciable drop in thermal resistance due to winds up to 11 m.p.h. when the permeability of the cover was high, it was considered desirable to experiment with a wider range of wind velocities in order to differentiate more closely between the effects of the low permeability covers. More information was also desirable on the effect of wind direction, and it was decided to try the effect of wind striking

TABLE III

THERMAL RESISTANCE OF DOUBLE PILE FABRICS WITH AND WITHOUT COVER IN STILL AIR AND IN WIND OF 11 m.p.h., 30° TO SURFACE

Test No.	Permeability of cover	Air movement	Underlying fabric	
			A	*B*
1	No cover	No wind	2.70	2.44
2	No cover	Wind	1.71	1.42
3	0	No wind	2.95	2.70
4	0	Wind	2.52	2.32
5	33	Wind	2.21	—
6	66	No wind	—	2.70
7	66	Wind	—	2.02
8	100	Wind	2.04	—
9	165	Wind	2.00	—
10	205	Wind	1.97	—

the surface at angles of 90° and 45°, as well as at 30°. The results of these experiments are given in Tables IV and V. The same results are presented in another form in Tables VI and VII, in which they have been corrected so as to represent the thermal resistance of the fabrics only, without that of the air over them. The correction is explained in the discussion that follows.

Thermal Resistance of Boundary Air Layer

The thermal resistance determined in most of our tests was that of the fabric and the boundary air layer combined. In order to calculate the resistance of the fabric itself, it is necessary to know that of the air layer. The correction could have been made by the use of data obtained by others, but the information published was meagre and there was some doubt as to the extent to which it was applicable to our experiments. It was thought preferable to repeat some of the experiments and measure the surface temperature of the fabric as well as that of the air. In this way it was possible to calculate the thermal transmission through the fabric separately from that through the air layer. Although the calculation of the resistance of the fabric offered no difficulty, the calculation of the resistance of the air layer necessitated a knowledge of the air temperature. In our initial experiments, the air temperature was taken as that of the grid, and, to apply a correction to the results, it would be sufficient to know the value of the resistance of the air between the surface of the fabric and the grid under the conditions of the experiments. However, in order to compare the results with theoretical figures or with results reported by other investigators the temperature of the air or room is required.

Measurement of the temperature of the air or of the walls of the room was not as easy as anticipated. Attempts made to measure the temperature of the room showed that there were appreciable variations due to drafts, and the temperatures of the walls varied significantly with the position of the thermocouple. The ceiling, 14 ft. above the floor, was generally a few degrees

TABLE IV

THERMAL RESISTANCE (CLOS) OF PILE FABRIC WITH AND WITHOUT COVER AND FOR VARIOUS WIND VELOCITIES (UNCORRECTED)

Wind velocity, m.p.h.	Permeability of cover					
	0	8	13	38	193	∞
	Thermal resistance, clos					
Wind at 90°						
0	2.30	—	2.31	2.21	2.24	1.96
	(2.26)	—	—	(2.38)	(2.36)	(1.95)
3	1.75	—	—	—	—	1.36
	(1.84)	—	—	—	—	—
5	—	1.74	1.68	—	(1.78)	—
	—	—	(1.96)	(1.83)	(1.73)	—
6	—	—	(1.72)	—	(1.75)	—
8	1.80	—	—	—	1.46	0.73
	(1.74)	—	—	—	—	—
9	—	—	—	1.70	—	—
11	1.76	—	—	—	—	—
13	1.68	—	—	1.22	—	—
14	—	1.50	—	—	1.06	—
15	—	—	1.42	—	—	0.69
16	—	1.44	—	1.19	0.94	—
18	1.66	1.42	—	—	—	—
19	1.71	—	—	—	—	—
20	—	—	0.99	0.78	—	—
22	1.60	1.16	—	0.75	0.57	0.53
	—	1.14	—	—	—	—
24	—	1.15	—	—	—	0.50
26	1.64	1.08	—	(0.62)	0.54	0.49
	(1.53)	—	—	—	—	—
30	1.54	—	0.80	—	0.49	0.46
Wind at 45°						
30	1.66	—	1.10	0.93	0.70	0.55
	1.62	—	—	0.96	—	—
Wind at 30°						
8	2.08	—	—	—	1.78	—
9	2.05	—	—	—	—	—
10	1.98	—	—	—	—	1.35
13	1.85	—	—	1.70	1.67	1.17
	1.81	—	—	—	—	—
18	—	—	—	—	1.47	—
20	1.76	—	—	—	—	0.84
25	1.74	—	—	—	1.34	0.83
30	1.70	—	—	—	1.03	0.68
	1.69	—	—	—	1.05	—
Parallel wind						
3	(1.89)	—	—	—	—	—
3½	(1.90)	—	—	—	—	—
4½	(1.89)	—	—	—	—	—

NOTE.—*Figures in parentheses are those obtained when temperature of surface was measured directly in later experiments.*

TABLE V

THERMAL RESISTANCE (CLOS) OF DOUBLE PILE FABRIC *B* WITH AND WITHOUT COVER AND FOR VARIOUS WIND VELOCITIES (UNCORRECTED)

Wind velocity, m.p.h.	Permeability of cover			
	∞	44	8	0
	Thermal resistance, clos			
0	2.40[1]	—	2.44	2.69[1]
2	—	—	—	2.45
3½	2.10	—	—	2.32
4½	1.95 1.97	—	—	—
6½	1.43	—	—	—
9	1.26	1.91	2.30	2.30 2.33
26	0.37	0.61	1.22	2.14 2.11

[1] *Mean of five measurements.*

warmer than the walls. The temperature variation around the room was also appreciable and there was sometimes a difference of a few degrees between the temperature of the walls and that of the air, the air being generally cooler at such times. As the apparatus was in a corner of the room in close proximity to two walls, it was decided to use the temperature of these walls, a short distance above the level of the apparatus, as the air temperature. Where there was an induced air movement to simulate the effect of wind, the air temperature was measured directly in front of the fan.

Air Resistance with No Wind

The thermal resistance provided by the boundary air layer and determined as above under comparatively still air conditions was found to vary in the different tests from 0.53 to 0.64 clo for surface to grid and between 0.68 and 0.76 clo for surface to wall, with mean values of 0.58 and 0.72 clo, respectively. These values are for a temperature gradient of about 12° F. from surface to air, this temperature gradient being that which applied to most of our earlier experiments.

In order to find out how the resistance of the air layer varied with temperature, a number of tests were carried out in which the heat input was varied within fairly wide limits in order to give different temperature gradients. The results of one particular set of tests are given in Table VIII while results of all such tests are given in Fig. 1, in which a straight line has been drawn through the points. This line has an intercept of 1.6° F. on the temperature axis and a slope of 1.79 B.t.u. per degree corresponding to 0.63 clo insulation. These results will be discussed presently.

TABLE VI

THERMAL RESISTANCE (CORRECTED) OF PILE FABRIC WITH AND WITHOUT COVER AND FOR VARIOUS WIND VELOCITIES

Wind velocity, m.p.h.	Permeability of cover					
	0	8	13	38	193	∞
	Thermal resistance, clos					
Wind at 90°						
0	1.72	—	1.73	1.63	1.66	1.38
	(1.67)	—	—	(1.63)	(1.67)	(1.35)
3	1.51	—	—	—	—	1.12
	(1.69)	—	—	—	—	—
5	—	1.56	1.50	—	(1.56)[1]	—
	—	—	(1.64)	(1.64)	—	—
6	—	—	(1.59)	—	1.67	—
8	1.65	—	—	—	1.30	0.57
	(1.64)	—	—	—	—	—
9	—	—	—	1.56	—	—
11	1.65	—	—	—	—	—
13	1.59	—	—	1.11	—	—
14	—	1.42	—	—	0.95	—
15	—	—	1.34	—	—	0.57
16	—	1.38	—	1.10	0.84	—
18	1.63	1.38	—	—	—	—
19	1.68	—	—	—	—	—
20	—	—	0.97	0.71	—	—
22	1.60	1.15[1]	—	0.70	0.49	0.43
24	—	1.12	—	—	—	0.40
26	1.70	1.14	—	(0.74)	0.49	0.40
	(1.63)					
30	1.65	—	0.86	—	0.45	0.37
Wind at 45°						
30	1.65[1]	—	1.16	0.90[1]	0.64	0.46
Wind at 30°						
8	1.92	—	—	—	1.62	—
9	1.90	—	—	—	—	—
10	1.82	—	—	—	—	1.20
13	1.71[1]	—	—	1.58	1.54	1.04
18	—	—	—	—	1.36	—
20	1.67	—	—	—	—	0.73
25	1.68	—	—	—	1.26	0.74
30	1.66[1]	—	—	—	0.96[1]	0.59
Parallel wind						
3	(1.74)					
3½	(1.74)					
4½	(1.67)					

[1] *Mean of two measurements.*

NOTE.—*Figures in parentheses are those obtained directly from surface temperature measurements and not by difference from Table IV.*

TABLE VII

THERMAL RESISTANCE (CORRECTED) OF DOUBLE PILE FABRIC *B* WITH AND WITHOUT COVER AND FOR VARIOUS WIND VELOCITIES

Wind velocity, m.p.h.	Permeability of cover			
	∞	44	8	0
	Thermal resistance, clos			
0	1.82	—	1.86	2.11
2	—	—	—	2.17
3½	1.87	—	—	2.09
4½	1.75 1.77	—	—	—
6½	1.26	—	—	—
9	1.11	1.77	2.16	2.16 2.19
26	0.28	0.59	1.28	2.20 2.17
				Mean 2.14

TABLE VIII

PROTECTION GIVEN BY BOUNDARY AIR FOR VARIOUS TEMPERATURE GRADIENTS BETWEEN SURFACE AND AIR

Δt, surface to air, ° F.	Thermal resistance, clos	
	Surface–grid	Total
12.5	0.60	0.74
15.7	0.57	0.71
17.9	0.57	0.70
22.3	0.55	0.69
25.4	0.51	0.66

Determinations of the thermal resistance were also made with the grid at various distances from the surface, with results given in Table IX.

These results show that the position of the grid between ½ in. and 2 in. above the surface of the fabric was not critical and that its temperature was practically constant between these limits.

The results obtained for the air resistance might be compared with those given for flat plates by other investigators. In order to compare results, it is desirable to break up the heat lost from the surface into heat lost by radiation and heat lost by convection. The heat lost by radiation is readily obtained from theoretical considerations. Assuming that, for the difference in temperature with which we are concerned, the heat radiated is proportional to the temperature difference, θ, between surface and air, we can write $H_r = h_r \theta$, where H_r is the total heat loss per square foot per hour and h_r represents the

heat loss per square foot per hour per degree difference in temperature. If θ is of the order of 10° to 12° F. as in most of our experiments, $h_r = 1.10$ B.t.u. when the emissivity is 1.0. As the emissivity of the fabrics used in our experiments was probably closer to 0.90, h_r might be taken as 1.0 B.t.u.

TABLE IX

VARIATION OF AIR RESISTANCE BETWEEN SURFACE AND GRID FOR DIFFERENT POSITIONS OF THE GRID

Distance above surface, in.	Thermal resistance, clos
0.2	0.38
0.3	0.48
0.6	0.53
0.9	0.52
1.2	0.51
1.5	0.53
1.8	0.54
8	0.58
18 (to one side near wall)	0.68

To calculate the heat lost by convection, we may similarly use H_c as the heat loss per square foot per hour and h_c as the heat loss per square foot per hour per degree difference in temperature.

However, in this case, h_c itself is dependent on temperature. To find h_c we may use Nussel's formula $h_c = 0.39\ \theta^{1/4}$ for loss of heat from a vertical pipe, applying the correction + 6% suggested by Rosin for plane surfaces (9, p. 96). This gives $h_c = 0.77$ B.t.u. when $\theta = 12°$ F. Griffiths and Davis (3) use a similar formula in which the coefficient is 0.38 instead of 0.39 while King (5) gives a coefficient of 0.36 (0.275 + 30% correction for horizontal surfaces). These two coefficients yield values of $h_c = 0.71$ and 0.67 B.t.u., respectively. Hampton (4) uses a formula of the same type which gives $h_c = 0.60$ B.t.u. The sum of $h_r + h_c$ can therefore be taken as somewhere between 1.60 and 1.77 B.t.u. This corresponds to a resistance of 0.71 to 0.64 clo. Our figures are therefore in good agreement with those generally accepted.

It follows from the above that $H_c = 0.38\ \theta^{5/4}$, using the coefficient 0.38 given by Griffiths and Davis, and $H_r = 1.0\ \theta$, so that $H_c + H_r$ is not a linear function of temperature and the straight line drawn in Fig. 1 is only an approximation, while the slope of the line represents simply a mean of the experimental values of $\frac{H_r + H_c}{\theta}$ within the range of temperatures investigated. The values calculated from the formula $H_r + H_c = 1.0\ \theta + 0.38\ \theta^{5/4}$ have been represented by open circles in Fig. 1. Taking the extreme temperature differences used to obtain Fig. 1, we have for a 26° difference a heat loss of 1.85 B.t.u. per hr. per ft.^{2} per ° F. corresponding to a resistance of 0.61 clo, and for a 6° difference, a heat loss of 1.60 B.t.u. per hr. per ft.^{2} per ° F.,

corresponding to a resistance of 0.71 clo. The resistance calculated from the slope of the line in Fig. 1 is 0.63 clo. The calculated values for $H_c + H_r$ are somewhat higher than most of the experimental values found. The deviation may be due to the factor 0.38 being too high or the emissivity might be lower than the 0.90 assumed. However, it might be pointed out also that the temperature difference that controls the radiation loss in our experiments is not necessarily the same as that affecting the convection losses, since the latter would depend mostly on the air temperature around the apparatus, while the radiation would depend more on the temperature of the walls or other surfaces in the room. In other words $H_r + H_c = 1.0\ \theta_1 + 0.38\ \theta_2^{5/4}$, where θ_2 is different from and generally smaller than θ_1 in our experiments. Since θ_1, the temperature difference between the surface of the fabric and the

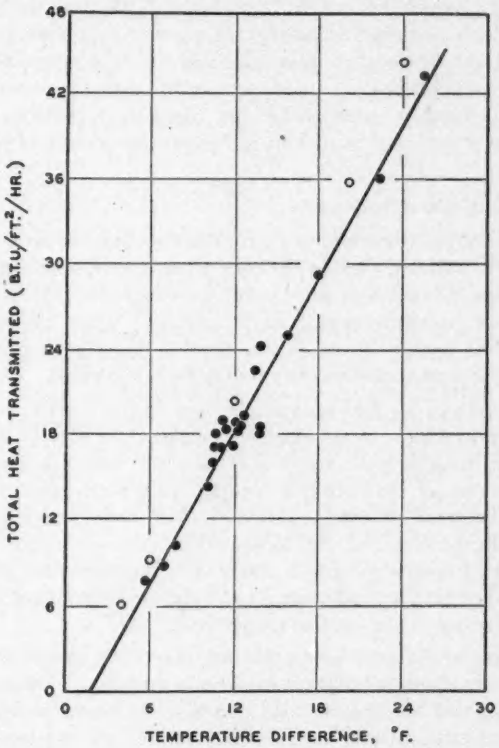

FIG. 1. *Relation of heat loss to temperature difference between surface of fabric and room.*

walls of the room, was used in plotting Fig. 1, the experimental points would be expected to be too high with respect to temperature if the above explanation is correct. It is of course possible that all three factors just mentioned are

jointly responsible for the deviations noted, but, whichever explanation is correct, it is evident that the line expressing the relation between heat loss and temperature difference should pass through the origin. The intercept of 1.6° F. on the temperature axis given by our curve indicates that our temperature differences were either too high, at least for the lower points, or that the line changes direction for low temperature differences. This point was not considered of sufficient importance to merit further study.

In order to obtain the resistance of the fabric itself under 'no wind' conditions, it was decided then to subtract 0.58 clo from the total for fabric plus boundary air layer, between surface and grid, this figure being considered the most probable mean value under the conditions of our test. The results given in Table IV thus yield 1.72 clo for the resistance of the pile fabric covered with the impermeable cover. This is the figure reported in Table VI, which contains such corrected values for all other tests. The repeated tests in which the surface temperature was measured directly gave 1.67 clo as the mean of six determinations, in good agreement with the previous result. The correction is further justified by the agreement between the direct measurements and those calculated by difference for covers of permeability 38, 193, and ∞.

Resistance of Air Under Circulation

The resistance of the boundary air layer discussed in the preceding section was for so-called 'still air', but it is evident that any body at a different temperature from the ambient air cannot be surrounded by still air since there will always be convection currents resulting from the difference in temperature. The term 'still air' or 'no wind' is therefore relative only and signifies that there was no deliberately induced air movement.

The correction to be applied for the air layer in the results obtained with various wind velocities is not so readily calculated as for conditions of no wind. However, the thermal resistance of the air in such cases is quite small and any small error in the correction would have little effect on the total resistance. As before, tests were repeated in which surface temperatures were determined while the material was subjected to air movement. It was not deemed necessary to carry out a wide series of such experiments, as the initial tests indicated that the thermal resistance of the air became quite small even at low wind velocities. The results are given in Table X.

Available formulae for calculating the heat loss through forced convection apply either to wind parallel to plane surfaces or to pipes. Data obtained by Winslow, Gagge, and Herrington (11) can also be used, but the formulae apply to the human body and not to a flat surface. Nevertheless, work on heat loss by natural convection has shown that a plane horizontal surface has a heat loss comparable to that of a pipe 4 in. or more in diameter. Assuming that this similarity holds for forced air circulation, then one could justify the use of a formula derived from data on the human body, as Rees (7) has done.

TABLE X

THERMAL RESISTANCE OF BOUNDARY AIR LAYER UNDER WIND CONDITIONS

Wind velocity, m.p.h.	Permeability of cover, cu. ft./ft.²/min. at ½ in. water pressure	Thermal resistance of air layer, clos		
		Surface–grid	Total	Total calc.
0.4	0	0.58	0.72	0.71
0.6	0	0.33	0.35	0.63
1.1	0	0.33	0.43	0.52
2.4	0	0.25	0.30	0.39
3.5	0	0.18	0.32	0.34
4.5	0	0.13	0.29	0.30
4.5	0	0.17	0.31	0.30
4.5	13	0.20	0.32	0.30
4.5	160	0.10	0.15	0.30
5.5	38	0.20	0.27	0.28
6.0	0	0.18	0.28	0.27
6.0	13	0.16	0.20	0.27
6.0	160	0.08	0.16	0.27
14	>750	0.05	0.06	0.19
26	0	0.06	0.09	0.14
26	38	0.03	0.04	0.14

Using the data of Winslow, Gagge, and Herrington, namely, a radiation loss of 3.35 kgm-cal. per m.² per hr. per °C. and a convection loss of $1.043\sqrt{v}$ kgm-cal. per m.² per hr. per °C. where v is the air velocity in centimetres per second, one gets by change of units a thermal resistance $R = \frac{1}{0.61 + 1.25\sqrt{v}}$ where v is in miles per hour.

The calculated values from this equation are given in the last column of Table X. Considering the difficulties involved in measuring such low resistances with any precision and the possible error in the determination of the wind velocity itself, it can be assumed that the above formula is applicable to our results obtained with an impermeable cover and for velocities above 1 to 2 m.p.h. For low velocities, the effect of natural convection currents predominates over the effect of forced air circulation, and the relation no longer holds, as Winslow, Gagge, and Herrington have pointed out in their paper.

The rate of heat loss by convection was calculated as follows from our observations under various wind velocities with the impermeable cover over the pile fabric. The value 1.65 clo, representing the thermal resistance of the fabrics, was subtracted from the total resistance found. The difference was taken as the resistance of the air over the fabric. The rate of heat loss by radiation was assumed to be 1.0 B.t.u. per sq. ft. per hr. per ° F., and, by subtracting this from the total heat loss through the air, the rate of heat loss by convection, h_c, was obtained. The various values of h_c thus found have been used in Fig. 2. The full dots in the upper curve represent values

calculated from a smooth curve drawn through the resistances found experimentally when plotted against $\sqrt{v}$, while the open circles are points derived directly from some of the observations. The upper curve represents the

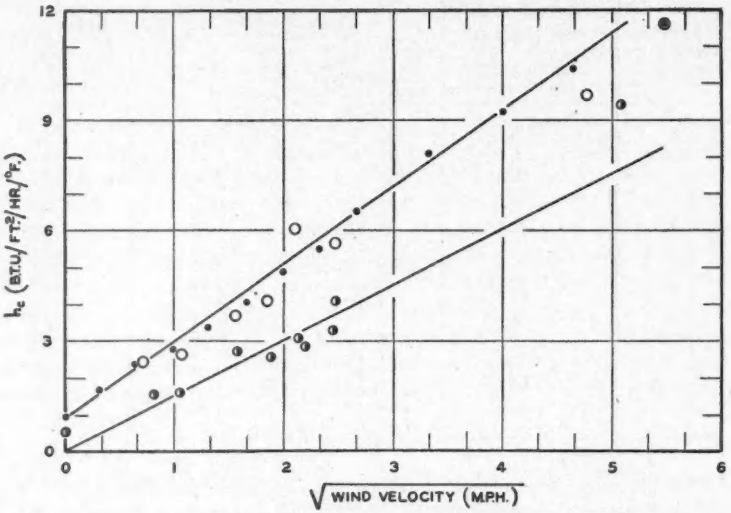

FIG. 2. *Relation between convective heat loss and wind velocity for the boundary air layer. Upper curve for layer between surface of fabric and grid. Lower curve for entire air layer.*

conductance for the air layer between surface and grid. The lower curve was drawn through points obtained in the later experiments when the surface temperature was measured directly, and it represents the conductance of the total boundary air layer (i.e., air layer between fabric and grid + the effective layer above the grid). It should be pointed out that owing to the difficulty in determining the air temperature between surface and air in most cases, the values for h_c are subject to a relatively large error. The values for conditions of 'no wind' have been placed at $v = 0$, but these points actually represent conductances with air under some movement. In Table X, the agreement between experimental values and calculated values is good if we take $v = 0.4$ m.p.h. for the 'no wind' condition. The slope of the lower line in Fig. 2 is 1.50. Although this is only approximate it gives an equation for the thermal resistance, $R = \dfrac{1}{0.88 + 1.32\sqrt{v}}$ clo, that compares with $R = \dfrac{1}{0.61 + 1.25\sqrt{v}}$ clo, obtained with the data of Winslow, Gagge, and Herrington. The average ratio of surface-to-grid resistance to the total air resistance is roughly $\frac{2}{3}$. The values calculated for the total resistance have therefore been multiplied by $\frac{2}{3}$ to obtain the correction to be subtracted from the experimental results of Tables IV and V. The few tests carried out with the covers of permeabilities 38 and 160 seem to indicate that the air protection is appreciably less when

the outer fabric is quite permeable (cf. Table X). This is perhaps due to the fact that the convection effect extends below the surface of the fabric when the covering fabrics are permeable. The comparative roughness of the surface in such cases may also play a role in diminishing the thermal resistance of the air by increasing the convection effects. It is therefore much more difficult to correct for the air layer resistance in these instances. Fortunately the corrections are small and any error resulting from the use of the wrong values will be small in comparison to the total resistance of fabric plus air.

The corrections to be applied when the wind is not perpendicular to the surface but makes angles of 30° and 45° to the horizontal can be taken to be the same as for the 90° wind. Table XI gives the figures for a horizontal wind calculated from the formula proposed by King and Knaus (6) and compared with the values for a vertical wind calculated as before. It will be seen that the two sets of values are comparable and it seems logical therefore to assume that any wind direction would give similar results.

TABLE XI

THERMAL RESISTANCE OF AIR LAYER FOR A 90° WIND COMPARED WITH THE RESISTANCE IN A HORIZONTAL WIND PARALLEL TO SURFACE

Wind velocity, m.p.h.	Thermal resistance, clos	
	Vertical wind	Horizontal wind
3	0.36	0.45
5	0.29	0.35
8	0.24	0.27
11	0.21	0.23
13	0.20	0.21
16	0.18	0.18
24	0.15	0.14
30	0.13	0.12

The effect of wind direction on the surface coefficient of flat surfaces has been investigated by Rowley and Eckley (8). They found that for winds below 15 m.p.h., the heat loss was practically the same for all angles between 15° and 90° but slightly less than that for a parallel direction. Above 15 m.p.h., the conduction decreased somewhat as the angle of the wind increased but at 25 m.p.h. the results for a 60° wind and a 90° wind were still about the same. In view of the low value for the thermal resistance of the boundary air at high wind velocities, no serious error is introduced by assuming the same values for all directions of the wind.

There is another correction to be made that has no connection with the boundary air layer but that is dependent on the wind. This is the reduction in thermal resistance resulting from the change in thickness of the materials due to the compressional effect of the wind pressure. This pressure will be

proportional of course to the square of the wind velocity. Direct determination of the change in thickness by means of a cathetometer showed that a wind of 30 m.p.h. resulted in a compression of about 2.2 mm. corresponding to a change in resistance of 0.30 clo when the impermeable fabric covered the pile fabric. With a cover of permeability 38 the change in thickness was only about half that, and with the cover of permeability 193 it was only one-fourth. For winds of velocity lower than 30 m.p.h. the compression has been assumed to be proportional to the square of the velocity. For angles other than 90°, the vertical component of the velocity has been used to calculate the compressional effect. This correction is of opposite sign to that applied for the change in resistance of the boundary air layer, and has to be added to the experimental results.

The results corrected for boundary air resistance and for compression due to wind pressure are given in Tables VI and VII. These figures represent therefore the thermal resistance of the pile fabric itself with the covers of various permeabilities and under various wind conditions.

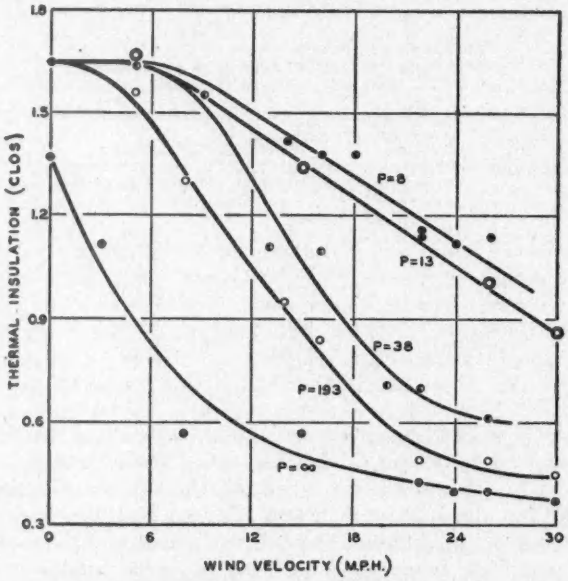

FIG. 3. *Curves showing the relation between change in thermal insulation and wind velocity for covers of different permeabilities.*

These results have been plotted in Figs. 3 and 4. Fig. 3 shows the variation in thermal resistance with varying wind velocity for covers of different permeabilities. In Fig. 4, the thermal resistance is given against the permeability for various wind velocities, the points having been taken from the curves of Fig. 3.

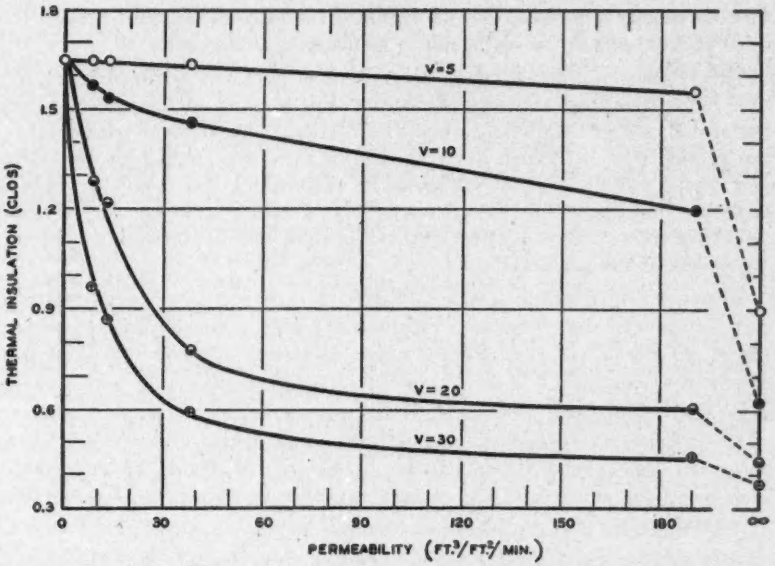

FIG. 4. *Curves indicating the change in thermal insulation with permeability of cover for various wind velocities.*

Discussion of Results

Effectiveness of Covers

Fig. 3 shows clearly that for low wind velocities, up to about 10 m.p.h., the permeability of the cover is not very important until a fairly high permeability is reached. It would appear also that as long as the permeability is not too high, say below 50 on our scale, the air behind the covering fabric is not appreciably disturbed when the wind velocity is not higher than 6 m.p.h. The sole effect of the wind up to this point is to change the resistance provided by the boundary air layer, and most of this change, as we have seen from Table X, occurs at low wind speeds.

Once the speed of the wind reaches 6 m.p.h., the reduction in thermal resistance of the fabric behind the cover is practically proportional to wind velocity for covers of low permeability, at least up to 30 m.p.h. It is evident, however, that this relation cannot hold for all velocities and that at some higher velocity the curves for the low permeability covers must level off and become asymptotic to the horizontal axis, as do the lines for the higher permeabilities at velocities of 24 to 30 m.p.h. The latter show a linear relation over a more limited range of wind velocities, and it would appear that the higher the permeability, the shorter the linear portion of the curve becomes.

It is also clear that at very high wind velocities the lines approach one another and that again the permeability becomes relatively unimportant, since the thermal resistance is small in any case. The curve for $p = \infty$

(uncovered pile fabric) is a special case but it indicates the limit to which the other curves tend as the permeability is indefinitely increased.

The relative protection given by covers of different permeabilities will therefore depend on the wind velocity. For a wind of low velocity, the permeability is of little importance within fairly wide limits of permeability, but at high wind velocities, say 20 m.p.h. or more, to get the best protection one should employ a cover of as low a permeability as possible. This is probably best shown by the curves of Fig. 4, which indicate that at wind velocities of 20 to 30 m.p.h., most of the drop in thermal resistance occurs in the covers of low permeability.

Although the relation between change of resistance and permeability is not a linear one, for purposes of calculation within a narrow range of permeabilities it can be assumed that the reduction in thermal resistance is proportional to permeability. For example, for a wind of 30 m.p.h. and between zero permeability and a permeability of 10, the drop in resistance is about 0.70 clo and we can therefore say that the resistance decreases by 0.07 clo for every unit change in permeability. This sort of calculation is useful in comparing the efficacy of two or more windbreaks that differ somewhat in permeability but that are all low in permeability.

It should be borne in mind that the results given indicate only the general relation between wind, permeability of cover, and change in thermal resistance. The magnitude of the change will depend not only on the permeability of the cover but also on the nature of the fabric under the cover. This is shown by comparing the results for the double pile fabric with those obtained with the single pile. Whereas a change in resistance of 1.54 clo was obtained for the double pile fabric without cover when the wind was 26 m.p.h. as compared with the 'no-wind' condition, the single pile fabric showed only a corresponding drop of 0.98 clo. Comparing the figures for the cover of permeability 44 over the double pile with those for the cover of permeability 38 over the single pile and the change occurring when the wind is increased from 9 to 26 m.p.h., we have a drop of 1.18 clo for the double pile and 0.82 clo for the single pile fabric. This difference could hardly be due to the small difference in permeability. It is more likely due to the more open construction of the double pile and to the fact that the pile was much more uneven in thickness (fibre length) than in the single pile fabric of mohair fibres fairly closely packed and sheared so as to give a uniform pile thickness.

Differences due to the nature of the underlying fabric itself are also evident from the results given in Tables II and III. The results given in Table II show clearly that the more open the structure of the fabric, the larger the effect of the wind, as is to be expected. Table III indicates that fabric *A* was more open than fabric *B*, for the drop between 'no wind' and wind conditions with the cover of permeability 66 was 0.83 clo (interpolated) for fabric *A* versus 0.68 clo for fabric *B*. Comparison of the 12 m.p.h. results in Table II also reflect the more open structure of fabric *A* relative to fabric *B*.

Applying the corrections for the resistance of the boundary air layer to the results of Table II, it is possible to show that, except for the fabrics of more open structure, the effect of a horizontal wind is small. In the case of fabric *B* with no cover, for example, we have 1.86 clo for 'no wind', 1.93 clo for a wind of 9 m.p.h., 1.97 clo for a wind of 12 m.p.h., and 1.91 clo for a wind of 13 m.p.h.; on the other hand, fabric *A* shows a change from 2.25 clo for 'no wind' to 2.06 clo for a wind of 12 m.p.h., again indicating a more open structure for fabric *A*.

The advantage to be derived from a cover is well shown by the two results obtained for the loose pad of wool. While the thermal resistance decreased by only 0.25 clo with the cover, the change was 3.07 clo with no cover, for a horizontal wind of 7 m.p.h.

Regarding the effect of the angle at which the wind strikes the fabric, the number of tests carried out are insufficient to enable a generalization to be made but the results reported in Table VI seem to indicate that the effect is proportional to the vertical component of the wind; in other words the effect of the 30° wind is roughly the same as that obtained with a 90° wind of half the velocity, while the 45° results should correspond to that of a 90° wind with a velocity of 0.7 that of the 45° wind. For example, the insulation for $P = \infty$ at 30 m.p.h. at 30° is 0.59 clo, while that for 15 m.p.h. at 90° is 0.57 clo. For 45° we have 0.46 clo, while for a 21 m.p.h. (0.7×30) wind at 90° we have 0.43+ clo. The relation apparently falls down at low wind velocities, but we have seen that convection currents interfere with the correction at low velocities and that the convection currents are also largely dependent on the openness of the fabric. If we take the figures for a cover of permeability $P = 193$ we have, for 30 m.p.h. at 30°, 0.96 clo, and 0.90 clo for 15 m.p.h. at 90°, or 1.36 clo for 18 m.p.h. at 30° and $\backsim$ 1.26 clo for 9 m.p.h. at 90°. The relation can be considered only a rough one, however, until more data are available. The results for the 45° wind, for example, do not agree so well with those for the 21 m.p.h. wind at 90°.

In conclusion it might be objected that the results given in this paper apply to flat surfaces only and may not be applicable to the same materials worn on the body. We hope to show in a later paper that the general conclusions drawn from our results also hold for vertical cylinders. However, it can be argued that the conditions under which clothing is worn are so variable that one cannot hope in ordinary laboratory experiments to duplicate exactly these conditions. The information obtained in the laboratory serves rather to evaluate the relative merits of different fabrics, and this can be done more conveniently on a flat plate apparatus than on a cylindrical one.

References

1. CLEVELAND, R. S. J. Research Natl. Bur. Standards, 19 : 675-684. 1937.
2. GAGGE, A. P., BURTON, A. C., and BAZETT, H. C. Science, 94 : 428-430. 1941.
3. GRIFFITHS, E. and DAVIS, A. H. Food Investigation Board Special Report, 9. D.S.I.R. London. 1922.
4. HAMPTON, W. M. Nature, 481. 1946.

5. KING, W. J. Mech. Eng. 54 :347-353. 1932.
6. KING, W. J. and KNAUS, W. L. Refrigerating Data Book, A.S.R.E. 1937-1938.
7. REES, W. H. J. Textile Inst. 37 : P132-P153. 1946.
8. ROWLEY, F. B. and ECKLEY, W. A. Heating, Piping, Air Conditioning, 3 : 870-874. 1931.
9. SCHACK, A. Industrial heat transfer. *Translated by* H. Goldschmidt and E. P. Partridge. John Wiley & Sons, Inc., New York. 1933.
10. SCHIEFER, H. F. and BOYLAND, P. M. J. Research Natl. Bur. Standards, 28 : 637-642. 1942.
11. WINSLOW, C.-E. A., GAGGE, A. P., HERRINGTON, L. P. Am. J. Physiol. 127 : 505-518. 1939.

PERMEABILITY STUDIES

II. SURFACE AREA MEASUREMENTS OF INORGANIC PIGMENT POWDERS[1]

By J. C. Arnell[2]

Abstract

The modified Kozeny equation has been found to be satisfactory for the measurement of the specific surface of inorganic pigments having particle diameters of the order of 0.1 to 0.2 μ to within $\pm 10\%$. These powders were too fine for visual microscope counting or standard sedimentation methods of specific surface measurement. The results obtained from experimental data were checked against those calculated from electron microscope counting for two of the powders studied and found to be in satisfactory agreement.

Introduction

A modification of the Kozeny equation for the measurement of the specific surface of fine powders by permeability methods has been presented in a previous paper (3). This modification was introduced for the case of gases permeating through porous media, where the average size of the channels through the media was of the same order of magnitude as the mean free path of the gas. The modified equation may be written as:

$$Q = \frac{Ah\rho_{Hg}g\epsilon}{LS_v(1-\epsilon)}\left[\frac{\epsilon^2}{k\eta S_v(1-\epsilon)} + \frac{8}{3}\sqrt{\frac{2R_0T}{\pi M}}\frac{\delta\alpha}{\bar{P}\rho_{Hg}g}\right], \qquad (1)$$

where Q = rate of gas flow in cubic centimetres per second,
A = cross-sectional area of the bed in square centimetres,
h = pressure head in centimetres of mercury,
ρ_{Hg} = density of mercury in grams per cubic centimetre,
g = acceleration due to gravity,
L = length of the bed in centimetres,
ϵ = volume of pore space per unit volume (porosity),
S_v = specific surface of the powder in square centimetres per cubic centimetre,
α = fraction effective void area,
k = shape factor,
η = viscosity of the gas in poises,
δ = variable factor, having a value of approximately 0.9,
R_0 = gas constant,
T = absolute temperature,
M = molecular weight of the gas, and
$\bar{P} = (p_1 + p_2)/2$ = mean pressure in centimetres of mercury.

[1] *Manuscript received February 2, 1947.*
Contribution from the Defence Research Chemical Laboratories, Ottawa, Canada.
[2] *Research Chemist.*

This equation was tested against the data obtained from the flow of air through a bed of finely ground quartz at different mean pressures and also against the data of Hodgins, Flood, and Dacey (7), who measured the flow of both permanent and non-permanent gases through a sintered glass plug at different mean pressures.

In this paper, additional data are presented for the flow of air through beds of finely ground quartz and a number of inorganic pigments over a fairly wide range of porosities. These results permit a closer examination of the above equation and bring out some of the relations between the porosity and such variables as the shape factor, which cannot be determined accurately.

Apparatus and Technique

The apparatus employed for the permeability studies is illustrated in Fig. 1, and was a modified form of that used by Rigden (9).

The powder to be studied was packed, in increments, in a small tube, *A*, by means of a hand press of the type used by Pechukas and Gage (8) to give a bed 1.00 cm. long. The first tubes used were made of lengths of glass tubing, selected with a uniform cross-section. These tubes were later discarded in favour of tubes machined out of Lucite rods. All the tubes used had a cross-sectional area of about 0.245 sq. cm. and were about 4.5 cm. long. The packed tube was attached to two glass adapters by means of rubber pressure tubing and mounted across the top of the two mercury towers, *B*.

The two mercury towers were about 110 cm. long and had a cross-sectional area of 3.99 sq. cm. They were connected across the bottom to form a large manometer and were half-filled with mercury. The right-hand tower was connected through a null manometer, *C*, to a mercury manometer, *D*.

The technique of measuring permeabilities was as follows. After the packed tube was in position, stopcock S_1 was closed, and, with stopcock S_2 open, the left-hand tower was slowly evacuated through stopcock S_3. The evacuation was continued until a pressure difference of between 12 and 20 cm. of mercury, depending on the mean pressure of the experiment, was attained across the two towers, and stopcock S_3 was then closed. Stopcock S_4 was closed when the mercury in the two arms of the null manometer was approximately level. The gas volume between the top of the mercury in the left-hand arm of the null manometer and stopcock S_4 was sufficiently small as to be negligible when compared to the total gas volume in the mercury towers. Stopcock S_2 was closed and stopcock S_1 opened slowly to connect the two towers through the bed of powder. As the gas flowed through the bed of powder, the drop in the mercury level in the left-hand tower with time was followed by means of a cathetometer. The decrease in the pressure head was logarithmic with time and from a plot of the logarithm of the pressure head against time, the rate of gas flow could be calculated, by the method to

be given later in this paper, for any required pressure difference. When sufficient readings had been obtained, stopcock S_2 was opened slowly and the equilibrium pressure, p_0, was obtained on the mercury manometer, D, by balancing the two arms of the null manometer, C, with stopcock S_4 open, by the proper manipulation of stopcock S_5.

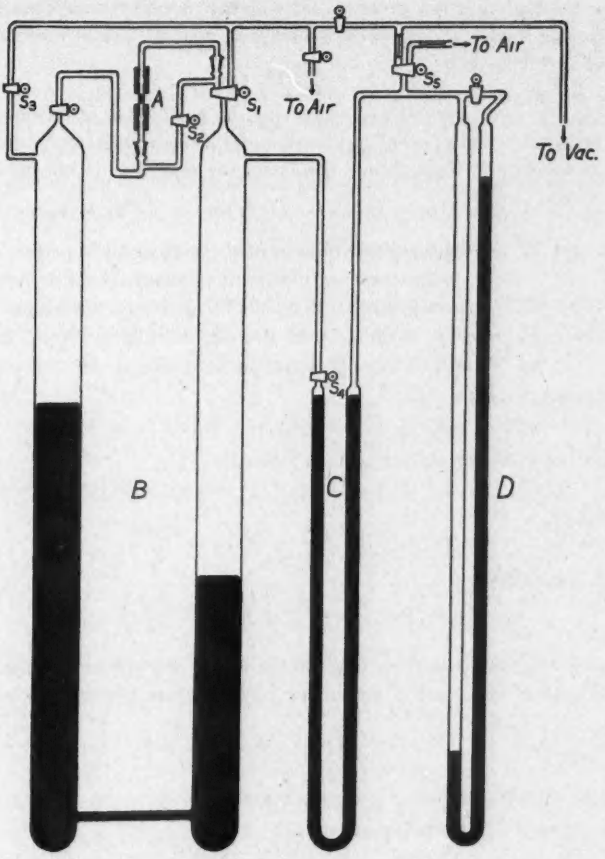

FIG. 1. *Diagram of decay apparatus.*

In the normal operation of the apparatus, the drop of the mercury level with time was generally followed from a pressure difference of just over 10 cm. of mercury to just under 5 cm. of mercury and the rates of flow were calculated for pressure heads of 5 and 10 cm. of mercury. If the pressure difference at the start of an experiment was higher than that desired, some gas was bled through stopcock S_2 until the required difference was obtained.

Theory of the Decay Apparatus

For the sake of completeness, the treatment followed here will be carried through the final integration, but, as will be shown later, the resulting equation has been used in its differential form.

In Fig. 1, if p_1 and p_2 are the pressures in centimetres of mercury, at any instant on the high and low pressure sides of the mercury towers respectively, and if h be the instantaneous pressure head in centimetres of mercury across the bed of powder, then

$$p_1 - p_2 = h. \tag{2}$$

Equating the sums of the masses of gas on both sides of the bed at any moment with the total mass of gas in the equilibrium position, and assuming isothermal conditions throughout, the following equation is obtained:

$$p_1(V_1 + A_0h/2)\rho_1 + p_2(V_2 - A_0h/2)\rho_1 = p_0(V_1 + V_2)\rho_1, \tag{3}$$

where V_1 and V_2 = equilibrium volumes of the high and low pressure sides of the mercury towers respectively in cubic centimetres,

A_0 = cross-sectional area of the towers in square centimetres,

$\rho_1 = \rho/p$ = density of the gas at unit pressure, and

p_0 = equilibrium pressure in centimetres of mercury.

Rearranging Equation (3),

$$p_1V_1 + p_2V_2 + (p_1 - p_2)A_0h/2 = p_0(V_1 + V_2).$$

Eliminating p_2 by substituting from Equation (2),

$$p_1(V_1 + V_2) - V_2h + A_0h^2/2 = p_0(V_1 + V_2),$$

and therefore,

$$p_1 = p_0 + \left(\frac{h}{V_1 + V_2}\right)\left(V_2 - \frac{A_0h}{2}\right). \tag{4}$$

Similarly, eliminating p_1,

$$p_2 = p_0 - \left(\frac{h}{V_1 + V_2}\right)\left(V_1 + \frac{A_0h}{2}\right). \tag{5}$$

The mass of gas entering the bed per second at any moment is equal to the rate of change of the mass of gas in the high pressure tower, which is:

$$G = -\frac{d}{dt}[p_1(V_1 + A_0h/2)\rho_1],$$

where G = rate of gas flow in grams per second.

Substituting for p_1 from Equation (4),

$$G = -\frac{d}{dt}\left[(V_1 + A_0h/2)\left\{p_0 + \left(\frac{h}{V_1 + V_2}\right)(V_2 - A_0h/2)\right\}\rho_1\right],$$

which on differentiation becomes

$$G = -\rho_1\left[\frac{A_0p_0}{2} + \frac{V_1V_2}{V_1 + V_2} - \frac{A_0(V_1 - V_2)h}{V_1 + V_2} - \frac{3A_0^2h^2}{4(V_1 + V_2)}\right]\frac{dh}{dt}. \tag{6}$$

Equation (6) has been used for all the calculations of gas flow reported in this paper. The equilibrium volumes, V_1 and V_2, were determined by the

expansion of known volumes of air in the apparatus and the use of Boyle's law, and the cross-sectional area of the towers was determined by liquid displacement.

If v_1 is the volume of gas entering the bed per second, and v_2 is the volume of gas leaving the bed per second, and the flow of gas is assumed to be governed by the Poiseuille equation, then

$$p_1v_1 = p_2v_2 = \frac{(p_1 + p_2)}{2}(p_1 - p_2)X, \tag{7}$$

where X = a constant for any particular bed of powder, and is analogous to the constant $\pi\rho_{H_2}gr^4/8\eta L$ in the Poiseuille equation for the flow of a compressible fluid through a capillary tube.

The mass of gas entering the bed per second may also be represented by $p_1v_1\rho_1$, and therefore

$$G = p_1v_1\rho_1 = \frac{(p_1 + p_2)}{2}(p_1 - p_2)X\rho_1.$$

Substituting for p_1 and p_2 from Equations (4) and (5) and combining with Equation (6), the following equation is obtained:

$$\left[p_0 - \frac{(V_1 - V_2)h}{2(V_1 + V_2)} - \frac{A_0h^2}{2(V_1 + V_2)}\right]hX = -\left[\frac{A_0p_0}{2} + \frac{V_1V_2}{V_1 + V_2} - \frac{A_0(V_1 - V_2)h}{V_1 + V_2} - \frac{3A_0^2h^2}{4(V_1 + V_2)}\right]\frac{dh}{dt}.$$

Rearranging and integrating

$$X\int_{t_1}^{t_2} dt = -\int_{h_1}^{h_2} \frac{\frac{A_0p_0}{2} + \frac{V_1V_2}{V_1 + V_2} - \frac{A_0(V_1 - V_2)h}{V_1 + V_2} - \frac{3A_0^2h^2}{4(V_1 + V_2)}}{p_0 - \frac{(V_1 - V_2)h}{2(V_1 + V_2)} - \frac{A_0h^2}{2(V_1 + V_2)}} \cdot \frac{dh}{h}.$$

The right-hand side can be integrated by factoring in the form:

$$[Xt]_{t_1}^{t_2} = -\int_{h_1}^{h_2}\frac{B}{h}dh - \int_{h_1}^{h_2}\frac{Ch + D}{p_0 - \frac{(V_1 - V_2)h}{2(V_1 + V_2)} - \frac{A_0h^2}{2(V_1 + V_2)}}dh,$$

where B, C, and D are constants and have the values:

$$B = \frac{A_0}{2} + \frac{V_1V_2}{(V_1 + V_2)p_0},$$

$$C = \frac{A_0V_1V_2}{(V_1 + V_2)^2p_0} - \frac{A_0^2}{2(V_1 + V_2)}, \text{ and}$$

$$D = \frac{V_1V_2(V_1 - V_2)}{2(V_1 + V_2)^2p_0} - \frac{3A_0(V_1 - V_2)}{4(V_1 + V_2)}.$$

Evaluation of these integrals and collection of terms leads to the following relation between the pressure head and the time:

$$[Xt]_{t_1}^{t_2} = \left[\left\{\frac{A_0}{2} + \frac{V_1V_2}{(V_1 + V_2)p_0}\right\} \ln h - \left\{\frac{V_1V_2}{(V_1 + V_2)p_0} - \frac{A_0}{2}\right\} \ln \left\{p_0 - \frac{(V_1 - V_2)h}{2(V_1 + V_2)} - \frac{A_0h^2}{2(V_1 + V_2)}\right\} - \frac{A_0(V_1 - V_2)}{\sqrt{(V_1 - V_2)^2 + 8A_0p_0(V_1 + V_2)}} \ln \frac{2A_0h + (V_1 - V_2) + \sqrt{(V_1 - V_2)^2 + 8A_0p_0(V_1 + V_2)}}{2A_0h + (V_1 - V_2) - \sqrt{(V_1 - V_2)^2 + 8A_0p_0(V_1 + V_2)}}\right]_{h_2}^{h_1} \quad (8)$$

For all practical purposes, it was found that the second and third terms in the expression on the right-hand side of Equation (8) were sufficiently small in the region between $h = 5$ cm. and $h = 10$ cm. for the apparatus used, that they could be neglected and Equation (8) written:

$$[Xt]_{t_1}^{t_2} = \left[\left\{\frac{A_0}{2} + \frac{V_1V_2}{(V_1 + V_2)p_0}\right\} \ln h\right]_{h_2}^{h_1}. \quad (9)$$

With beds of very fine powders, such as were used in these experiments, the simple Poiseuille equation is no longer valid and a second term must be introduced to account for 'slip'. In the previous paper of this series (3), this matter was discussed and the simple Poiseuille equation was replaced by:

$$G = \frac{(p_1 + p_2)}{2}(p_1 - p_2)X\rho_1 + (p_1 - p_2)Y\rho_1 = p_1v_1\rho_1, \quad (10)$$

where Y = a constant for any particular bed of powder and is analogous to the Knudsen flow equation constant, $\frac{4}{3}\sqrt{2\pi}\sqrt{\frac{R_0T}{M}}\frac{r^3}{L}$.

Equation (10) can be combined with Equation (6) and integrated in the same manner as above with Equation (7). This yields a more complicated result than Equation (8), but one having the same form. Again for all practical purposes, two terms on the right-hand side may be neglected for the apparatus used here, and the final simplified form is:

$$[t]_{t_1}^{t_2} = \left[\left\{\frac{\frac{A_0p_0}{2} + \frac{V_1V_2}{V_1 + V_2}}{p_0X + Y}\right\} \ln h\right]_{h_2}^{h_1}. \quad (11)$$

When Y becomes very small, Equation (11) reduces to Equation (9).

This equation can be readily checked against the flow of air through calibrated capillary tubes.

Test of the Decay Apparatus Theory

Before any permeability measurements were made on beds of powder, the theory presented in the previous section was checked with three capillary tubes. Two of these capillary tubes consisted of thermometer tubing, while the third was a piece of fine Pyrex capillary tubing. The tubes had the following characteristics:

Type of tubing	Radius, cm.	Length, cm.
−50° C. to 50° C. alcohol thermometer	0.0311	25.4
Pyrex capillary tubing	0.0229	26.5
−10° C. to 110° C. thermometer	0.00816	20.0

With the apparatus filled with air, the capillary tube under test was mounted with suitable adapters across the top of the two mercury towers, B, and, after evacuating the left-hand tower, the air was allowed to flow through the capillary until equilibrium was attained. As the air was flowing through the capillary, the level of the mercury in the left-hand tower was periodically read on a cathetometer and the time of each reading noted on a stopwatch having two second hands for interval timing. From a knowledge of the cathetometer reading of the mercury level at equilibrium, it was possible to evaluate the pressure head corresponding to any reading of the mercury level in the left-hand tower, since a calibration showed that the cross-sectional areas of the two towers were sufficiently uniform that the expected linear relation between the pressure head and the reading of the mercury level in the left-hand tower held over the entire working range.

Fifteen runs were made with the alcohol thermometer capillary over an equilibrium pressure (p_0) range of 0.9 to 20 cm. of mercury, six runs were made with the other thermometer capillary over an equilibrium pressure range of 14 to 64 cm. of mercury, and 11 runs were made with the Pyrex capillary tubing over an equilibrium pressure range of 0.5 to 26 cm. of mercury.

In all cases, when the logarithm of the pressure head was plotted against time, a straight line was obtained, which was considered sufficient justification for the use of Equations (9) and (11) above. Further, when the rates of gas flow in grams per second were calculated using Equation (6) for pressure heads of 1, 5, and 10 cm. of mercury, where such calculations were possible, and plotted against the corresponding mean pressures, $(p_1 + p_2)/2$, calculated from Equations (4) and (5), straight lines were obtained, which almost passed through the origin. This was as expected, since the correction for 'slip' in the Poiseuille equation is very small when applied to tubes of these radii.

As little is to be gained by reproducing all the data obtained with the capillary tubes, only data applying to the Pyrex capillary tubing is presented here.

Typical lines obtained when the logarithm of the pressure head was plotted against the time are shown in Fig. 2. It is possible to calculate the slopes of these lines from Equation (11) by introducing the necessary apparatus constants. The equilibrium volumes, V_1 and V_2, of the apparatus, with the capillary tube adapters in place, were determined by inserting a solid glass rod in place of a capillary tube between the two adapters and observing the pressure change inside one half of the apparatus, when the mercury level was changed by varying the pressure in the other half. The accompanying volume change was calculated from the change in the mercury level and the cross-sectional area of the tower* being calibrated. The equilibrium volume was then cal-

* *The two tubes that were used for the two towers were calibrated before the apparatus was built and were found to have an average cross-sectional area of 3.99 sq. cm. over the working length.*

culated by means of Boyle's law. The equilibrium volumes were found to be: $V_1 = 233$ cc. and $V_2 = 265$ cc.

Introducing the Poiseuille and Knudsen flow equation constants in Equation (11) and letting $\delta = 0.9$, as recommended by Adzumi (1), the equation becomes:

$$[t]_{h_1}^{h_2} = \left[\left\{ \frac{\frac{A_0 p_0}{2} + \frac{V_1 V_2}{V_1 + V_2}}{\left(\frac{\pi r^4}{8\eta L} p_0 \rho_{Hg} g + 0.9 \times \frac{4}{3} \sqrt{2\pi} \sqrt{\frac{R_0 T}{M}} \frac{r^3}{L} \right)} \right\} \ln h \right]_{h_2}^{h_1}, \quad (12)$$

where r = radius of the capillary tube in centimetres. The term $\rho_{Hg} g$ has been introduced into the denominator above to permit the use of centimetres of mercury as the unit of pressure head.

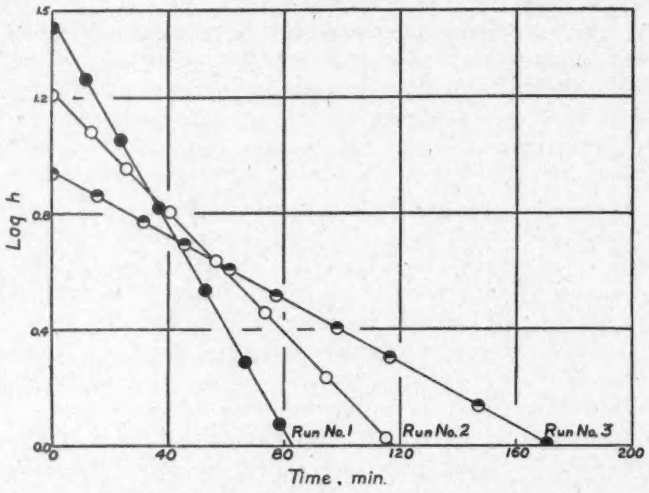

FIG. 2. *Logarithm of pressure head plotted against time. Abscissa—Time, min. Ordinate—log h.*

Rearranging Equation (12), it can be written:

$$\ln h = Kt + \ln h_0, \quad (13)$$

where $1/K$ = the expression in the brace $\{\}$ in Equation (12), and
h_0 = pressure head at time $t = 0$.

From this it can be seen that the slopes obtained from the graphs of the logarithm of the pressure head versus the time should be given by the reciprocal of the expression in the brace in Equation (12). The calculated values of the slopes are listed with the experimental values in Table I, together with the rates of air flow in grams per second at a pressure head of 1.0 cm., calculated by means of Equation (6).

TABLE I

FLOW OF AIR THROUGH PYREX CAPILLARY TUBE

Run No.	Equilibrium pressure, p_0, cm. Hg.	Slope of ln h vs. t		Flow at h = 1 cm. G, gm./sec.	Mean pressure at h = 1 cm., $\bar{P}$, cm. Hg
		Observed	Calculated		
11	25.72	0.0431	0.0435	11.92×10^{-5}	25.78
1	23.72	0.0411	0.0414	11.20	23.78
2	11.50	0.0239	0.0236	5.59	11.56
6	6.54	0.0141	0.0144	3.05	6.60
3	5.65	0.0126	0.0127	2.72	5.71
7	3.15	0.00749	0.00741	1.54	3.21
4	2.75	0.00666	0.00661	1.37	2.81
8	1.58	0.00397	0.00396	0.79_7	1.64
5	1.37	0.00349	0.00352	0.70_5	1.43
9	0.76	0.00207	0.00210	0.40_9	0.82
10	0.49	0.00146	0.00147	0.28_9	0.55

The relation between the rate of air flow, G, and the mean pressure, $\bar{P}$, is given by Equation (10), which may be rewritten with the capillary tube constants as:

$$G = \frac{\pi r^4}{8\eta L} h\rho_{Hg} g \rho_1 \bar{P} + 0.9 \times \frac{4}{3}\sqrt{2\pi}\sqrt{\frac{R_0 T}{M}}\frac{r^3}{L} h\rho_1 . \qquad (14)$$

Substituting for the various constants in Equation (14), the equation for the rate of air flow through the Pyrex capillary tube is found to be:

$$G = 4.74 \times 10^{-6} h\bar{P} + 6.33 \times 10^{-7} h. \qquad (15)$$

The values of G from Table I are shown plotted against the mean pressure in Fig. 3, together with the line given by Equation (15).

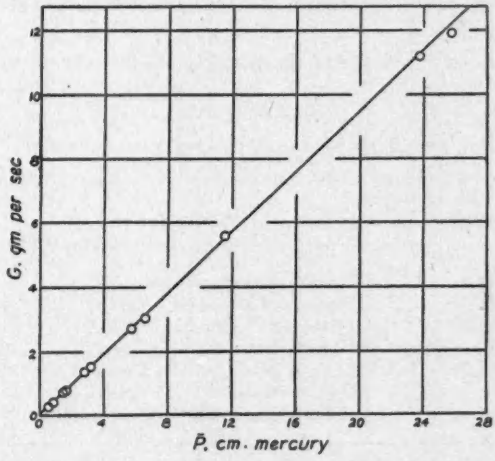

FIG. 3. *Rate of mass flow plotted against mean pressure. Abscissa—$\bar{P}$ (centimetres of mercury). Ordinate—G (grams per second).*

From the results of these experiments, the equations developed for use with the decay apparatus appeared to be valid and the permeabilities of beds of fine powders were then investigated.

Experimental Results

Decay curves were obtained on beds of finely ground quartz and a number of inorganic pigments over as wide a range of porosities as was feasible. The limiting values of porosity were governed by the minimum amount of powder that would form a solid bed and withstand a full atmosphere pressure difference across its length at high porosities, and by the maximum amount of powder that could be compressed into the required length using the small hand press at low porosities. In general, the decay curves were determined at five different mean pressures, all below atmospheric pressure, on each bed and further runs were made only when there appeared to be some discrepancy in the data.

From the decay curves, the rates of mass flow, G, were calculated using the Equation (6) for pressure heads of 5 and 10 cm. of mercury and these values were then plotted against the corresponding mean pressures $\overline{P}$. These plots all proved to be straight lines and could be expressed by an equation of the form:

$$G = \frac{Ah}{L}(B\overline{P} + C) . \qquad (16)$$

The runs were all made at room temperature (20° to 25° C.), as it was found that the temperature seldom varied by more than 1° C. during the runs on any one bed, and the constants B and C of Equation (16) were all reduced to 20° C. to permit direct comparison between the different beds and powders studied.

The pertinent data for each of the powders studied are listed in Table II.

TABLE II

DATA ON THE POWDERS USED FOR PERMEABILITY STUDIES

Kind of powder	Source	Density, gm./cc.[1]
Finely ground quartz	Laboratory preparation	2.65
Mapico Red No. 297	Binney and Smith, New York	5.18
Mapico Yellow Lemon	Binney and Smith, New York	3.82
Hydrated yellow iron oxide	C. K. Williams and Co., Easton, Pa.	4.0
Hydrated chromic oxide	C. K. Williams and Co., Easton, Pa.	3.12
Pure red iron oxide	C. K. Williams and Co., Easton, Pa.	5.15
Pure chromic oxide	C. K. Williams and Co., Easton, Pa.	5.2

[1] *Except for the powdered quartz, the values of the densities of the powders were all supplied by the manufacturers.*

The values of the apparatus constants that are needed for the calculation of the rate of mass flow and the porosity of the bed are given in Table III.

TABLE III

CONSTANTS OF THE DECAY APPARATUS

Area of the permeability cell, sq. cm.	0.243
Length of the bed of powder, cm.	1.00
Area of the mercury towers, B, sq. cm.	3.99
Equilibrium volume (with adapter), V_1, cc.	234.5
Equilibrium volume (with adapter), V_2, cc.	268.5

In Table IV are listed the constants B and C of Equation (16) and the porosities for the various beds studied.

TABLE IV

SUMMARY OF EXPERIMENTAL DATA

Porosity	Constants—Equation (16) at 20° C.	
	B	C
Powdered Quartz		
0.610	4.09×10^{-6}	4.16×10^{-6}
0.621	6.53	5.02
0.604	4.18	3.68
0.584	3.35	3.32
0.619	4.31	4.17
0.585	2.97	3.13
0.528	1.51	2.29
0.514	1.47	2.11
0.498	1.05	1.83
0.439	0.85	1.55
0.537	2.16	2.76
0.428	0.63	1.32
0.517	1.45	2.15
0.545	2.21	2.80
0.475	1.41	2.10
0.510	1.24	1.99
0.425	0.60	1.23
0.475	1.03	1.66
0.563	3.54	3.63
Mapico Red No. 297		
0.766	11.81×10^{-6}	3.48×10^{-6}
0.752	14.08	2.80
0.718	7.60	2.29
0.692	4.25	1.88
0.677	4.24	1.99
0.721	6.81	2.31
0.636	2.05	1.54

TABLE IV—*Concluded*

SUMMARY OF EXPERIMENTAL DATA—*Concluded*

Porosity	Constants—Equation (16) at 20° C.	
	B	*C*
Mapico Yellow Lemon		
0.807	7.05×10^{-6}	8.33×10^{-6}
0.780	3.01	5.72
0.754	2.77	4.88
0.767	2.54	4.83
0.704	1.37	3.35
0.700	1.08	2.81
0.676	0.95	2.60
Hydrated yellow iron oxide		
0.778	2.68×10^{-6}	4.08×10^{-6}
0.771	1.99	3.99
0.781	2.91	5.04
0.747	1.72	3.75
0.721	0.89	2.63
0.702	0.77	2.64
Hydrated chromic oxide		
0.682	6.36×10^{-9}	1.20×10^{-6}
0.664	7.26	1.24
0.656	4.07	0.80
0.711	38.85	3.30
0.706	26.85	2.52
0.691	15.51	1.92
Pure red iron oxide		
0.552	12.80×10^{-9}	2.15×10^{-6}
0.583	21.53	2.80
0.491	4.90	1.32
0.479	5.98	1.50
0.568	20.43	2.93
0.543	11.15	1.93
Pure chromic oxide		
0.526	26.8×10^{-9}	1.85×10^{-6}
0.464	3.53	1.08
0.521	23.5	1.91
0.487	7.27	1.28
0.493	5.64	1.49

Discussion

In the derivation of Equation (1), which has been given in the preceding paper of this series (3), the fraction effective void area, α, was introduced only into the term corresponding to Knudsen-type flow, and the part of the equation including the original Kozeny equation was left in its original form. The derivation of the original Kozeny equation contains a substitution of v/ϵ for v_0, where v is the approach velocity of the fluid and v_0 the mean velocity of the fluid in the bed. As the fraction effective void area, α, is generally smaller than the fraction void volume, ϵ, the v/ϵ term should be replaced by v/α in the above-mentioned substitution. This change would result in α being introduced in place of an ϵ in the first term of the right-hand side of the modified equation (Equation (1)) with a corresponding change in the shape factor k. As $G = Q\overline{P}\rho_1$, it is possible to rewrite Equation (1) with these modifications in terms of mass flow G as:

$$G = \frac{Ah\epsilon\alpha\rho_1}{LS_v(1-\epsilon)}\left[\frac{\epsilon\rho_{H_0}g\overline{P}}{k_0\eta S_v(1-\epsilon)} + \delta \times \frac{8}{3}\sqrt{\frac{2}{\pi}}\sqrt{\frac{R_0T}{M}}\right], \tag{17}$$

where k_0 = a new shape factor.

It has already been pointed out that the experimental data can be represented by the equation:

$$G = \frac{Ah}{L}(B\overline{P} + C), \tag{16}$$

where B and C are constants.

From a comparison of Equations (16) and (17), the following relations are obtained:

$$B = \frac{\rho_{H_0}g\epsilon^2\alpha\rho_1}{k_0\eta S_v^2(1-\epsilon)^2}, \tag{18}$$

and

$$C = \frac{8}{3}\sqrt{\frac{2}{\pi}}\sqrt{\frac{R_0T}{M}}\,\frac{\delta\epsilon\alpha\rho_1}{S_v(1-\epsilon)}. \tag{19}$$

An expression for the specific surface, S_v, in terms of ϵ and α can be obtained by rearranging Equation (19) to give:

$$S_v = \frac{8}{3}\sqrt{\frac{2}{\pi}}\sqrt{\frac{R_0T}{M}}\,\frac{\delta\epsilon\alpha\rho_1}{C(1-\epsilon)}. \tag{20}$$

It is possible to evaluate S_v using Equation (20), provided that the value of α, the effective void area, is known. It appears to be very difficult to measure α experimentally and little is known of its nature as a function of the porosity, although Furnas (6) has pointed out that α generally has a value of 0.1 to 0.2 when ϵ is 0.4 to 0.6. In the previous paper of this series (3), an empirical relation between α and ϵ was found to be satisfactory for the data under consideration and it can also be used here. This relation is:

$$\log \alpha = 1.41\epsilon - 1.40. \tag{21}$$

The values of S_v, calculated from the experimental data given in Table IV by means of Equations (20) and (21), are listed in Table V.

With a knowledge of the values of S_v for the different powders, it is now possible to determine the values of the shape factor, k_0, from Equation (18). The values obtained for k_0 from the experimental data in Table IV are listed in Table V.

TABLE V

VALUES OF THE SPECIFIC SURFACE, THE SHAPE FACTOR, AND THE ADZUMI PORE RADIUS CALCULATED FROM THE EXPERIMENTAL DATA

Porosity	Specific surface, S_v, sq. cm./cc.	Shape factor, k_0	Pore radius, R, cm.
Powdered quartz			
0.610	1.1×10^5	2.4	2.98×10^{-5}
0.621	0.9	1.7	3.94
0.604	1.0	2.2	3.44
0.584	1.0	2.2	3.07
0.619	1.0	2.6	3.14
0.585	1.1	2.5	2.88
0.528	1.0	2.6	2.00
0.514	0.9	2.3	2.11
0.498	1.0	2.7	1.74
0.439	0.7	1.7	1.65
0.537	0.9	2.0	2.38
0.428	0.8	2.0	1.45
0.517	0.9	2.4	2.05
0.545	0.9	2.1	2.39
0.475	0.7	1.5	2.04
0.510	1.0	2.6	1.88
0.425	0.9	2.1	1.48
0.475	0.9	2.1	1.88
0.563	0.8	1.6	2.96
	$0.9_1 \times 10^5$	2.2	
Mapico Red No. 297			
0.766	4.0×10^5	3.4	1.03×10^{-5}
0.752	4.4	2.3	1.52
0.718	4.0	2.7	1.01
0.692	4.0	3.5	0.69
0.677	3.4	2.9	0.65
0.721	4.1	3.2	0.89
0.636	3.2	3.7	0.40
	$3.8_7 \times 10^5$	3.1	
Mapico Yellow Lemon			
0.807	2.4×10^5	2.3	2.56×10^{-5}
0.780	2.8	3.5	1.59
0.754	2.6	2.6	1.72
0.767	2.9	3.4	1.59
0.704	2.4	2.7	1.24
0.700	2.9	3.3	1.16
0.676	2.5	2.7	1.11
	$2.6_4 \times 10^5$	2.9	

TABLE V—*Concluded*

VALUES OF THE SPECIFIC SURFACE, THE SHAPE FACTOR, AND THE ADZUMI PORE RADIUS CALCULATED FROM THE EXPERIMENTAL DATA—*Concluded*

Porosity	Specific surface, S_v, sq. cm./cc.	Shape factor, k_0	Pore radius, R, cm.
Hydrated yellow iron oxide			
0.778	3.8×10^5	2.4	1.99×10^{-5}
0.771	3.3	2.4	1.51
0.781	3.2	2.3	1.75
0.747	3.2	2.4	1.39
0.721	3.6	3.2	1.02
0.702	3.1	2.9	0.88
	$3.3_5 \times 10^5$	2.6	
Hydrated chromic oxide			
0.682	5.8×10^5	—	1.60×10^{-5}
0.664	4.9	—	1.78
0.656	7.1	—	1.55
0.711	2.7	—	3.56
0.706	3.3	—	3.23
0.691	3.9	—	2.42
	4.6×10^5		
Pure red iron oxide			
0.552	1.2×10^5	2.5	1.80×10^{-5}
0.583	1.2	2.1	2.33
0.491	1.3	3.3	1.12
0.479	1.0	2.4	1.21
0.568	1.0	1.9	2.11
0.543	1.2	2.6	1.75
	$1.1_4 \times 10^5$	2.5	
Pure chromic oxide			
0.526	1.1×10^5	0.9	4.41×10^{-5}
0.464	1.3	3.4	1.00
0.521	1.1	1.0	3.72
0.487	1.3	2.1	1.72
0.493	1.1	2.9	1.15
	$1.1_6 \times 10^5$	2.1	

From Table V it can be seen that the values of the specific surface for any given powder show a maximum deviation of about $\pm 10\%$, which is the maximum error suggested by previous workers for specific surface measurements on coarse granules. The one exception in Table V is hydrated chromic oxide, which shows no consistent value for the specific surface. From electron microscope photographs, this powder appears to be extremely heterogeneous

and to have no definite form. It is therefore quite possible that some deformation of the particles occurred during the packing of the beds and that the resultant beds were of variable porosity throughout their length, which would render the values of the over-all porosity meaningless.

The average values of the shape factor vary from 2.2 to 3.1 for the different powders and appear to be of the right order of magnitude. In the original Kozeny equation, the shape factor, k, was taken as a constant equal to 5, but with the replacement of an ϵ by an α in the modified equation, the corresponding new shape factor, k_0, varies from 1.8 at $\epsilon = 0.4$ to 3.5 at $\epsilon = 0.8$. It is also interesting to note that with most of the powders studied, the values of the shape factor for any given powder in Table V show a decrease with increasing porosity. As Carman (4) has pointed out, the shape factor embodies a term which relates the actual length of the conduits through the bed with the over-all length of the bed and which he considers to be a factor of about $\sqrt{2}$. It seems reasonable to assume that, as the porosity of a bed of powder increases, the ratio of the length of the conduits to the length of the bed would decrease and thus cause a decrease in the value of the shape factor, similar to that found experimentally.

A further comparison between Equation (17) and the equation put forward by Adzumi (2) is of particular interest. The Adzumi equation may be written as:

$$G = \frac{Ah\rho_1}{L}\left[\frac{\pi\rho_{H_0}gE_0\bar{P}}{8\eta} + \frac{4}{3}\sqrt{2\pi}\sqrt{\frac{R_0T}{M}}\,\delta F_0\right], \tag{22}$$

where E_0 and F_0 are constants for any given bed of porous media. Adzumi considered the significance of the constants E_0 and F_0 and concluded that the average radius of the pores (R) in a porous bed was given by the ratio E_0/F_0. Evaluating the values of E_0 and F_0 in terms of Equation (17) and working out the ratio E_0/F_0, the following expression is obtained for the Adzumi pore radius:

$$R = \frac{4\epsilon}{k_0(1-\epsilon)S_v}. \tag{23}$$

If the shape factor, k_0, has a value of 4 in Equation (23), the equation reduces to the definition of hydraulic radius, which forms the basis of both the original Kozeny equation and the modified equation being considered here. The value of the shape factor, as discussed above, appears to vary from 2 to 4 over the normal working range of porosities, and it therefore seems reasonable to conclude that the average pore radius arrived at by Adzumi by a method of summation applied to a system considered to be composed of a large number of fine circular capillaries, connected both in parallel and series, is practically the same as the hydraulic radius.

The value of the Adzumi pore radius in terms of the experimental data is useful for purposes of calculation and may be obtained from a comparison of Equations (16) and (22). This leads to the result:

$$R = \frac{32}{3}\sqrt{\frac{2}{\pi}}\sqrt{\frac{R_0T}{M}}\,\frac{\delta B\eta}{\rho_{H_0}gC}. \tag{24}$$

The values of the Adzumi pore radius calculated from Equation (24) using the data in Table IV are listed in Table V.

In order to check the calculated specific surface of several of the powders, a series of electron microscope photographs were taken of dispersions of two of the powders at a magnification of approximately 17,000×. The plates were examined under a visual enlarger, which gave a final magnification of about 130,000×. The diameters of the particles on a number of plates were measured across their horizontal axes, and the distributions of the particle diameters obtained are summarized in Table VI.

TABLE VI

DISTRIBUTION OF PARTICLE DIAMETERS OF TWO OF THE POWDERS STUDIED

Size range		Number of particles	
		Mapico Red	Yellow iron oxide
Less than 0.05μ		5	58
Between 0.05 and 0.10μ		37	57
0.10	0.15	58	24
0.15	0.20	31	26
0.20	0.25	4	24
0.25	0.30		14
0.30	0.35		15
0.35	0.40		19
0.40	0.45		13
0.45	0.50		6
0.5	0.6		7
0.6	0.7		4
0.7	0.8		6
0.8	0.9		1
0.9	1.0		4
	Total	135	278

Fair and Hatch (5) quote an expression for calculating the specific surface from a particle distribution, such as those above. This expression may be written:

$$S_v = K \frac{\Sigma nd^2}{\Sigma nd^3}, \tag{25}$$

where K is a shape factor depending on the form of the particles and varies from 6.0 for spheres to 7.7 for angular particles.

Equation (25) can be applied to the data in Table VI after a consideration of the particle shapes. From the electron microscope photographs, the Mapico Red particles are nearly spherical and appear to have smooth surfaces. These particles would be considered Rounded in the Fair and Hatch nomenclature and K would equal 6.1. The yellow iron oxide is in the form of needles, which appear on the average to be about eight times as long as they are wide. Fair and Hatch make no provision for particles of this shape, but an estimate of the shape factor can easily be made for different needle-like

shapes by comparing the surface of the shape under consideration with that of a sphere of equal volume and multiplying by 6, since the surface–volume ratio of a sphere is equal to 6 divided by the diameter of the sphere. Applying this method, the following shape factors are obtained for various figures having a length–width ratio of 8:

Shape of figure	Shape factor
Tetragonal prism	10.4
Triangular prism	13.4
Regular pyramid (octahedron)	21.3

From the shape of the yellow iron oxide crystals, which tend to be tapered towards the ends, it seems reasonable to assume a shape factor of 16 to 18 for K.

Substituting these values of the shape factor in Equation (25), together with the calculated sums of the squares and cubes of the diameters from Table VI, the specific surface of Mapico Red is found to be 4.1×10^5 sq. cm. per cc. and of the yellow iron oxide to be 2.9 to 3.3×10^5 sq. cm. per cc., both of which are in excellent agreement with the average values calculated from the permeability data (Table V).

It would appear that this method of measuring the specific surface of fine powders, which are too fine to be counted under an ordinary microscope and also too fine for measurements using the standard sedimentation methods, is reliable to within $\pm 10\%$. The greatest error with the method appears to lie in the packing of the bed, as slight changes in porosity through the bed are magnified in the values of the specific surface. Even though all the beds studied were packed in small increments, it was almost impossible to apply the same pressure to each increment during the packing with the small hand press used. If this could be done, it is quite possible that the error involved in the measurements would be appreciably reduced.

As the specific surface is calculated from the intercept of the mass flow equation (Equations (16) and (20)), which corresponds to the contribution that Knudsen-type flow makes to the total flow, it is very likely that the low pressure region, where the entire flow is of the Knudsen type, would be the most satisfactory for measurements of specific surface, if a suitable apparatus was used for the measurements.

Acknowledgments

The author would like to express his thanks to Dr. W. M. Barss, Physics Division, National Research Council of Canada, for supplying the pigment samples and for the electron microscope photography; to former Lieut. G. O. Henneberry for assisting in the construction of the apparatus and for making some of the early measurements; and to Mr. J. W. McWade for assisting in some of the latter experimental work.

References

1. ADZUMI, H. Bull. Chem. Soc. Japan, 12 : 292-303. 1937.
2. ADZUMI, H. Bull. Chem. Soc. Japan, 12 : 304-312. 1937.
3. ARNELL, J. C. Can. J. Research, A, 24 : 103-116. 1946.
4. CARMAN, P. C. Trans. Inst. Chem. Engrs. London, 15 : 150-166. 1937.
5. FAIR, G. M. and HATCH, L. P. J. Am. Water Works Assoc. 25 : 1551-1565. 1933.
6. FURNAS, C. C. Flow of gases through beds of broken solids. U.S. Department of Commerce, Bureau of Mines Bull. 307. 1929.
7. HODGINS, J. W., FLOOD, E. A., and DACEY, J. R. Can. J. Research, B, 24 : 167-177. 1946.
8. PECHUKAS, A. and GAGE, F. W. Ind. Eng. Chem., Anal. Ed. 18 : 370-373. 1946.
9. RIGDEN, P. J. J. Soc. Chem. Ind. 62 : 1T-4T. 1943.

ERRATA

PERMEABILITY STUDIES. I. Surface Area Measurements Using A Modified Kozeny Equation. By J. C. Arnell. Can. J. Research, A, 24 : 103-116. November, 1946.

Page 104. Equation (3) should read:

$$Q = \frac{h\rho g A}{5S_v^2\eta L} \cdot \frac{\epsilon^3}{(1-\epsilon)^2} \tag{3}$$

Page 105. Line 8 should read:

. . . a constriction may have the . . .

Page 108. Equation (16) should read:

$$Q = \frac{\pi(p_1 - p_2)}{8L}\left[\frac{R^4}{\eta} + \frac{1 + c_1 p}{1 + c_2 p}\frac{32}{3\pi}\sqrt{2\pi}\sqrt{\frac{R_0 T}{M}}\frac{R^3}{p}\right] \tag{16}$$

Equation (17) should read:

$$Q = \frac{\pi(p_1 - p_2)E}{8\eta} + \gamma\frac{4}{3}\sqrt{2\pi}\sqrt{\frac{R_0 T}{M}}\frac{(p_1 - p_2)F}{p} \tag{17}$$

THE GAMMA-RAY MEASUREMENT OF RADIUM ORE CONCENTRATES[1]

By W. J. Hushley[2] and W. R. Dixon[2]

Abstract

A method is described for measuring the radium content of substances in which the radium concentration is of the order of micrograms per gram of material. The gamma-ray activities of the unknown material and of a standard radium capsule are compared by means of Geiger-Müller counters. Corrections for self-absorption and distance are given for rectangular and cylindrical sources. The effect of radiation scattered by the source into the detector is discussed. Synthetic bulk sources made up with known quantities of radium were used for the experimental work.

Introduction

In order to measure a quantity of radium by comparing its gamma-radiation with that of a known standard, it is necessary to correct for the absorption of radiation in the radium-bearing material and its container. Several authors (2–7) have described methods of obtaining absorption corrections in the measurement of radium salts. In these methods the container is usually a cylinder less than a centimetre in diameter, and the radiation is measured in a direction from the cylinder that is at right angles to its axis. The total absorption correction may be a few per cent, most of which is due to the container, and the expected accuracy in the radium content is about 0.1%. The absorption coefficients must be obtained by measurements on other similar salts and containers.

It was the purpose of the present investigation to determine whether such techniques are applicable to the measurement of radium ore concentrates in which the radium concentration is of the order of micrograms per gram, and is to be determined to within 1%. In order to obtain a radiation intensity convenient to measure, a few hundred grams of the material is required. In comparing such bulk sources with the usual radium standards, absorption corrections as high as 30% may be necessary. Since the samples to be measured may vary considerably in density, size, and composition it might be thought desirable to measure the absorption coefficient of each independently rather than use predetermined coefficients. It was found, however, that over the range of densities and of sizes of containers studied, the measured value of the absorption coefficient usually gives a value of the absorption correction that is too high. The error for large sources is about 1% or greater and is believed to be due to radiation scattered from other parts of the bulk source into the detector. Thus in using this method for the determination of the

[1] *Manuscript received in original form October 29, 1946, and, as revised, April 2, 1947. Contribution from the Division of Physics, National Research Laboratories, Ottawa, Canada. Issued as N.R.C. No. 1563.*

[2] *Physicist.*

radium content it is desirable to have the source of a size for which the appropriate mass absorption coefficient is known or for which it is known that the measured value will give the proper correction.

Form of Corrections

The accuracy of radium content determinations depends mostly upon the accuracy of the absorption corrections, since other sources of error may be largely eliminated. For bulk sources the correction for absorption in the radium-bearing material is much larger than the correction for absorption in the container; the latter correction may be made small by using a thin-walled container. For purposes of calculation it is assumed that the radium is uniformly distributed throughout the material in a container, that all the gamma-radiation is due to radium in equilibrium with its products of disintegration, and that the measured radiation is essentially homogeneous. It is also assumed that the distance between the source and the detector is several times larger than the maximum dimension of either the source or the detector, in order that corrections due to the finite extent of source and detector shall be small.

Cylindrical containers were used throughout as they were more readily obtained than those of other shapes. However, it is more convenient to measure the absorption coefficient and to calculate the absorption correction in an object having a rectangular cross-section. If a cylinder is placed with its axis in the line joining the source and the detector it will be referred to as a rectangular source; while if it is placed with its axis at right angles to the source–detector axis it will be referred to as a cylindrical source.

Radiation from a Rectangular Source

Referring to Figs. 1(*a*) and 1(*b*), consider a source whose cross-section is rectangular in the plane passing through both the source and the detector.

Let L_c = distance from the centre of the source to the detector G,
L_f = distance from the front face of the source to the detector G,
h = length of source in the direction of the detector,
μ = linear absorption coefficient of the source.

To calculate the correction due only to absorption in the source, consider the radiation from an element of thickness dx at a distance x from the origin 0 and integrate for the intensity over the length of the source. Then the ratio of the intensity received at G with absorption to the intensity with no absorption in the source is

$$1/P = (1/\mu h)\,(1 - e^{-\mu h}), \qquad (1)$$

where P is the factor by which a measured radiation equivalent must be multiplied to correct it for absorption in the source. A source is said to be the radiation equivalent of a given quantity of radium, at the same or a given distance, if the intensity of its gamma-radiation is the same as that of the radium, provided there is no absorption of the radiation in the reference source

of radium or in its container. Expression (1) applies to both Figs. 1(*a*) and 1(*b*) and in effect replaces the bulk source with an equivalent surface source at the origin.

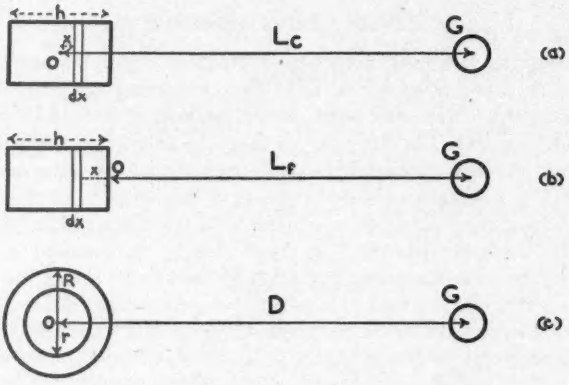

FIG. 1. *Container cross-sections for which absorption corrections are considered.*

Let t = the thickness of the container, and λ = linear absorption coefficient of the container material. Then the intensity is further reduced because of absorption in the container by a factor $e^{-\lambda t}$.

Since the various elements of the source are at different distances from the detector it may be necessary to apply an inverse square correction. If the distance L_c from the detector is measured to the centre of the source the ratio of intensities when the source is distributed throughout the container to that when it is concentrated in the plane $x = 0$ is

$$\frac{1}{h}\int_{-h/2}^{h/2}\frac{L_c^2}{(L_c - x)^2}\,dx = \frac{1}{1 - h^2/4L_c^2}.$$

Combining the corrections for absorption in the sample and for distance as in Fig. 1(*a*), one obtains a ratio of measured to corrected intensities of

$$\frac{1}{P_c} = \frac{1}{h}\int_{-h/2}^{h/2} e^{-\mu(h/2 - x)}\frac{L_c^2}{(L_c - x)^2}\,dx \qquad (2)$$

$$= \frac{1}{\mu h}(1 - e^{-\mu h}) + \frac{h}{L_c}\left(\frac{\mu h}{6} - \frac{\mu^2 h^2}{12} + \frac{\mu^3 h^3}{40} + \ldots\right)$$

$$+ \frac{h^2}{4L_c^2}\left(1 - \frac{\mu h}{2} + \frac{\mu^2 h^2}{5} - \frac{\mu^3 h^3}{120} + \ldots\right) + \ldots\ldots$$

If μh and h/L_c are small it may be permissible to neglect the inverse square correction when distances are measured to the centre of the source. For example, if $\mu h = 0.2$ and $h/L_c = 0.05$, $P = 1.1033$, whereas $P_c = 1.1014$.

If the distance L_f is measured to the front face the ratio of intensities for the source distributed to the source concentrated in the plane $x = 0$ is

$$\frac{1}{h}\int_0^h \frac{L_f^2}{(L_f + x)^2}\,dx = \frac{1}{1 + h/L_f}.$$

Combining the corrections for absorption in the sample and for distance as in Fig. 1(*b*), one obtains the ratio of measured to correct intensities,

$$\frac{1}{P_f} = \frac{1}{h}\int_0^h e^{-\mu x}L_f^2/(L_f + x)^2\,dx \qquad (3)$$

$$= \frac{1 - e^{-\mu h}}{\mu h} - \frac{h/L_f}{1 + h/L_f} + \sum_{m=1}^{\infty} \frac{(-1)^m(\mu h)^m}{m!}\left[\sum_{n=1}^{\infty} \frac{n+1}{n+m+1}(-1)^n(h/L_f)^n\right].$$

In Table I are given a few values of P_e and P_f for μh values up to 0.40 and for h/L values up to 0.10.

TABLE I

COMBINED CORRECTIONS FOR ABSORPTION IN THE SOURCE AND FOR THE DISTANCE EFFECT ALONG THE LENGTH OF THE SOURCE IN A RECTANGULAR SAMPLE. P_e AND P_f ARE THE CORRECTIONS WHEN THE DISTANCE IS MEASURED TO THE CENTRE AND TO THE FRONT FACE OF THE SAMPLE RESPECTIVELY

	P	P_e					P_f				
h/L / μh	0.00	0.02	0.04	0.06	0.08	0.10	0.02	0.04	0.06	0.08	0.10
0.00	1.000	0.9999	0.9996	0.9991	0.9984	0.9975	1.020	1.040	1.060	1.080	1.100
0.02	1.010	1.010	1.009	1.009	1.008	1.007	1.030	1.050	1.070	1.091	1.111
0.04	1.020	1.020	1.019	1.019	1.018	1.017	1.040	1.061	1.081	1.101	1.121
0.06	1.030	1.030	1.029	1.029	1.028	1.027	1.051	1.071	1.091	1.112	1.132
0.08	1.041	1.040	1.040	1.039	1.038	1.037	1.062	1.082	1.102	1.123	1.143
0.10	1.051	1.050	1.050	1.049	1.048	1.046	1.072	1.092	1.113	1.133	1.154
0.12	1.061	1.060	1.060	1.059	1.058	1.056	1.082	1.103	1.124	1.144	1.165
0.14	1.072	1.071	1.070	1.069	1.068	1.066	1.093	1.113	1.134	1.155	1.176
0.18	1.093	1.092	1.091	1.090	1.088	1.087	1.114	1.135	1.156	1.177	1.199
0.20	1.103	1.102	1.101	1.100	1.099	1.097	1.125	1.146	1.167	1.189	1.210
0.22	1.114	1.113	1.112	1.111	1.109	1.107	1.135	1.157	1.178	1.200	1.221
0.24	1.125	1.124	1.123	1.121	1.119	1.118	1.146	1.168	1.189	1.211	1.233
0.26	1.136	1.135	1.133	1.132	1.130	1.128	1.157	1.179	1.201	1.222	1.244
0.28	1.147	1.145	1.144	1.142	1.140	1.138	1.168	1.190	1.212	1.234	1.256
0.30	1.157	1.156	1.155	1.153	1.151	1.149	1.179	1.201	1.223	1.245	1.267
0.32	1.168	1.167	1.166	1.164	1.162	1.159	1.191	1.213	1.235	1.257	1.279
0.34	1.180	1.178	1.176	1.175	1.172	1.170	1.202	1.224	1.246	1.268	1.291
0.36	1.191	1.189	1.187	1.185	1.183	1.181	1.213	1.235	1.258	1.280	1.302
0.38	1.202	1.200	1.199	1.197	1.194	1.191	1.225	1.247	1.269	1.292	1.314
0.40	1.213	1.212	1.210	1.207	1.205	1.202	1.236	1.259	1.281	1.304	1.326

Radiation from Cylindrical Source

Consider a cylinder of unit length whose axis is at right angles to the direction of the detector. Absorption corrections for this arrangement have been given by several authors (3–8) and are included here for comparison and

reference purposes only. Referring to Fig. 1 (*c*), let r and R be the inside and outside radii of a container that is completely filled with the source material. Let μ and λ be the linear absorption coefficients of the source and container materials as before.

Considering absorption in the source only, let there be an element at (x, y) emitting gamma-radiation in the direction of the detector G. Then the ratio of the intensity with absorption in the source to that with no absorption is

$$\frac{2}{\pi r^2}\int_0^r \int_{-(r^2-y^2)^{\frac{1}{2}}}^{(r^2-y^2)^{\frac{1}{2}}} e^{-\mu\left\{(r^2-y^2)^{\frac{1}{2}}-x\right\}}\,dx\,dy \qquad (4)$$
$$= 1 - (8/3\pi)\mu r + \tfrac{1}{2}\mu^2 r^2 - (32/45\pi)\mu^3 r^3 + \ldots$$

The equivalent rectangular source is approximately that for which $1 - (8/3\pi)\mu r = 1 - \mu h/2$, or $h = 1.68\,r$.

Considering the absorption in the circular container only, the ratio of the intensity with absorption to that with no absorption is

$$\frac{2}{\pi r^2}\int_0^r \int_{-(r^2-y^2)^{\frac{1}{2}}}^{(r^2-y^2)^{\frac{1}{2}}} e^{-\lambda\left\{(R^2-y^2)^{\frac{1}{2}}-(r^2-y^2)^{\frac{1}{2}}\right\}}\,dx\,dy$$
$$= 1 - \lambda R[1 - (8/3\pi)r/R - (1/8)r^2/R^2 - (1/64)r^4/R^4 - \ldots] \qquad (5)$$
$$+ \frac{\lambda^2 R^2}{2}[1 - (16/3\pi)r/R + \tfrac{1}{2}r^2/R^2 + (8/15\pi)r^3/R^3 + \ldots] + \ldots$$

If the container correction is small a good degree of approximation may be obtained by defining an effective thickness t by

$$t = R[1 - (8/3\pi)\,(r/R) - (1/8)\,(r^2/R^2) \ldots\ldots]. \qquad (6)$$

and the absorption correction is then given by $e^{-\lambda t}$. For more accurate work a graphical integration is usually performed.

If the cylindrical source and container corrections are large and an accurate result is required the two expressions (4) and (5) must be combined before integration since the corrections cannot be applied separately as they can for a rectangular source.

Obliquity Corrections

If the distance between the source and the detector is of the same order as the lateral dimensions of either the source or the detector, it may be necessary to apply obliquity corrections. The form of such corrections has been given by Backhurst (1). In the experimental work described here obliquity corrections were usually negligible.

Experimental

Experimental work was performed on several bulk sources of known radium content, so that errors arising from using the wrong absorption coefficient, or from using an undesirable geometrical arrangement, would become evident.

Measurements were made of the radiation equivalent of each source as a rectangular source, and an absorption coefficient was measured to see whether it could be used to give the proper absorption correction. Typical results are given in Table III for the sources that are described below.

The direct measurement of the absorption coefficient of the bulk source was made by measuring the reduction in intensity of the radiation from a standard capsule placed behind it. Thus if

I_s is the intensity due to the standard capsule alone;

I_{su} is the intensity due to the standard capsule and to the unknown, placed so that radiation from the standard is absorbed in the unknown before reaching the detector;

and

I_u is the intensity due to the unknown alone,

then the measured value of μh is

$$\mu h = \ln I_s/(I_{su} - I_u) - 2\lambda t, \tag{7}$$

where λt refers to the container walls. The measured values of μh given in Table III were obtained with the standard capsule touching the centre of the back face of the bulk source.

Description of Sources

The sources used in the experimental work are listed in Table II, U-1 to U-10 being especially prepared bulk sources, and S-1 to S-4 being National Research Council secondary radium standards.

Sources U-1, U-2, and U-3 were prepared from capsules of radium bromide that previously had been measured against the National Research Council secondary standards with both an ionization chamber and a Geiger-Müller counter. The contents of each capsule was dissolved in dilute hydrobromic acid and mixed with enough barium carbonate to give the desired concentration. The tools and dishes used in the mixing were sealed in another container and their radiation equivalent later measured to determine how much radium was lost. This amounted to a few micrograms. It is considered that the radium content of U-1, U-2, and U-3 is known with an accuracy of at least 0.5%.

Sources U-4 to U-8 were prepared to show the effect of containers of different sizes. The material used for each was from the same sample of radium ore concentrate, consisting of 92% barium carbonate and 7% aluminium oxide, which had been obtained from Eldorado Mining and Refining Co. Subsequent measurements of these five sources indicated that the most likely radium concentration was 11.00 μgm. per gm., and the true content of each source was calculated on this basis.

Sources U-9 and U-10 contain pitchblende ore that had been chemically analysed and then mixed with inert rock to contain 32.0 and 48.0%, respectively, of U_3O_8. These ore samples were obtained from the Bureau of Mines, Department of Mines and Resources, Ottawa. By assuming the ratio of

TABLE II

DESCRIPTION OF SOURCES. THE SOURCE MATERIALS ARE: *A*—MIXTURE OF RADIUM BROMIDE AND BARIUM CARBONATE; *B*—A SAMPLE OF RADIUM BARIUM CARBONATE OBTAINED IN THE REFINING OF ORE; *C*—CANADIAN PITCHBLENDE ORE; *D*—RADIUM SULPHATE

Description of source					Description of container				
Source number	Radium content, mgm.	Material	Weight, gm.	Density, gm./cm.³	Material	Wall thickness, cm.	Inside diameter, cm.	Inside length, cm.	Volume, cm.³
U-1	1.118	*A*	125.6	1.39	Steel	0.025	5.49	3.81	90.2
U-2	2.150	*A*	179.7	1.97	Steel	0.025	5.49	3.86	91.4
U-3	2.070	*A*	131.3	1.49	Steel	0.025	5.49	3.71	87.8
U-4	0.656	*B*	59.6	1.85	Steel	0.025	3.79	2.85	32.2
U-5	1.262	*B*	114.7	1.88	Steel	0.025	4.79	3.38	60.9
U-6	1.811	*B*	164.6	1.80	Steel	0.025	5.49	3.86	91.4
U-7	2.486	*B*	226.0	1.85	Steel	0.025	6.04	4.27	122.3
U-8	1.103	*B*	100.3	1.66	Steel	0.025	7.59	1.34	60.6
U-9	0.025	*C*	267.5	2.05	Steel	0.025	7.50	2.95	130.3
U-10	0.050	*C*	363.3	2.68	Steel	0.025	7.50	3.07	135.6
	Rad. Eq.								
S-1	0.0906	*D*			Glass				
S-2	0.528	*D*			Glass				
S-3	0.942	*D*			Glass				
S-4	1.977	*D*			Glass				

TABLE III

TYPICAL EXPERIMENTAL RESULTS ON SOURCES DESCRIBED IN TABLE II. INTENSITIES ARE GIVEN AS COUNTING RATES PER MINUTE, SCALE-OF-64. FILTER WAS 1 CM. LEAD SURROUNDING THE G-M TUBE

Unknown source	Standard source	Distance unknown, L_c, cm.	Distance standard, L_s, cm.	Intensity unknown, I_u	Intensity standard, I_s	Radiation equiv., mgm. Ra	Measured $\mu_m h$
U-1	S-3	75.0	75.0	87.6	81.5	1.013	0.199
U-2	S-4	110.0	110.0	73.7	78.0	1.868	.299
U-3	S-4	75.0	75.0	162.6	171.9	1.870	.203
U-4	S-2	70.0	70.0	56.0	50.2	0.589	.196
U-5	S-3	100.0	100.0	51.0	42.9	1.119	.230
U-6	S-4	97.6	100.0	80.4	95.0	1.594	.256
U-7	S-4	100.0	100.0	98.8	90.3	2.163	.292
U-8	S-4	100.0	100.0	47.6	89.8	1.048	.078
U-9	S-1	33.0	33.0	9.4	38.2	0.0223	.254
U-10	S-1	34.0	34.0	17.2	35.7	0.0436	.364

radium to uranium to be 3.4×10^{-7} the amount of radium in each of U-9 and U-10 was calculated.

For purposes of measurement a given sample of radium ore concentrate is thoroughly mixed to ensure a homogeneous distribution and packed into a container that is then sealed and put away until the disintegration products

come into equilibrium with the radium. Steel cylindrical containers of height about 4 cm., radius 2.5 cm., and wall thickness 0.025 cm. have been found convenient, since they were readily available commercially. These containers hold about 150 gm. of barium carbonate.

Apparatus

The radiation intensities due to the radioactive sources were measured by means of Geiger-Müller counters. In order to minimize scattering from the walls and tables into the Geiger-Müller tube, the apparatus was located centrally in a room approximately 20 ft. square. The Geiger-Müller tube was mounted about twenty inches above the edge of one table, and the sources and filters were placed on an optical bench that stretched across to another table. Mountings to hold the Geiger-Müller tube and the sources were made of light wood. The usual distance between the sources and the counters was of the order of 100 cm. The general arrangement is shown in Fig. 2.

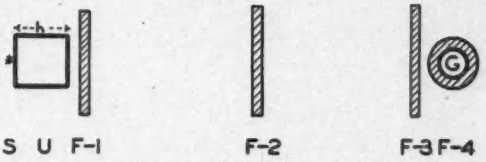

FIG. 2. *Arrangement of standard radium capsule S, the unknown bulk source U, filters F-1 to F-4, and Geiger-Müller counter G.*

The detecting apparatus consisted of a self-quenching Geiger-Müller tube, a stabilized high voltage supply, a scaler, and a recorder. The G-M tubes were made with brass cathodes of cross-section 14 by 2 cm. Counting rates were of the order of 100 counts per sec. All the measurements were corrected for resolving time losses and the natural background, and sufficient counts were taken to reduce statistical errors to the order of 0.1%.

Positions of Filters

Owing to the complex nature of the gamma-radiation emitted by the disintegration products of radium it is necessary to use a filter to improve the homogeneity of the radiation that reaches the detector. Four possible locations of the filter are illustrated in Fig. 2. In choosing the best arrangement of the filter, consideration must be given to the radiation scattered from the walls and tables, and to the radiation scattered from the filter itself into the counter.

The wall and table scattering was measured experimentally by placing a lead brick, 25 cm. long and 10 cm. square in cross-section, in the path of the direct radiation from a 5 mgm. source placed 150 cm. from the counter. The following counting rates were observed:

No filtering	238.0
25 cm. lead filter in direct beam	20.4
25 cm. lead filter in direct beam plus 3 mm. lead surrounding the G-M tube	2.7
25 cm. lead filter in direct beam plus 1 cm. lead surrounding the G-M tube	1.5
Natural background, 1 cm. lead surrounding G-M tube	1.4
Lead filter 1 cm. in direct beam	108.5

Thus the wall and table scatter comprises roughly 10% of the total radiation reaching the counter in this particular geometry, if no lead is used about the G-M tube. If a lead filter of 1 cm. thickness is used next to the source, and no lead is placed about the G-M tube, the wall and table scatter may be as much as 20% of the total. Three millimetres of lead about the G-M tube cuts out most of the scattered radiation since it is much softer than the direct, owing to the large angles through which it has been scattered.

Scattering from the lead filter itself may be as much as 10% of the total radiation reaching the counter. This may be demonstrated by placing a lead filter close to the source, Fig. 2, F-1; midway between the source and the counter, F-2; and close to the counter, F-3. The recorded counting rate is always less for the filter in the midway position. For a lead filter 18 cm. by 15 cm. and 1 cm. thick, the counting rate was observed to be 10% less than for either of the other two positions. This is to be expected from a consideration of the solid angles subtended by the filter at the source and by the counter at the filter. A more complete discussion of the radiation scattered into the detector from a filter has been given by Tarrant (8).

Since the amount of radiation scattered from the filter depends upon the distance between the filter and the source, the inverse square law as applied to distance between the source and the detector does not hold. Table IV gives results that were obtained with different positions of the filter and sources. It is seen that divergent values are obtained when use is made of

TABLE IV

EXPERIMENTAL RESULTS FOR SOURCES U-3 AND S-4 FOR DIFFERENT ARRANGEMENTS OF FILTERING AND DISTANCES. INTENSITIES ARE GIVEN AS COUNTING RATES PER MINUTE, SCALE-OF-64

Distance unknown, U-3, L_o, cm.	Distance standard, S-4, L_s, cm.	Lead filtering	Intensity unknown, I_u	Intensity standard, I_s	Calculated content, mgm. Ra
72.6	75.0	3 mm. F-4, 1 cm. F-1	130.5	126.5	2.116
97.6	100.0	" "	72.6	71.6	2.115
152.6	155.0	" "	30.2	30.6	2.093
72.6	70.7	" "	129.2	145.6	2.049
72.6	75.0	3 mm. F-4, 1 cm. F-2	119.2	117.3	2.083
152.6	155.0	" "	25.5	26.1	2.073
72.6	75.0	1 cm. F-4	173.5	171.9	2.070

the inverse square law, except when the filter is placed about the detector. The arrangement adopted has been to place a 1 cm. lead cylinder around the G-M tube even though there is considerable radiation scattered from the lead cylinder into the counter tube.

Absorption Corrections

If the form of the absorption corrections given above is to be used, it is necessary to find that value of μh for which the corresponding P (Equation (1), (2), or (3)) gives the correct radium content. This value of μh is found most accurately from sources of which the true radium content is known, and of which the radiation equivalent has been measured. Coefficients obtained by other means then may be compared with this value.

It will be found convenient to distinguish three different absorption coefficients. μ_p will be used to indicate the 'appropriate' coefficient which when used to calculate the correction factor P gives the correct result. μ_m will be used to indicate the measured coefficient as calculated from Equation (7). μ_t will be used to indicate the true coefficient, i.e., that which would be measured if radiation scattered from other parts of the source were not allowed to reach the detector. It has been found that μ_m is usually less than μ_t but greater than μ_p, the differences being due to scattered radiation reaching the detector. Scattered radiation increases the apparent radiation equivalent of the bulk source, requiring a lower value of μ_p, and this is not always compensated for by the scattered radiation which reaches the counters during the measurement of the coefficient μ_m.

The appropriate corrections for absorption are shown for sources U-1 to U-10 in Table V. The corresponding value of $\mu_p h$ was found from Table I, and the mass absorption coefficient μ_p/ρ was found by dividing $\mu_p h$ by $h\rho$, where ρ is the density. The results show that μ_p/ρ varies with the dimensions

TABLE V

COMPARISON OF APPROPRIATE AND MEASURED ABSORPTION COEFFICIENTS AND ABSORPTION CORRECTIONS FOR SOURCES OF KNOWN RADIUM CONTENT. CORRECTION FOR ABSORPTION IN THE CONTAINER WALL WAS TAKEN TO BE 1.010

Source No.	h/L_c	$P(\mu_p h)$	$\mu_p h$	μ_p/ρ, cm.²/gm.	μ_m/ρ, cm.²/gm.	$P(\mu_m h)$	$\frac{P(\mu_m h)}{P(\mu_p h)}$
U-1	0.051	1.093	0.185	0.035	0.038	1.100	1.007
U-2	0.035	1.139	0.272	0.036	0.039	1.155	1.013
U-3	0.050	1.096	0.191	0.035	0.037	1.102	1.006
U-4	0.041	1.103	0.203	0.038	0.037	1.099	0.996
U-5	0.034	1.117	0.229	0.036	0.036	1.118	1.001
U-6	0.040	1.125	0.244	0.035	0.037	1.131	1.005
U-7	0.043	1.138	0.270	0.034	0.037	1.151	1.011
U-8	0.013	1.042	0.083	0.037	0.035	1.039	0.997
U-9	0.090	1.098	0.200	0.033	0.042	1.124	1.024
U-10	0.090	1.143	0.287	0.035	0.044	1.184	1.036

of the sources. The radium content of the sources is not known accurately enough to determine whether it also varies with the density.

The accuracy with which μh must be known may be found by differentiating the correction factor $P = \mu h/(1 - e^{-\mu h})$

with respect to μh. This gives

$$\Delta P/P = (1 - Pe^{-\mu h})\Delta\mu h/\mu h.$$

For $\mu h = 0.10$, the relative error in μh is about twenty times the relative error in P; for $\mu h = 0.20$, about ten times; and for $\mu h = 0.30$, about seven times. The error in using a value $\mu/\rho = 0.035 \pm 0.001$ cm.^{2} per gm. for sources U-1 to U-3 is then about $0.001 \times 0.1 \times 100/0.035 = \pm 0.3\%$.

The measured values of μ_m/ρ are also shown in Table V, but these values may have an appreciable error because the density within a bulk source may not be uniform. The observed coefficient μ_m/ρ shows a significant decrease for a thin sample and is much higher for a small radius, a value of 0.045 being obtained when a lead brick with a hole through it of radius half a centimetre was placed in front of the absorbing sample. Increase of the radius beyond about two centimetres seemed to have little effect, probably because of the large angle through which the radiation had to be scattered in order to reach the counter. The measured coefficient also increases as the distance between the source and the absorber is increased owing to the smaller amount of scattered radiation reaching the counter.

The correction factor P calculated from the measured value $\mu_m h$ is usually higher than the 'appropriate' value. The error in using the former value of P may be seen from the last column of Table V. Although this error is only a little greater than the experimental errors in measurement, a discussion is given below to show how it might arise.

Effect of Scattered Radiation

The effect of scattered radiation in the determination of the 'appropriate' and measured coefficients may be written in terms of the fraction of radiation scattered. Let us consider the fraction J_s/I_s arising in the direct measurement of the absorption coefficient, and the fraction J_u/I_0 arising in the measurement of the radiation equivalent of a bulk source, where

J_s is the intensity of the radiation from the standard capsule scattered into the counter during the measurement of μh,

I_s is the intensity of radiation due to the standard capsule alone,

J_u is the intensity of the radiation from the unknown bulk source scattered into the counter from other parts of the source, and

I_0 is the intensity due to the unknown with no absorption.

If μ_t, μ_m, and μ_p are the coefficients already defined, then

$$J_s/I_s = e^{-\mu_m h} - e^{-\mu_t h}, \tag{8}$$

and

$$J_u/I_0 = 1/P(\mu_p h) - 1/P(\mu_t h). \tag{9}$$

Experimental values of these scattered fractions for sources U-1 to U-8 are shown in Table VI, as calculated from Equations (8) and (9), taking $\mu_t/\rho = 0.050$ cm.^{2} per gm. This value of μ_t/ρ was measured by using an absorbing sample of small cross-section and a separation of standard capsule and absorber of several centimetres. It agrees with a value obtained by Perry (7).

The 'appropriate' coefficient μ_p/ρ may be written in terms of the measured coefficient μ_m/ρ from Equations (8) and (9), if the approximations $P = e^{\frac{1}{2}\mu h}$ and $x = \ln(1 + x)$ for small x are used, giving

$$\mu_p/\rho = \mu_m/\rho + (1/h\rho)(J_s/I_s)e^{\mu_t h} - (2/h\rho)(J_u/I_o)e^{\frac{1}{2}\mu_t h}. \qquad (10)$$

If a measured coefficient is to be used for the calculation of the absorption correction, it is then necessary that the approximate ratio of the scattered fractions be

$$\frac{J_s/I_s}{J_u/I_0} = 2\,e^{-\frac{1}{2}\mu_t h}, \qquad (11)$$

or, more accurately, simply the ratio of Equation (8) to Equation (9) with μ_p substituted for μ_m. The latter relation has been used to calculate the required ratio in Table VI. The experimental value of this ratio is also given in Table VI. Since J_u/I_0 is fixed by the geometry of the unknown source it is necessary to find those conditions in the measurement of μh for which the scattering would compensate the effect of scattering in measuring the radiation equivalent of the bulk source, if a measured coefficient is to be used.

TABLE VI

FRACTIONS OF RADIATION SCATTERED IN MEASURING AN ABSORPTION COEFFICIENT AND A RADIATION EQUIVALENT OF A BULK SOURCE AND THEIR RATIO

Source	J_s/I_s Equation (8)	J_u/I_0 Equation (9)	The ratio $(J_s/I_s)/(J_u/I_o)$	
			Exptl.	Req'd.
U-1	0.053	0.034	1.6	1.9
U-2	0.057	0.043	1.3	1.8
U-3	0.059	0.036	1.6	1.9
U-4	0.054	0.026	2.1	1.9
U-5	0.067	0.037	1.8	1.8
U-6	0.068	0.042	1.6	1.9
U-7	0.072	0.050	1.4	1.8
U-8	0.030	0.013	2.3	2.0

Scattering presumably also has an effect upon the correction for absorption in the container walls. However, the total wall correction for 0.025 cm. of steel is 1% so that variations in this correction due to scattering may be neglected. The effect of container walls was further investigated by measuring source U-2 with a brass collar 0.3 cm. thick fitting snugly around it. The collar increased the measured radiation equivalent by about 1% owing to increased scattering. A container wall of 0.025 cm. would, therefore, introduce no appreciable error.

Conclusions

The main features of the experimental method for the determination of the radium content of unknown bulk sources are the measurement of the radiation equivalent of the source, as found by comparing the intensity of gamma-radiation from it to that from a standard radium capsule, and the correction for self-absorption made on the basis of an absorption coefficient measured with the capsule touching the centre of the back face of the bulk source. This method gives an error in the radium content that is less than 2% for the radium ore concentrates studied.

The measurements on the synthetic sources, consisting chiefly of barium carbonate, indicate that the mass absorption coefficient required to give the proper absorption correction varies with the dimensions of the source. An accurate value of a directly measured absorption coefficient is difficult to obtain, and, because this value frequently does not give an appropriate absorption correction, it is desirable to have the source of a size for which the appropriate mass absorption coefficients are known, or for which it is known that the measured value will give the proper correction. The error in using the directly measured absorption coefficient arises because scattering conditions in the measurement of the coefficient differ from those in the measurement of the radiation equivalent of a bulk source.

References

1. BACKHURST, I. Proc. Phys. Soc. London, 38 : 277-290. 1926.
2. KAYE, G. W. C., ASTON, G. H., and PERRY, W. E. Brit. J. Radiol. 7 : 540-556. 1934.
3. ODDIE, T. H. Proc. Phys. Soc. London, 51 : 905-931. 1939.
4. OWEN, E. A. and FAGE, W. E. Proc. Phys. Soc. London, 34 : 27-32. 1921.
5. OWEN, E. A. and NAYLOR, B. Proc. Phys. Soc. London, 34 : 92-97. 1921.
6. PATERSON, C. C., WALSH, J. W. T., and HIGGINS, W. F. Proc. Phys. Soc. London, 29 : 215-246; discussion, 246-249. 1917.
7. PERRY, W. E. Proc. Phys. Soc. London, 57 : 178-190. 1945.
8. TARRANT, G. T. P. Proc. Cambridge Phil. Soc. 28 : 475-489. 1931.

NEW PHOTOGRAPHIC EMULSIONS SHOWING IMPROVED TRACKS OF IONIZING PARTICLES[1]

By Pierre Demers[2]

Abstract

The photographic emulsion method of registering the tracks of ionizing particles suffers from certain disadvantages that are mainly due to the relatively large size of grains forming the tracks and their large spacing. These disadvantages are mostly removed in new emulsions that have been prepared after numerous tests. The tracks of ionizing particles in these emulsions consist of grains of diameter $d \sim 0.2\ \mu$, which often form continuous lines.

Grain spacing is no longer the main cause of apparent straggling, except below a range of 3 to 4 mm. of air. The standard deviation in determining energy from a single measurement of range is 3.25 to 3.5% for protons of 0.6 to 2.4 Mev., and 1.3 to 1.9% for α-rays of 4 to 8.5 Mev. The latter deviation is one-half to one-quarter that obtained in commercial emulsions. Ease of finding the tracks, especially of protons, is considerably increased. The tracks of fission fragments have a characteristic appearance and are easily found amidst the faint or invisible tracks of α-rays and protons. Slow electron tracks have occasionally been seen.

The action of certain sensitizing and desensitizing chemicals is described and discussed in terms of the theory of the photographic process.

The grain spacing is related to the diameter of the grain, the concentration of silver bromide in the emulsion, and the average probability of development of the grains touched by the ionizing particle. A quantitative theory is given for the probability of development in terms of the specific energy loss and a sensitivity parameter of the emulsion. The observed variation of the grain spacing with residual range of protons, α-rays, and fission fragments can be approximately explained by the theory.

Introduction

1. *General Remarks*

The cloud chamber and the photographic emulsion methods were introduced as new techniques into nuclear physics at about the same time (1910-1912); both make visible the tracks of individual electrified particles. As is well known, the cloud chamber method is due to C. T. R. Wilson. The photographic emulsion method originated from the work of several authors, notably Kinoshita (11) and Reinganum (20). The principle is as follows. An ionizing particle passes through a layer of emulsion, which consists of silver bromide crystals embedded in gelatine, and leaves a modification called a latent image in some of the crystals, which renders them developable. After these crystals have been reduced to silver, the track is visible as a row of silver grains under a magnification of 100 to 1500 times. (In the processing some crystals are developed outside the track, thus producing what is called fog.)

[1] *Manuscript received August 29, 1946.*

Contribution from the Montreal Laboratory, Nuclear Physics Branch, Division of Atomic Energy of the National Research Council of Canada. Issued as N.R.C. No. 1450. This work was mostly done in 1945, the first original results being obtained in May 1945. Publication was withheld owing to security restrictions. In December 1945, a brief account was sent in the form of a Letter to the Editor for publication in the Physical Review, but its appearance was delayed until July 15, 1946. The results of this paper were briefly presented at the Toronto meeting (May 20, 1946) of the Royal Society of Canada.

[2] *Physicist, National Research Council; now at the University of Montreal, Montreal, Que.*

By this technique the tracks of mesotrons, protons, and heavier ions have been recorded by various experimenters. Electrons and γ-rays fog the emulsions without usually leaving recognizable tracks.

2. *Photographic Emulsions That Have Been Used to Record Tracks*

The properties of photographic materials are dealt with by Mees (13) and Webb (26), and emulsion-making by Baker (1), Wall (24), and Carroll (7). Shapiro (21) and Wilkins (27) have written useful reviews of the emulsion technique in nuclear physics.

Photographic emulsions usually contain about 40% silver bromide in the form of minute crystals or grains, the balance being gelatine, with occasional minor constituents. The diameter of the grains may range from a few hundredths of a micron to several microns. The mean diameter is smallest (about 0.03 μ) in the Lippmann emulsions and largest (1 to 2 μ) in fast negative material. The dried emulsion forms a layer 10 to 20 μ thick on a support of glass or a cellulose derivative.

The early experimenters were able to record the tracks of α-rays but not of protons. In 1925 Miss Blau (3) found that certain emulsions could be sensitized to protons by pinakryptol yellow or green. Plates are now commercially available that will respond to the action of protons without a sensitizing dye. Some of these are *Eastman fine grain α-particle* (Eastman Kodak, U.S.A.) or *Eastman α* for short, *Ilford Special Halftone* (Ilford, U.K.) and *Agfa K* (Agfa, Germany). Ilford has recently produced a series of improved emulsions, which came to the writer's attention while this work was being written (19).

There is no information in the technical literature on how these commercial emulsions are made. Jdanov (10) has recommended one emulsion (called E_3) for recording proton tracks, without giving its complete formula. Myssowsky and Tschishow (15) have discussed the recording of α-ray tracks in an emulsion of given recipe.

3. *Advantages and Limitations of the Photographic Emulsion Technique*

In order to appreciate the value of the photographic emulsion technique, it may be compared with the cloud chamber method. The photographic emulsion acts as a continuously sensitive device for recording the tracks of ionizing particles, while a cloud chamber is sensitive only about one-thousandth of the time that it is in operation. The volume of air equivalent to the emulsion is usually greater than that contained in a cloud chamber. Moreover, the photographic plate has the great convenience of small size. On the other hand, when the thin thread-like tracks in a cloud chamber are compared with the tracks seen in the usual emulsions, the limitations of the latter are evident. Since the grains are large and relatively scarce, the tracks are hard to find and the accuracy possible in range and angular measurements is severely limited. These limitations may be seen in Figs. 13*A*, 13*B* and 18, which show tracks obtained in Eastman α-plates. Powell (18) has found that α-ray energies of a few million electron volts can be measured with a

standard deviation of 0.25 Mev. and protons with a standard deviation of 0.15 Mev. in Ilford halftone plates. The writer has found somewhat higher deviations in Eastman α-plates. Moreover, in addition to the rather large standard deviations, there is usually little difference in appearance between the tracks of protons and α-rays. Sometimes it has even been difficult to recognize the tracks of the strongly ionizing fission fragments among the tracks of α-rays. Perfilov (17) and Borst and Floyd (6) have recently succeeded, however, in recording and recognizing the tracks of the fission fragments from uranium without confusion with the α-rays.

4. *Desired Improvements in Emulsions*

In view of the causes of the limitations pointed out in the previous section, the following improvements may be aimed at: (i) smaller grain size, and (ii) closer grains, which will result in a better definition of the track, (iii) differential sensitivity of the grains so that the various particles may be distinguished and identified, (iv) every grain touched by the ionizing particle must develop, and (v) excessive fog must be avoided. How these desired results may be brought about can be seen in part from the considerations that follow.

Jdanov (10) has introduced a useful relation that correlates the mean grain spacing $\triangle$, the grain diameter d, and the concentration c:

$$\triangle = 4.2\, d/c.$$

It is easily derived from geometrical considerations on the assumptions that the grains are spherical, the track linear, and every grain touched by the track is ultimately developed. $\triangle$ and d are conveniently expressed in microns and c in grams of silver bromide per cubic centimetre of emulsion. Owing to the absence of information on grain sizes before development, the apparent diameter after development will be used for d throughout this paper. If not every grain touched is developed but a fraction P of them, Jdanov's formula can be modified as follows:

$$\triangle = 4.2\, d/cP = \triangle_0/P,$$

where $\triangle_0$ is the expression written above. The variables d, c, and P are not generally independent, for they are related through the process of emulsion making. The concentration c is usually determined by the quantities of chemicals used; how to effect changes in d and P is a complicated physico-chemical problem.* While c is nearly 1 gm. of silver bromide per cc. of the usual emulsions, it may be increased to a maximum of 6.5 gm. per cc., which is the density of pure silver bromide. If P is less than unity, sensitizing the grains may be useful.

** Very small values of d, about 0.03 μ, are found in Lippmann emulsions. Unsuccessful attempts have been made by Blau and Wambacher (4) and by Jdanov to show α-ray tracks in these emulsions. Their failure may be attributed to the values of c and P being too small under their conditions.*

5. *Brief Survey of the Present Work*

After making numerous tests, emulsions have been prepared that have very small grain size and grain spacing. In these the tracks of ionizing particles often look like narrow and continuous threads, except under high resolving power when the individual grains can be seen. The improvements effected may be judged from Figs. 13 to 34. Differential sensitivity has been attained. β- and γ-rays fog these plates quite slowly. In a few instances it is believed that the last few centimetres of the tracks of electrons have been seen.

Following a brief account of the microscopic technique, the preliminary work on previous kinds of emulsions will first be reviewed. Second, the making, processing, and application of new emulsions will be described. Third, some nuclear physical experiments using the emulsion technique will be described. Fourth, the actions of certain sensitizing and desensitizing substances will be included. Fifth, a quantitative theory that correlates grain spacing and several other factors will be put forward.

Microscopic Technique

The best optical conditions are necessary to bring out the details in the finest grained emulsions. A Spencer binocular mono-objective microscope with inclined eyepieces was used. The illumination was provided by a Bausch and Lomb lantern, and the image of its diaphragm was accurately focused in the plane being examined by a 1.4 N.A. condenser. Oil immersion was used between the condenser and the plate and between the plate and the objective. The latter was a 1.3 N.A. 90 × Apochromat. The eyepieces were usually 12.5 × compensated, and the over-all magnification 1125. A scale divided into hundredths or into two-hundredths of a millimetre was used. The resolving power in white light should be approximately

$$1.22\ \lambda/2\ \text{N.A.} = 1.22 \times 0.55\ \mu/2.6 = 0.26\ \mu.$$

In practice it was possible to detect the presence of as many as three or four grains per micron and to estimate the diameter of a grain down to 0.1 μ.

Photomicrographs were taken in white light, which showed a resolving power not as good as that calculated above (Figs. 13*A* and 26 to 34). Photographs were also taken with a blue filter, consisting of a liquid cell filled with a solution of copper nitrate and malachite green, which transmits a band around 0.48 μ. With this filter the theoretical resolving power of 0.24 μ was actually attained, judging from the enlargements (Figs. 13*B* to 25).

Preliminary Work

1. *Eastman* α

The tracks of α-rays were obtained in Eastman α-emulsions (Fig. 18) by soaking the plates in dilute uranium or thorium nitrate, drying, and keeping them for some time before development. The emulsions were developed for 20 min. in Eastman's D-19 diluted 1 : 20. The mean grain spacing was

found to be 1.6 μ along the whole range of the α-rays from thorium C′. The stopping power of the emulsion from measurements on these tracks was 1415 times that of air at 15° C. and a pressure of 1 atm.

Long proton tracks (Figs. 13*A*, 13*B*, 34) were obtained by irradiating plates with neutrons from a mixed polonium and beryllium source. The grain spacing Δ, which varied from 2.2 μ to 10 μ, is plotted in Fig. 1*A* against the residual range of the proton in Figs. 13*A* and 13*B*.

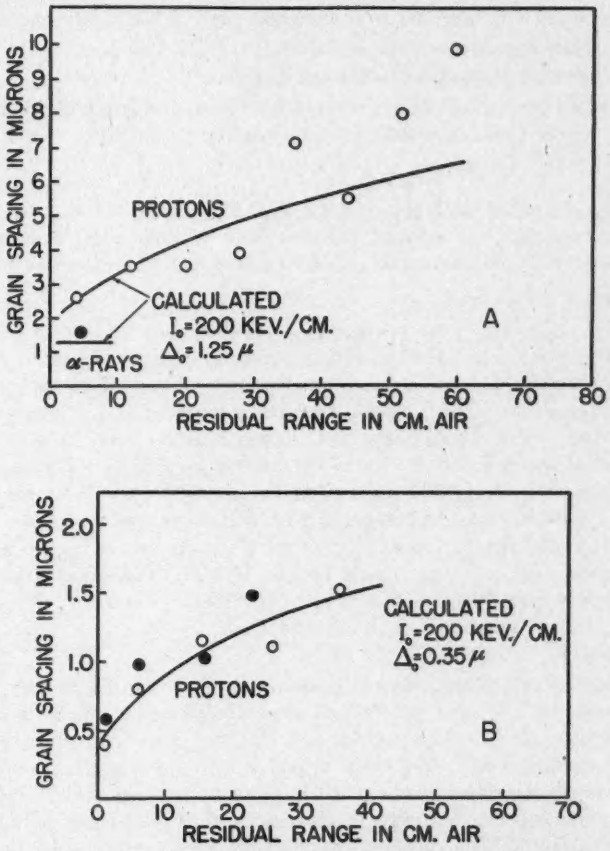

FIG. 1. *A. Measured grain spacing in microns is plotted against the residual range in centimetres of air for tracks of protons and α-rays in Eastman α-emulsion. Concentration c = 1 gm. silver bromide per cc. emulsion, and grain diameter d = 0.6 μ. The curves were calculated from the proposed theory, using the indicated values of the parameters.*

B. Measured grain spacing in microns is plotted against the residual range in centimetres of air for tracks of protons in Eastman α-emulsion concentrated by centrifuging. Concentration c = 4 gm. silver bromide per cc. emulsion, and grain diameter d = 0.6 μ. The curve was calculated with one parameter the same as in A, the other parameter different.

The composition of the Eastman α-emulsions was obtained as follows. The thickness of the gelatine layer on a plate was measured with the microscope. A plate was weighed, fixed, washed, dried, and weighed again. The loss in weight represents the silver bromide originally present. The weight of gelatine was obtained after the plate had been scrubbed free of gelatine and weighed again. The results were as follows:

Silver bromide: 40% of emulsion by weight
$c = 1.04$ gm. silver bromide per cc. emulsion
Density of emulsion = 9 mgm. per cm.^{2}, 2.6 gm. per cc.
Thickness of emulsion = 34.5 μ
Density of gelatine = 1.6 gm. per cc.

The developed grains were seen to be quite uniform and had a mean diameter of 0.6 μ. From these data the minimum spacing should be

$$\triangle_0 = 4.2 \times 0.6\ \mu/1.04 = 2.4\ \mu,$$

which does not agree with the spacing of 1.6 μ found in α-ray tracks. It seems unlikely that the composition was 50% in error, and a more likely explanation is that the mean grain diameter was only 0.4 μ before development.

2. *Eastman α Centrifuged*

In order to increase the concentration of silver bromide in an emulsion, centrifuging was tried. It was convenient to start with Eastman α-plates and to remove the emulsion by soaking in water. When the melted emulsion was centrifuged, the silver bromide grains accumulated at the bottom of the tube, leaving a clear liquid above. The plug of silver bromide was melted, coated on a glass plate, and allowed to set and dry before use. The concentration was approximately 93% silver bromide or $c = 5$ gm. silver bromide per cc. emulsion, which may be compared with $c = 1$ gm. per cc. in the original emulsion. If the size and sensitivity of the grains have not been changed in the operations, the spacing should be one-fifth of its original value. The measured spacings along proton tracks, plotted in Figs. 1*A* and 1*B*, are approximately in this ratio. (Development was for 5 to 10 min. in D-19 at full strength.)

The effect of centrifuging on the appearance of proton tracks may be seen in Figs. 13*B*, 13*C*, 33, and 34. These show the proton tracks in Eastman α and in centrifuged Eastman α-emulsion. In the latter case the grains are practically contiguous. Fog was tolerable in the instance reproduced, although in other cases it was bad. Development spreads from isolated fog grains as well as from the grains in the tracks, thus producing black clumps. Although careful control of conditions might have led to consistently good results, it appeared preferable to avoid centrifuging and to try finer grained material.

3. *Eastman Type V-O*

Spectroscopic plates Type V are recommended for minimum graininess. Development was for 5 to 10 min. in D-19 at full strength. The tracks of

α-rays were seen in these plates with a grain size of 0.8 μ and a spacing of 2.1 μ. As these values are very high, no further work was done.

4. *Eastman Type 548*

Eastman Type 548 emulsions are extremely fine grained (grain diameter not greater than 0.1 μ) and have been recommended for making graticules. By the procedure described for Eastman α-plates, it was found that the thickness of emulsion Type 548 is 20 μ and the composition about the same: $c = 1.04$ gm. per cc. or 40% silver bromide. If d is taken to be 0.1 μ, $\Delta_0 = 0.4$ μ.

Some plates were irradiated with neutrons and then strongly developed for 15 min. in Eastman developer D-82. Proton tracks were occasionally seen, but they were weak and very difficult to find in the strong fog. Only a small fraction of the proton tracks present could be found. Figs. 2 and 3 show the grain spacing along the tracks, varying from 0.9 to 1.6 μ. The grain size after development was 0.2 μ.

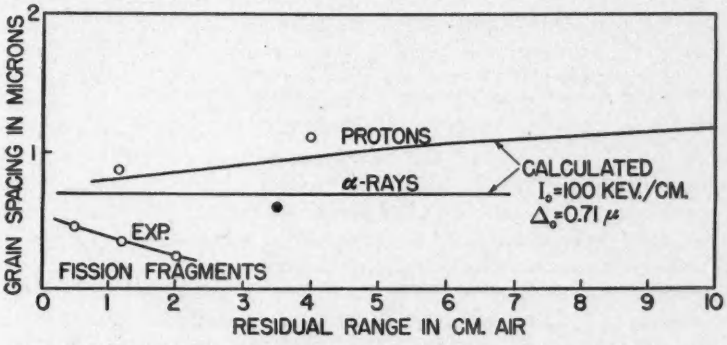

FIG. 2. *Measured grain spacing in microns is plotted against the residual range in centimetres of air for tracks of protons, α-rays, and fission fragments in Eastman 548 emulsion. Concentration $c = 1$ gm. silver bromide per cc. emulsion, and grain diameter $d \leq 0.1$ μ. The curves for protons and α-rays were calculated with the common pair of parameters shown.*

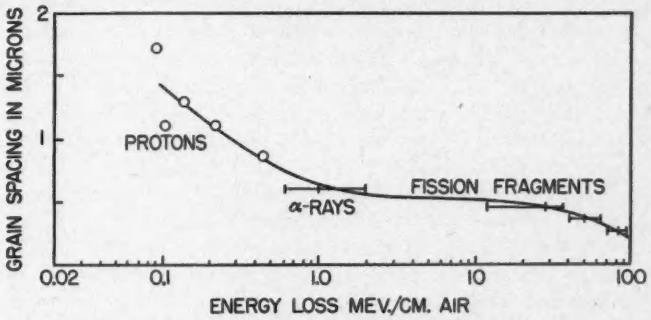

FIG. 3. *Measured grain spacing in microns is plotted against the specific energy loss in million electron volts per centimetre of air on a logarithmic scale, for tracks of protons, α-rays, and fission fragments in Eastman 548 emulsion.*

The tracks of α-rays could be brought out with a five minute development in D-19, which is insufficient to bring out proton tracks. The grain spacing along the α-ray tracks was 0.6 μ (Figs. 2, 3), and the size of the grain increased with increasing development. The stopping power of the emulsion for the α-rays of thorium C′ was 1415 times that of air. The standard deviation on the range of these α-rays was found to be 1.8%, while it was 2.5% on the shorter tracks of the α-rays of thorium C.

Reasonably good tracks of fission fragments were obtained in this emulsion (Fig. 26); a more complete description of this work will be given later.

5. *Emulsions Made by Jdanov*

The first series of emulsions to be made from the separate constituents followed the lines indicated by Jdanov (10), whose results, reproduced in Table I, will be discussed in this section. Two solutions are made up; Solution I

TABLE I

EMULSIONS MADE BY JDANOV (10)

EMULSION E_1

Solution I: 4 gm. potassium bromide, 3.5 gm. gelatine, 52.5 cc. water.

Solution II: 5 gm. silver nitrate, 1.75 gm. gelatine, 52.5 cc. water.

Add Solution II to Solution I at 60° C.

Emulsions E_2, E_3, and E_4 are made from similar recipes.

EMULSION L

Solution I: 5 gm. potassium bromide, 20 gm. gelatine, 300 cc. water.

Solution II: 6 gm. silver nitrate, 10 gm. gelatine, 300 cc. water.

Add Solution II to Solution I at 39° C.

Emulsions L_1, L_2, L_3, L_4, and L_5 are mixed at other temperatures.

Type	Temp., t, ° C.	d, μ	Concentration of AgBr in emulsion[1]			Δ_0, μ	α-Rays Δ, μ	Protons Δ, μ
			c, gm./cc.	%, vol.	%, wt.			
E_1	60	1	1.4	22	51	3.0	2.7	Weak
E_2	60	0.4	0.7	11	33	2.2	2.2	—
E_3	60	0.8	2.5	39	72	1.2	1.5	2–4.2[2]
E_4	60	1.2	3.7	57	84	1.2	1.4	None[2]
L	39	0.03				0.43	None	—
L_1	40	—	0.34	5.2	18	—	Very weak	
L_2	45	—					Weak	
L_3	50	—	(0.30)[3]	(4.7)[3]	(16)[3]	—	Moderate	
L_4	55	—					Clear	
L_5	60	0.2–0.4				4.3	~4.3 clear	—

[1] *Washed to remove soluble salts and dried.*

[2] *No proton tracks were observed after an 8 to 10 min. treatment with pinakryptol yellow in concentrations 1/5000 to 1/2000, and a 40 to 50 min. washing in running water.*

[3] *Calculated for the emulsions dried but not washed.*

contains potassium bromide and gelatine, and Solution II contains silver nitrate and gelatine. Solution II is added to Solution I while stirring proceeds. Concentrations and excess of bromide over silver vary from one emulsion to another, as well as the temperature t at which mixing is done. Emulsion E_3, used by Jdanov and co-workers, was recommended for proton tracks. The L-series of emulsions is interesting for the diameter d of the grains is varied from 0.03 to 0.3 μ by changing the temperature t while the concentration c is held constant at 0.3 gm. silver bromide per cc. emulsion. In this case

$$\Delta = \frac{4.2}{0.3}\frac{d}{P}.$$

The probability P of development is nearly unity when $d = 0.3\ \mu$, and must be very small when $d = 0.03\ \mu$ for then no tracks were seen (Table I).

6. *Extension of Jdanov's Work*

The writer followed Jdanov's formula for the L-emulsions and confirmed his results. In addition to repeating the work on these emulsions, the writer made exhaustive tests on the possibilities of formulas of the same type, which are labelled X1, X2, X3, X4, and X10 and which contain twice, three times, etc., respectively, the amounts of salts in the two solutions used for X1. The emulsions were poured on glass plates (7 cc. on a plate 8 by 11 cm.) and allowed to set. While X1 and X2 dried satisfactorily, the more concentrated ones containing too much soluble salts had to be washed and dried before use. If the temperature is low during the mixing of the two solutions or the concentrations of salts high, the gelatine may partially set during the reaction and a dirty emulsion results. Table II contains the information obtained from these experiments. It is seen that the average grain size increases as the temperature at the time of mixing is raised and also as the concentration of silver bromide is increased.

A modified series of X-emulsions was prepared in which about 5% of the silver was present as the iodide. (Such a proportion is often found in commercial light-sensitive emulsions.) The only noticeable change was a slight reduction in the size of grain.

The emulsions of the X-series were tested for recording the tracks of α-rays and fission fragments. A uranium disk was placed on the surface of the plate and irradiated with slow neutrons. The plate was developed for five minutes in D-19. In the case of α-ray tracks in X2 it is seen (Table II) that the grain spacing Δ decreases at first and then increases as the temperature t at the time of mixing is raised. The tracks of α-rays and fission fragments can be distinguished when Δ has nearly its minimum value; for larger grain sizes all tracks are alike, while for still smaller sizes, the tracks are invisible. Fig. 4 shows these results graphically; in plotting it plausible assumptions have been made on grain size, as exact measurements are not feasible below 0.2 μ.

If a comparison is made between X2 and Eastman 548, which have about the same values of c and d, the latter is better as regards differentiation of

TABLE II

Extension of Jdanov's work

Emulsion X1

Solution I: 0.5 gm. potassium bromide, 2 gm. gelatine, 30 cc. water.
Solution II: 0.6 gm. silver nitrate, 1 gm. gelatine, 30 cc. water.
Add Solution II to Solution I while stirring continuously.
Emulsions X2, X3, X4 and X10 are made with 2, 3, 4, and 10 times amounts of salts used for Emulsion X1.
d, Δ and Δ_0 are expressed in microns.

Emulsion	X1				X2				X3				X4			X10		
Gm. AgBr/gm. emulsion, %	18.1				30.7				39.9				46.9			69.0		
Cc. AgBr/cc. emulsion, %	5.15				9.8				14.0				17.8			35.2		
Gm. AgBr/cc. emulsion, ϵ	0.335				0.637				0.912				1.16			2.29		
Temp., ° C.	d	Δ_0	Δ_α	Δ_f	d	Δ_0	Δ_α	Δ_f	d	Δ_0	Δ_α	Δ_f	d	Δ_0	Δ_α	d	Δ_0	Δ_α
20, 25	—	—	—	—	$\ll 0.2$ d	$\ll 1.3$	i	i	—	—	—	—	<0.2 -0.3 d	<1.1	0.9	—	—	—
30	—	—	—	—	<0.2	<1.3	1.6 w	0.8 w	—	—	—	—	—	—	—	0.3 d	0.6	0.8
35	—	—	—	—	<0.2	<1.3	0.8 w	0.5 w	—	—	—	—	—	—	—	0.3 d	0.6	0.8
40	<0.2 c	<2.5	i	i	<0.2	<1.3	0.8	0.5	—	—	—	—	0.3	1.1	1	0.3 d	0.6	0.8
45	—	—	—	—	<0.2	<1.3	1.0	i	—	—	—	—	—	—	—	0.4 d	0.8	1.0
50	<0.2 -0.3 c	<3.8	>5	i	—	—	—	—	0.2	0.9	1.6	i	—	—	—	—	—	—
65	—	—	—	—	0.2	1.3	1.3	—	—	—	—	—	0.5	1.8	1.1	—	—	—
80	0.3 c	3.8	5	—	—	—	—	—	—	—	—	—	—	—	—	—	—	—

Code: α = *α-ray tracks,* f = *fission fragment tracks,*
i = *invisible tracks,* d = *dirty emulsion,*
w = *weak tracks,* c = *clear tracks.*

track, spacing of grains, and amount of fog. It is possible that the differences are due to the rather large range of grain sizes in X2.

Some tests were made on X2- and X4-emulsions centrifuged at about 50° C. Grains smaller than 0.2 μ in diameter did not settle completely. The mass formed at the bottom of the tube of the centrifuge, after being washed and

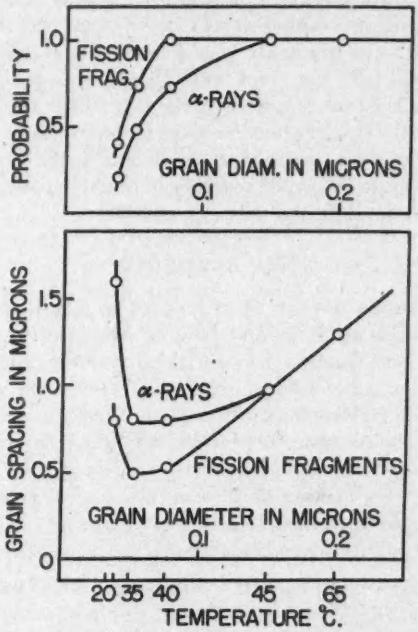

FIG. 4. *Upper. Probability of development is plotted against the grain diameter in microns for tracks of α-rays and fission fragments in Emulsion X2.*

Lower. Measured grain spacing in microns is plotted against the grain diameter in microns for tracks of α-rays and fission fragments in Emulsion X2.

The grain diameter is varied by changing the temperature at which the emulsion is made. The curves are not accurate, but their general behaviour is significant.

dried, had the following typical composition: 93% silver bromide by weight, 76.5% silver bromide by volume, and $c = 5.17$ gm. silver bromide per cc. emulsion. This emulsion does not melt or dissolve easily, hence it is difficult to spread it evenly on a plate.

In one case an X4-emulsion made at 40° C., in which d was 0.2 μ and Δ was 0.8 μ in the tracks of α-rays, was centrifuged, and in the concentrated emulsion d was 0.3 μ and Δ was 0.4 μ. The grains were practically contiguous in the track. Emulsions having the smaller grain sizes were chosen from the series X2 and X4 and were centrifuged. These showed improved tracks of fission fragments (Figs. 27*A* and 27*B*), which were clearer and better

defined than those seen in Eastman 548 emulsion. (The stopping power was about 1800 times that of air.)

It should be noted that the vertical dip of tracks is modified by the shrinkage of these concentrated emulsions that occurs in processing. The thickness of the gelatine layer is reduced to ½ to ¼ of its original value in fixing.

In agreement with the tests on Eastman α-emulsions that had been concentrated by centrifuging, spreading development often occurred in the centrifuged X-emulsions if the grain size was greater than 0.2 μ. Sometimes the development spreads from the track to large numbers of surrounding grains, which then form a huge black object in the field (Fig. 31). There may also be a broadening of the track, which happens preferentially near the end where the ionizing power of the α-ray is great, producing a club-like appearance. It is well known that grains clumped together in much coarser grained emulsions have a tendency to develop as a unit (13, p. 832).

New Emulsions

If the solutions mixed to form silver bromide grains in gelatine are concentrated, the first grains are large and grow by Ostwald ripening, because the concentrated bromide solution favours the formation and growth of large crystals and the last grains formed are small. Since very small and uniform grains are desired in conjunction with a high concentration, the precipitation of silver bromide should proceed between *dilute* reagents from beginning to end. The procedure used was suggested by a remark by Carroll (7); it has also been described for making positive emulsions by Baker (1, p. 100), and is similar in principle to the one followed by Sheppard, Lambert, and Swinehart (23) to obtain dilute silver bromide sols in the absence of gelatine.

The new emulsions were prepared from three solutions as follows. Equivalent volumes of silver (*A*) and bromide (*B*) solutions are run simultaneously and at equal rates into a solution of gelatine (*C*), which is stirred continuously and as vigorously as possible without excessive foam production. The details for six new emulsions are given in Table III. The rates of flow are controlled so that there is a small excess of soluble bromide over silver; for example Solution *B* should be 0.5 to 1 cc. ahead of *A*, although an occasional slight excess of *A* over *B* is not important. For the quantities shown in Table III, it takes about 30 min. to add *A* and *B* to *C*. The rates of flow are controlled by drawn capillaries of adjusted length below the stopcocks on the burettes containing *A* and *B* or preferably by stainless-steel needle-valves. Solution *C* is kept in a tray of thermostatically controlled water usually at 40° C.

The emulsion is poured into a flat tray, 12 by 18 in., cooled in ice water to set. It is then washed with running cold water for six to eight hours to remove the large amount of potassium nitrate present. The emulsion is removed, melted, and coated on a glass slide (1 cc. on 2.5 by 7.5 cm.) and left to set. (Such a layer measures about 40 μ at the centre when dry). The relative humidity of the air should be 60 to 80%, otherwise the emulsion

TABLE III

NEW EMULSIONS

Solution A: 0.6 gm. silver nitrate per cc.
Solution B: 0.42 gm. potassium bromide per cc.

Formula	Solution			% AgBr	c, gm. AgBr/cc.	d, μ
	A, cc.	B, cc.	C			
I	30	30.5	75 cc. H_2O 4.5 gm. gel.	81.6	3.34	≤0.1
II	30	30.5	50 cc. H_2O[1] 4.5 gm. gel. 25 cc. alcohol	81.6	3.34	≤0.1
III[2]	30	30.5	75 cc. H_2O 4.5 gm. gel.	81.6	3.34	0.1–0.2
IV	30	30.5	25 cc. H_2O 1.5 gm. gel.	93	5.17	0.1–0.15
V	30	30.5	25 cc. H_2O 0.75 gm. gel.	96.4	5.6	~0.2
VI[3]	30	30.5	I or II	—	—	—

[1] *Melt gelatine in water, then add alcohol while solution is stirred.*
[2] *Temperature control was different from that in I and II.*
[3] *Chlorine or iodine partly or wholly replacing bromine in Solution B.*

is likely to peel off its glass support. This tendency to peel off, which is due to the high concentration of silver bromide, is reduced if the layer is thinner and of smaller area. As these emulsions are not very sensitive to light, all operations listed above can be performed in red or amber light.

Digesting occurs on keeping the emulsions; the sensitivity rises in the course of a few days whether the emulsion be in the form of a jelly or dried on plates. Since fog increases with time it is advisable to keep the plates in an ice-box.

Excellent tracks were obtained in Emulsions I and II: Formula II is most highly recommended. The use of denatured alcohol was suggested by Wall's statement that it prevents coarse grain formation in emulsions containing ammonia (24). Although the present emulsions contain no ammonia, alcohol does greatly reduce fog and clump formation. Very reproducible results were obtained.

Unlike Emulsion I, II after washing occasionally does not melt when heated. Syneresis occurs, the emulsion contracting by one-tenth to one-fifth of its volume and giving off a liquid that contains little or no gelatine. If the supernatant liquid is expelled, the remaining gel may be melted by heating and stirring.

Emulsion III is the same as I except for temperature control. Several tests were made in which Solution *C* was brought up to 50° C., then Solutions *A* and *B* were added while the temperature fell to 20° to 30° C. Froth appeared or the gelatine partially set below 30° C., and the resulting emulsion was dirty. Sometimes excellent proton tracks were obtained after weak development, and still denser tracks were obtained if the emulsion was concentrated by centrifuging (Fig. 32*A*, *B*, *C*). Even by mixing the solutions at a chosen temperature, consistently good emulsions of this character could not be produced.

Emulsion IV contains 93% silver bromide, which is the same as that obtained by centrifuging III. When heated after washing it suffers syneresis, the volume contracting to $\frac{1}{3}$; and when coated on glass it has a tendency to peel off. Good proton tracks have been recorded in IV.

Emulsion V suffers syneresis during the mixing of Solutions *A* and *B* into *C*. Since it does not adhere to glass very well it is not satisfactory.

Emulsion VI was made with iodine or chlorine partly or wholly replacing the bromine. Pure iodide emulsions are insensitive even to fission tracks. Pure chloride emulsions have occasionally shown proton tracks, but they fog too easily. If 25% of the bromine atoms are replaced by iodine, fission tracks can be recorded, but the emulsion is insensitive to other particles. If a few per cent of the bromine atoms are replaced by iodine or chlorine or both, no worthwhile improvement in sensitivity is found.

Development was for 5 to 15 min. in Eastman's D-19. A still stronger development was occasionally used: 5, 10, or even 15 min. in Eastman's D-82. Too strong a development brings out excessive fog; on the other hand, if it is too weak, only fission tracks appear. Fixing may be lengthy if the coating is thick; stirring of the fixing bath is then helpful.

Nuclear Physics Experiments with Emulsions

Some of the nuclear physics experiments were carried out in preliminary work and have been described in part above. Most of the best tracks were recorded in the new emulsions. Tables IV and V show some collected results.

1. *α-Rays of Uranium and Thorium C'*

Fig. 17 shows the track of an α-ray from uranium in the new Emulsion II. Standard deviations on the range and energy have been determined by measuring about 60 tracks in each case (see Table V). The two α-ray groups of U^{238} and U^{234}, which were recorded simultaneously, are easily distinguished. For the α-rays of thorium C' the standard deviation is 2% on the range or 1.3% on the energy. In Eastman 548, which contains less silver bromide, the corresponding values are 1.8% and 1.1%; but the visibility of the tracks is not as good as in Emulsion II. The main cause of these deviations is not the grain spacing but straggling of the range, which is known to increase with atomic weight. Gelatine shift may be a contributing cause of the deviations in range.

2. *Protons from* N^{14} (n, p) C^{14}

As gelatine contains 5 to 15% nitrogen, emulsions irradiated with slow neutrons show numerous short proton tracks from the reaction N^{14} (n, p) C^{14}. Figs. 15*A*, *B*, *C* are examples obtained with Emulsion II. The standard deviations are small for such short tracks, 5.2% on the range (1.06 cm.) and 3.5% on the energy (0.62 Mev. (12)). The deviations are nearly four times as great in Eastman α.

3. *Proton Recoils from* D^2 (d, n) He^3 *Neutrons*

Proton recoil tracks were recorded in emulsions placed near the target of the Ottawa high tension set. The neutrons from the reaction D^2 (d, n) He^3 that are emitted at an angle of 110 degrees from the beam of deuterons are monokinetic (2.4 Mev.). The proton recoils in the forward direction have therefore a small energy spread. The standard deviations were 3.35% on the energy and 5.4% on the range in the new emulsions.

4. *Proton Recoils from Po-*α*-Be Neutrons*

A large number of proton tracks, each equivalent to several cm. of air, have been seen. Figs. 13*D*, *E* show the beginning and end of a proton track having a range of 60 cm. in air (Emulsion II). The end of a proton track is usually defined within $\frac{1}{2}$ mm. of air; the beginning of tracks 60 to 100 cm. long is usually defined within 1 to 2 mm. of air and sometimes within $\frac{1}{2}$ mm. as in the example shown.

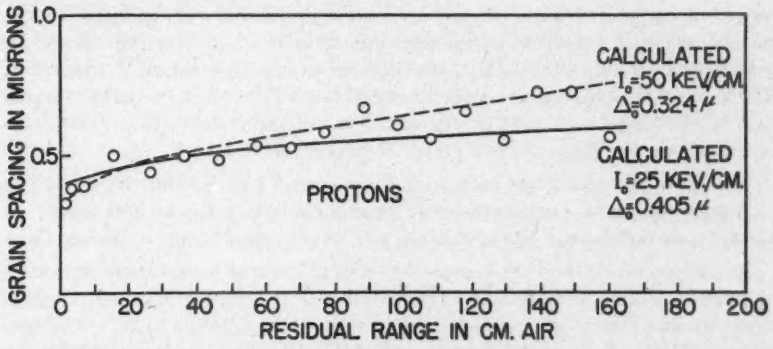

FIG. 5. *Measured grain spacing in microns is plotted against the residual range in cm. air for tracks of protons in Emulsion II. Concentration* $c = 3.3$ *gm. silver bromide per cc. emulsion, grain size* $d \leq 0.1$ μ. *The two curves were calculated from the proposed theory, using the parameters shown. These indicate the range of permissible choice.*

The advantage of the new emulsions is more marked on the short ranges. Reasonably good measurements are possible at 3 mm. of air, which corresponds to an energy of 200 kev. for protons and 400 kev. for α-particles. Grain spacing, grain size, and resolving power are the limiting factors. Grain spacing along proton tracks is plotted in Fig. 5.

The directions of proton tracks can now be ascertained very accurately. Deviations are visible in Figs. 32*A*, *B*, and *C*, especially near the end of the range. Four forks representing proton–proton collisions have been seen. Two of these nearly right-angled forks are shown in Figs. 28 and 29.

5. *Particles from the Reaction* Li^6 (n, α) H^3

Fig. 16 shows the tracks of an α-ray and a triton, obtained by irradiating Emulsion II containing lithium chloride with slow neutrons. This is a good example of differential sensitivity.

6. *Fission Tracks*

The tracks of fission fragments have been recorded in photographic emulsions by Myssowsky and Jdanov (14), Perfilov (17), and Borst and Floyd (6).

The writer has obtained numerous examples of the tracks of fission fragments in Eastman 548 and the new emulsions. Two variations of the technique have been employed. In the first method a disk of uranium metal was laid upon the emulsion, the two wrapped in black paper, and exposed to neutrons. In the early work the irradiation was performed for several hours in a paraffin box containing a source of neutrons consisting of 1 gm. of radium mixed with beryllium. The plate was shielded from the direct action of the γ-rays by 5 cm. of lead. Eastman 548 plates were processed in D-19 for five minutes. In nearly every field of view a few thick tracks were visible, which started at the surface and dipped into the emulsion. Their appearance is characteristic of fission fragments, as the tracks become thinner towards the end of the range, in agreement with the known ionizing properties. The effect of the α-rays was to form a netted background of light fog. The fog caused by γ-rays was tolerable until the plate had received a few hundred roentgens. The longest fission tracks recorded were about 17 μ or 2.4 cm. of air, which may be compared with 2.85 cm. obtained in a cloud chamber (5). The mean spacing $\triangle$ in the Eastman 548 emulsion was about 0.4 μ.

The same procedure was used with Emulsions X2 or X4 centrifuged. The fission tracks stand out prominently among the α-ray tracks and are much clearer than in Eastman 548 (Figs. 27*A*, *B*), as they appear like unbroken lines.

In the second method the complete tracks of pairs of fission fragments were recorded. Plates were soaked in uranium nitrate solution for five minutes, dried, and irradiated with slow neutrons from a chain reacting pile. The best concentration of uranium nitrate is 1/16% $UO(NO_3)_2 \cdot 6H_2O$. A smaller concentration shows too few tracks, while a larger concentration desensitizes the emulsion and the tracks contain fewer grains. Several complete tracks were measured. Their lengths show a distribution with a standard deviation of 5% from the mean value. This deviation is due mostly to the diverse mass and energy of the fragments, and not as in the cases of α-rays and protons to the ordinary straggling of ranges.

Fig. 26 shows the complete tracks of pairs of fission fragments in Eastman 548 emulsion, while Figs. 19 to 25 show complete tracks in the new emulsions.

It will be noted that the fission tracks stand out prominently amidst the tracks of α-rays and protons; an α-ray track is visible in Fig. 19. Figs. 17 and 19 show the tracks of α-rays and fission fragments in the same emulsion. The variation of the specific ionization from the centre of the pair of fission fragment tracks, where fission occurred, to the ends is clearly shown by the varying width. The point of fission cannot, however, be located very exactly by visual inspection. In Eastman 548 the grain spacing varied between 0.6 μ and 0.2 μ along the track. In the new emulsions the tracks are so well marked and dense that the single grains are not always recognizable and that grain spacing cannot be determined with its usual meaning.

Cloud chamber pictures of fission tracks, such as those of Bøggild, Brostrøm, and Lauritsen (5), show clearly numerous deviations and short side branches due to projected nuclei. Although the tracks in emulsions do not show as much of the detail, there are many examples of deviations and side branches, which may be due to hydrogen, carbon, nitrogen, oxygen, bromine, and silver nuclei (Figs. 19 to 24).

Figs. 25, *A* to *F*, show a complete pattern of tracks, which are not all contained in one plane. The three branches have comparable specific ionizations, possibly nearly the same mass, and not very different ranges (1 cm. for one track and 1.5 to 2.0 cm. for the others). The angles suggest conservation of momentum between three particles of about equal mass. If triple fission occurred the appearance could be like this. However, one of the branches may well be a silver or bromine nucleus knocked on by one of the pair of fragments, near the point of common origin.

The fission of thorium by fast neutrons was also shown by the emulsion technique. Thorium metal was laid on Eastman 548 emulsion, and irradiated for several days with a strong Po-α-Be source of neutrons. Dense tracks dipping into the emulsion, similar to those obtained from uranium, were seen after development.

7. *Electrons*

Whenever a very sensitive emulsion had been obtained, where grain spacing was very small at the beginning of long proton tracks, some faint complicated

TABLE IV

COMPARISON OF EMULSIONS

	New emulsions	Eastman α centrifuged	Eastman α	Ilford halftone
% AgBr, wt.	81.6	80–90	40	$\sim$ 40
Conc. c AgBr, gm./cc.	3.3	3–4	1.0	$\sim$ 1
Stopping power (rel. to air)	1600	1800	1400	$\sim$1400
Developed grain diam., μ	0.1–0.3	0.6	0.6	$\sim$ 0.5
Δ, cm. air, end of proton track	0.05	0.1	0.3	—
Δ, cm. of air, beginning 6 Mev. proton track	0.05–0.1	0.3	1	—

TABLE V

COMPARISON OF TRACKS

σ_1 = standard deviation on range in centimetres air.
σ_2 = standard deviation on energy in Mev.

Particles	New emulsions		Eastman α	Ilford halftone	Cloud chamber
	σ_1	σ_2	σ_2	σ_2	σ_2
UI α, 2.6 cm., 4.09 Mev.	0.065 2.5%	0.075 1.8%	0.24 5–6%	0.25 (18) —	— 0.4–0.6%
UII α, 3.2 cm., 4.7 Mev.	0.09 2.8%	0.09 1.9%	— —	— —	— —
ThC′ α, 8.5 cm., 8.78 Mev.	0.18 2%	0.16 1.3%	0.3 2.5%	— —	— —
Protons, 1.06 cm., 0.62 Mev.	0.055 5.2%	0.02 3.5%	0.08 14%	— —	— —
Protons, 9.0 cm., 2.4 Mev.	0.49 5.4%	0.08 3.35%	— —	0.15–0.2 6–8% (28)	— ~1.1%

tracks consistently appeared. These are attributed to electrons in the last one or two centimetres of their range, usually due to γ-rays or cosmic rays. One instance is reproduced in Fig. 30, although it is realized that the loss of detail in reproduction will make the track difficult to see.

Action of Various Chemicals on Emulsions

Emulsions to be tested were prepared according to Formula I or II, and sensitivity changes between treated and untreated parts of the same plate or of the same batch were estimated from the grain spacing in proton tracks. The treatment preceded irradiation.

1. *Dyes*

In some cases the dye was added to the emulsion before coating and amounted to 0.05% dye when dry; in other cases the dried plate was soaked in a 1 or ½% solution of the dye for three minutes.

No effect on sensitivity was observed from the following:

Acid fuchsin
Alizarin red S. (leaves reddish masses)
Bromo cresol green
Bromothymol blue
Chlorophenol red
Chromotropic acid (leaves yellow crystals)
Meta cresol purple
Phenol red.

Methylene blue induces a strong fog. The following dyes, which are known desensitizers, decrease the size of the grains either in the tracks or in the fog, and reduce sensitivity to some extent:

Neutral red
Rhodamine B
Rhodamine 6G.

Two dyes that are known to act either as sensitizers or as desensitizers occasionally reduced and never increased sensitivity in the tests:

Pinakryptol green
Pinakryptol yellow.

Three other dyes, the second of which is a known desensitizer, reduced sensitivity:

Diphenylamine blue
Phenosafranine (marked effect)
Tartrazine.

The following dyes improve sensitivity; they are listed in the approximate order of increasing effect observed:

Fluorescein
Dichloro R fluorescein
Chromotrope F 4B
Erythrosin (tetraiodofluorescein)
Methyl violet
Rose bengal
Eosin (tetrabromofluorescein).

Sensitizing occurred only when the emulsion was actually stained. A positive or negative effect on sensitivity appeared only with dyes that have known ability to be adsorbed on silver halides (Yoe and Sarver (29)). Eosin seems to be the most useful of these sensitizers. Fig. 6 was obtained from measurements on tracks in the two halves of the same plate, one untreated, one treated with eosin and dried. The best conditions are to bathe the plate

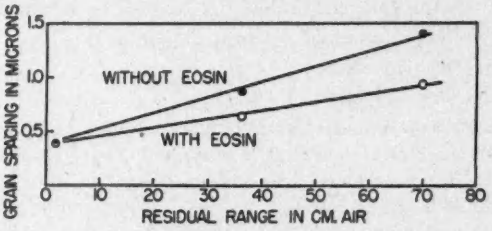

FIG. 6. *The reduction in grain spacing, brought about by eosin treatment, is shown for proton tracks in Emulsion II. Concentration* $c = 3.3$ *gm. silver bromide per cc. emulsion, grain size* $d \leq 0.1\ \mu$.

3 to 10 min. in a 1% solution of eosin. Prolonged treatment reduced the sensitivity, while a 0.001% solution has very little effect. It is not advantageous to add the dye to Solution *C* before making the emulsion.

2. *Nitrogen Compounds*

Since several nitrogen compounds produce complex salts with silver halides, some action is expected. Ammonia and triethanolamine are known to hypersensitize emulsions containing a colour sensitizing dye. Hypersensitizing may increase that part of the spectral sensitivity that is due to the action of the dye and even the part in the blue and violet region. Bathing plates already stained with various dyes in 1% ammonia for three minutes brought about an increase in sensitivity in all cases. The same effect of ammonia was also found for unstained emulsions.

The action of several organic compounds containing nitrogen was studied. Either 1% aqueous solutions or saturated solutions in weak alcohol were used. The treatment lasted three minutes. Nearly all substances having basic properties were active. The following decreased sensitivity and increased fog:

Diaminophenol hydrochloride (saturated)
Hydroxylamine hydrochloride.

Hydrazine induced strong fog and even blackened the undeveloped dried emulsion when it stood overnight, after soaking in a 1% solution. The following had little effect or decreased the sensitivity:

Diphenylamine (saturated solution)
Pyridine
Urea.

Ethylenediamine and hydroxyethylethylenediamine occasionally increase sensitivity, but they also increase grain size in the developed emulsion and may induce strong fog. The first is the more active. The following increased sensitivity without much increase in fog:

Acetonitrile
Aniline
Diethylamine
Diethylaniline
Hydroxyethylorthotoluidine (saturated solution)
α-Naphthylamine (saturated solution)
Triethanolamine
Trimethylamine.

Of these, the most promising are diethylamine, triethylamine, and triethanolamine, which are even more active than eosin and do not stain the emulsions. As the three act very much alike and the first two have objectionable smells, triethanolamine is most convenient to use. Prolonged treatment reduces both sensitivity and fog, which action is different from digesting. Plates treated with triethanolamine develop less fog on keeping than those treated with ammonia.

3. *Hydrogen Peroxide*

Hydrogen peroxide is a known intensifier of the latent image, if applied between irradiation and development (Neblette (16)). This effect on proton

tracks was observed, following a one- to five-minute treatment in 0.01% hydrogen peroxide.

4. *Chromic Acid*

(1) Chromic trioxide (2%) with sulphuric acid (1%) destroys sensitivity centres in five minutes according to Sheppard (22). Such a treatment was applied to Eastman α, Eastman 548, and X4 plates, which were then washed thoroughly. The Eastman α-plates showed α-ray tracks with increased grain spacing and no proton tracks, while the other plates recorded α-ray and fission tracks without much change. This is in general agreement with Wambacher (25), who found that chromic acid reduces sensitivity of certain emulsions to α-rays.

These experiments should now be interpreted as showing the importance of active centres in promoting sensitivity to protons and to a lesser extent to heavier particles. Presumably the same active centres are responsible for sensitivity to light and to ionizing particles.

(2) A one-minute treatment with 5% chromic trioxide and 2.5% sulphuric acid applied to Emulsions I or II removed fog to a remarkable extent, but it had little effect on sensitivity. On the other hand, a 15 min. treatment with $\frac{1}{2}$% chromic trioxide and $\frac{1}{4}$% sulphuric acid removed fog to the same degree, but it considerably affected sensitivity. These tests show that a chemical difference exists between fog or development centres, and active centres, in accord with other evidence. Further study by similar methods on the kinetics of the removal of both should bring important information on their nature. Active centres are known to contain less silver and more silver sulphide than development centres.

An emulsion so treated has lost to a variable degree its original sensitivity. Sensitivity may then be improved or restored by ageing or by a triethanolamine treatment in such a way that very dense proton tracks with very small grain size can be obtained with almost no visible fog.

(3) Emulsions may be prepared, coated, and dried in white light if they are afterwards treated with chromic acid in red light, which removes the latent fog. Emulsions suitable for recording the tracks of fission fragments against little background can be prepared in this way. Sensitivity to protons is negligible after this treatment, but it may increase with time.

5. *Ammonium Persu'phate*

Concentrations of 0.002 to 2% ammonium persulphate removed fog from emulsions but reduced sensitivity more than chromic acid for the same amount of fog removed.

Effect of Ionizing Particles on the Photographic Grain

1. *Proposed Mechanism*

In the theory of Gurney and Mott (9), which has also been described by Webb (26) and Berg (2), the action of light in forming a latent image is essentially as follows. A quantum of light of suitable wave-length is absorbed

by resonance in the silver bromide, and by photoelectric effect brings an electron from its normal state in a Br^- ion to an energy level in the conduction band of silver bromide. The electron may then migrate through the lattice, leaving behind a neutral bromine atom, which is a positively charged potential hole. The electron may become trapped on an active centre owing to its lower potential energy there. Active centres are specks of silver sulphide and silver on the crystal, which are essential for its sensitivity. The active centre, being negatively charged, attracts Ag^+ ions, which have the ability to migrate. In this way neutral silver atoms can accumulate on the active centre, which becomes a development centre if sufficiently enlarged with silver.

In the case of ionizing particles, the mechanism should be the same except for the first stage. Electrons are brought into the conduction band not by the photoelectric effect but by ionization by collision in the crystal. A few electrons may also come into the crystal after being produced in the gelatine immediately surrounding it. In gases the energy spent by a fast particle in producing an ion pair is about the same for all gases and all particles, about 30 ev. Professor N. F. Mott has pointed out to the writer that in silver bromide this energy should be much less. Nearly all the energy should be spent ultimately in bringing electrons into the conduction band, which requires a minimum expenditure of 3 ev. If an electron in this band possesses kinetic energy in excess of 3 ev., it will bring another electron into the conduction band. We may, therefore, expect a total energy of 3 to 6 ev., say 5 ev., spent per electron brought into the conduction band.

These views could be tested by experiments on the amount of visible image formation or on the photoconductance in silver bromide under the influence of α-rays, protons, β-rays, or γ-rays.*

An ordinary silver bromide grain to become developable requires the absorption of at least a few, say 10, and at most a few thousand quanta of light of about 3 ev., the average number being 100 or a total energy of 300 ev. It is interesting to compare this with the sensitivity of emulsions to the effect of various radiations. According to Eggert and Noddack (8), some 150 kev. energy is spent by X-rays per grain developed in one commercial emulsion. In one of the writer's emulsions the energy spent was 470 kev. for 100 grains developed, near the beginning of the track of a 12 Mev. proton. Since half of the volume was gelatine, about 250 kev. was spent in silver bromide or 2500 ev. per grain developed. Since not all the grains traversed by the proton were developed, but only a fraction of the order of one-fifth or one-tenth, the energy spent in each grain was therefore 250 to 500 ev. This corresponds to the release of 50 to 100 electrons if the energy spent per electron is 5 ev. If the energy spent per electron were 30 ev., it would correspond to 9 to 18 electrons released; such a sensitivity of the grain appears too high.

*Note added at the proof reading stage.—Van Heerden has proved that these views are correct, by measurement of the ionization current in silver chloride crystals caused by single rays: P. J. Van Heerden. "The crystal counter, a new instrument in nuclear physics". Thesis, Utrecht, 1944.

From the following two effects we would expect that the number of electrons required to be set free in a grain before it will develop is greater in the case of ionizing particles than in the case of light of a suitable intensity level.

The first effect is related to the failure of the reciprocity law at high intensity of illumination. It is known that in general a given flux of light will be most effective on an emulsion, when applied in a continuous exposure of duration t, for a certain optimum value of t. If the same total flux is applied using either a shorter time and a higher intensity, or a longer time and a lower intensity, the exposed plate is not blackened so much. The effect of an ionizing particle is completed in an exceedingly short time as compared with the times practicable in the case of light. The primary effect of the passing particle may last only 10^{-13} sec. or less. We may therefore expect as low an efficiency as can be obtained by reducing the exposure time t to the utmost.

The second effect has no exact parallel in the case of light. It is one of recombination of ions, and at present there is no direct experimental proof of its importance. Electrons and positive holes of potential when formed by the passing particle in the crystal are all located initially near a linear axis inside a cylinder of very small diameter in the silver bromide grain. The electrons tend at once to migrate away and reach the active centres; but this tendency may be strongly opposed by the high linear density of positive holes left in the crystal, if the latter migrate but slowly as is probable. This positive core creates a strong attractive field for the electrons, which have therefore a great chance of staying in that core, and of recombining with a positive hole, being then lost for the photographic process. Suppose the same number of electrons are created by light absorption in the same time; they would appear at points distributed at random throughout the volume of the crystal or on the surface, leaving on the average no particular regions where the positive holes of potential are densely grouped. Electrons produced by light, even under conditions of high intensity of illumination, are therefore more likely not to recombine with the positive holes, and to contribute finally to latent image formation.

Such an effect, which may be called a positive charge concentration effect, may come into play if the energy loss per unit length is large enough, and if the actual diameter of the cylindrical space where ionization is set up is small enough with respect to the dimensions of the crystal. These conditions are probably nearly fulfilled in the cases of α-rays and of protons of a few million electron-volts energy, in emulsions of not too small grains.

With the proposed mechanism, we may try to explain the sensitizing and the desensitizing effects observed. They are due exclusively to substances liable to be adsorbed, or forming compounds with the silver halide, in agreement with Vogel's law.

Optical sensitizing is due to increased absorption of light at the surface of the crystal, but as the stopping power is not changed by sensitizing, the improvement cannot be ascribed to increased production of electrons. It is not definitely connected with fluorescence, as the most active fluors are not

the best sensitizers. It appears rather to be connected with improved collection of electrons, and then of silver ions, by the active centres, whether the influence be through a modification of the active centre itself, of the surface, or of the mass of the crystal. A surface change seems most probable. That it is not due to an intensification of the latent image after its formation or to an effect enhancing development has been checked directly in the cases of eosin, ammonia, and triethanolamine.

The desensitizing effect is now accepted to be in most cases an oxidation phenomenon leading to regression of the latent image, and it does not seem impossible that the same substance be a sensitizer enhancing formation of an efficient latent image, and a desensitizer later oxidizing it, whether in the presence of air or not. Such consideration might explain the dual properties of pinakryptol yellow and green.

The fact that prolonged triethanolamine treatment decreases sensitivity and fog, while prolonged digesting decreases sensitivity and increases fog, suggests that sensitizing does not affect the formation and growth of the active centres in the same way as digesting. However, there may be an indication to the contrary in the following observation. The two effects seem to be complementary; a fully ripened emulsion is little improved by sensitizing, and a sensitized emulsion is little improved by ripening.

2. *Quantitative Theory*

The following theory gives a fair account in most cases of the grain spacings observed, while it is insufficient to explain certain other features.

Let l be the length of path of an ionizing particle in a grain, and E_l the corresponding energy spent by the particle. The path varies between zero and d, the diameter of the grain, which is assumed to be spherical. If E is the maximum energy that is spent in the grain ($l = d$) and I is the mean energy loss per unit length,

$$E_l = Il = El/d\,.$$

We shall assume that a grain having received energy E_l has the following probability of being developed:

$$1 - e^{-E_l/E_0}\,,$$

where E_0 is a constant of the emulsion. Let P be the probability that a grain be developed if the ionizing path goes through it at random. Assuming that equal elements of cross-section in the sphere have equal chances of being hit by the particle, whose track is assumed to be linear,

$$\begin{aligned} P &= \int_0^d (1 - e^{-El/E_0 d})\,\frac{2l\,dl}{d^2} \Big/ \int_0^d \frac{2l\,dl}{d^2} \\ &= 1 - (2/x^2)\,(1 - e^{-x} - xe^{-x}) \\ &= 2x/3 - x^2/4 + x^3/15 - x^4/72 \ldots\,, \end{aligned}$$

where $x = E/E_0 = I/I_0\,.$

In the formu'a for the grain spacing,

$$\Delta = \Delta_0/P = 4.2\, d/cP\,,$$

we may regard P as a function of E/E_0 or I/I_0, where I is the mean energy loss per unit length at the point considered, and I_0 is a constant. Sensitivity may be defined as the reciprocal of I_0. In this form, which contains only one adjustable parameter (I_0), the theory does not hold except as a rough approximation for large grains. On the other hand, if Δ_0 and I_0 are both regarded

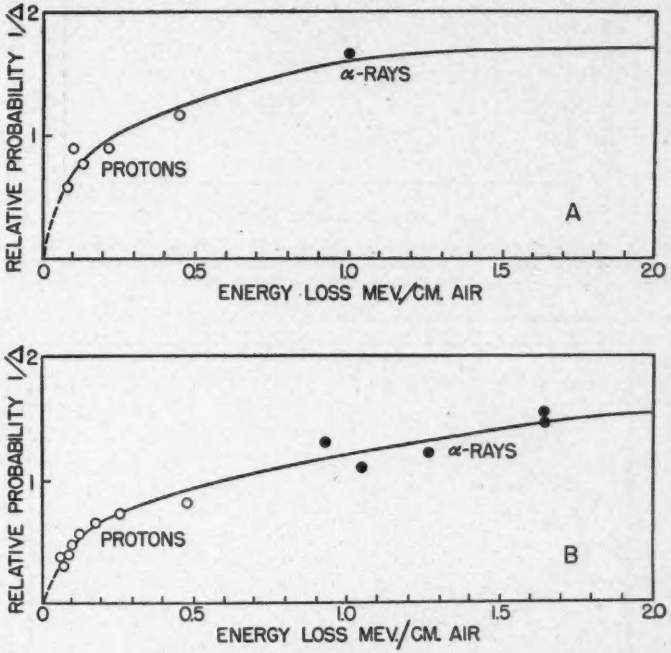

FIG. 7. *A. Relative probability of development or reciprocal of grain spacing is plotted against the specific energy loss in million electron volts per centimetre of air for tracks of protons and α-rays in Eastman 548 emulsion.*

B. Similar plot for Emulsion II with gelatine added. Concentration $c = 1$ gm. silver bromide per cc. emulsion and grain diameter $d \leq 0.1\ \mu$, for both emulsions.

as adjustable parameters the measured grain spacing can be approximately fitted for protons, α-rays, and fission fragments in most emulsions used.

For convenience, the probability P of development of the grains is plotted from the expression above against x ($= I/I_0$) in Fig. 8. The specific energy loss in million electron volts per centimetre of air, calculated from theoretical formulae (5, 12), is shown as a function of the residual range for protons, α-rays, and fission fragments in Fig. 9. These two figures are useful in fitting

experimental results to the theory and deriving the best values of the parameters $\triangle_0$ and I_0.

Calculated curves with suitable parameters are seen to fit the measured grain spacing plotted in Figs. 1, 2, and 5 for several emulsions. The similarity of the calculated probability curve (Fig. 8) with the experimental curves in

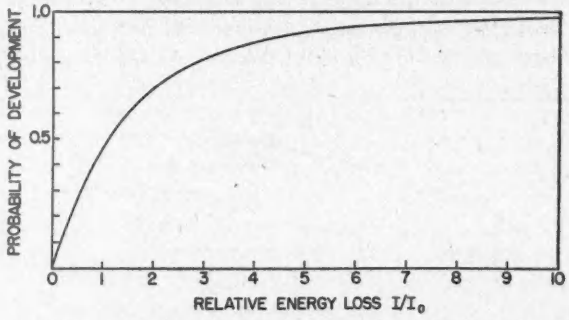

FIG. 8. *Probability of development is plotted against the relative energy loss I/I_0, on the basis of the proposed theory. The constant I_0 is a reciprocal sensitivity factor of the emulsion. The shape of the curve is similar to that of the experimental curves in Figs. 7A and 7B.*

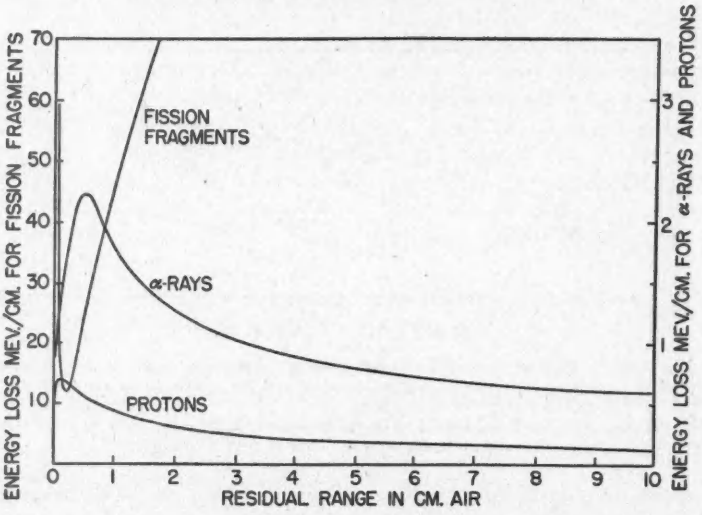

FIG. 9. *Specific energy loss in million electron volts per centimetre of air is plotted against the residual range in centimetres of air for protons, α-rays, and fission fragments. Theoretical formulas were used (5, 12).*

Figs. 7*A* and 7*B* should be noted. The values of I_0 required to fit the experimental results range from 25 kev. to 10 Mev. per cm. of air. In these emulsions proton tracks show well only if $I_0 < 100$ kev. per cm. Figs. 10, 11, and 12

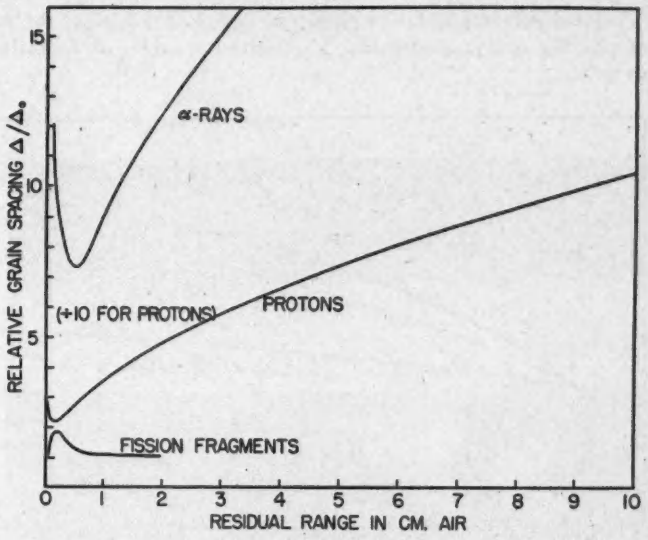

FIG. 10. *Relative grain spacing or Δ/Δ_0, calculated from the proposed theory (Figs. 8 and 9), is plotted against the residual range for tracks of protons, α-rays, and fission fragments. The parameter I_0 = 10 Mev. per cm. air.*

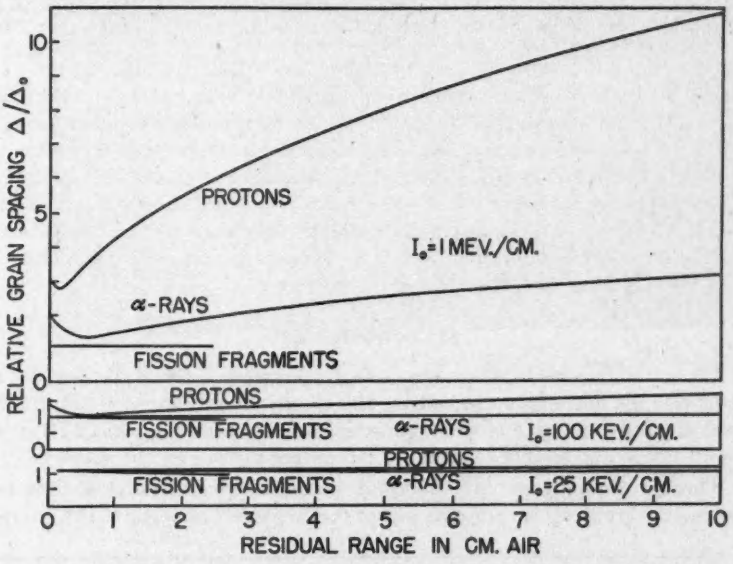

FIG. 11. *Relative grain spacing or Δ/Δ_0, calculated from the proposed theory (Figs. 8 and 9), is plotted against the residual range for tracks of protons, α-rays, and fission fragments. Chosen values of I_0 are 1 Mev. per cm., 100 kev. per cm., and 25 kev. per cm. air.*

show calculated curves of relative grain spacing plotted against the residual range of protons, α-rays, and fission fragments for values of I_0 likely to be encountered.

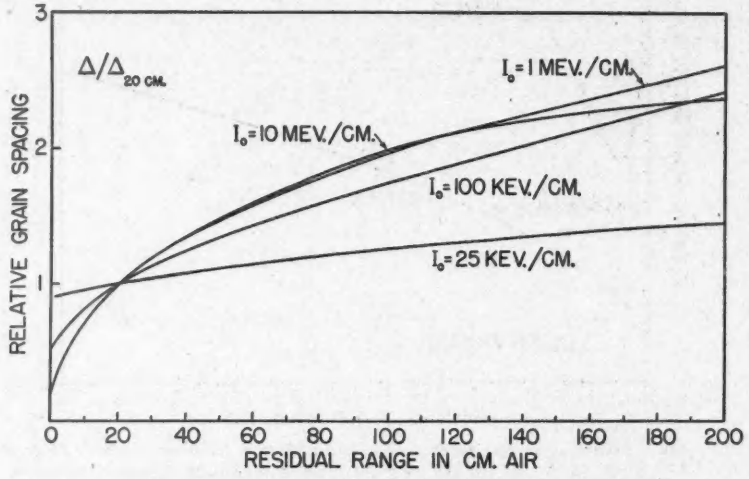

FIG. 12. *Relative grain spacing or* $\Delta/\Delta_{20\ cm.}$, *calculated from the proposed theory (Figs. 8 and 9), is plotted against the residual range of energetic protons. The variation in shape arising from the inverse sensitivity parameter* I_0 *is shown.* $\Delta_{20\ cm.}/\Delta_0 = 105, 14.9, 2.0,$ *and* 1.11 *at 10, 1, 0.1, and 0.025 Mev. per cm., respectively.*

The theory is not wholly satisfactory for the following reasons. (i) Certain curves of grain spacing as a function of residual range of protons cannot be fitted. These were obtained in very insensitive emulsions, in which the spacing was excessive at high energy. (ii) One pair of parameters Δ_0 and I_0 is not generally sufficient to fit the results for protons, α-rays, and fission fragments in the same emulsion. Usually the highest value of I_0 is required for the most strongly ionizing path. A very strong ionization appears therefore to bring a reaction from less sensitive grains.

Acknowledgments

The author wishes to thank Dr. J. D. Cockcroft and Dr. B. W. Sargent for their interest and encouragement in this work; also Prof. N. F. Mott, who read critically the part of the manuscript dealing with the formation of the latent image and modified several of the author's views on the subject.

Through the courtesy of the following, plates have been irradiated at various times: the group at the graphite pile of the Argonne Laboratory, the group at

---

Note:—Photomicrographs for Figs. 13A and 26 to 34 were taken with white light; those for Figs. 13B to 25 were taken with a blue-green filter, and show a better difinition.

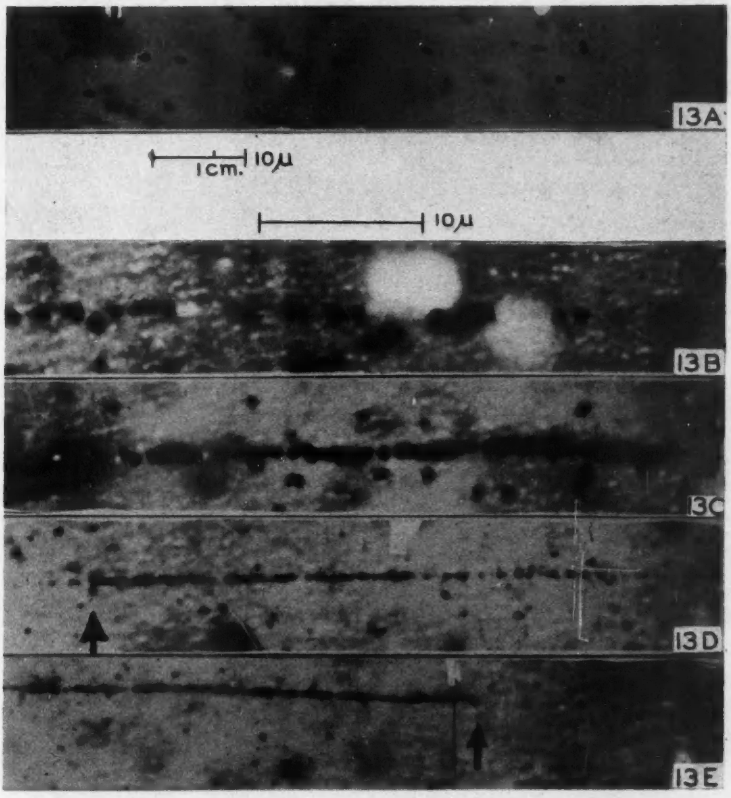

FIG. 13*A*. *Beginning of proton track of residual range 30 cm. air in Eastman α-emulsion.*
FIG. 13*B*. *End of proton track partly shown in Fig. 13A.*
FIG. 13*C*. *End of proton track in centrifuged Eastman α-emulsion.*
FIG. 13*D*. *Beginning of proton track of residual range 60 cm. air in Emulsion II.*
FIG. 13*E*. *End of proton track partly shown in Fig. 13D.*

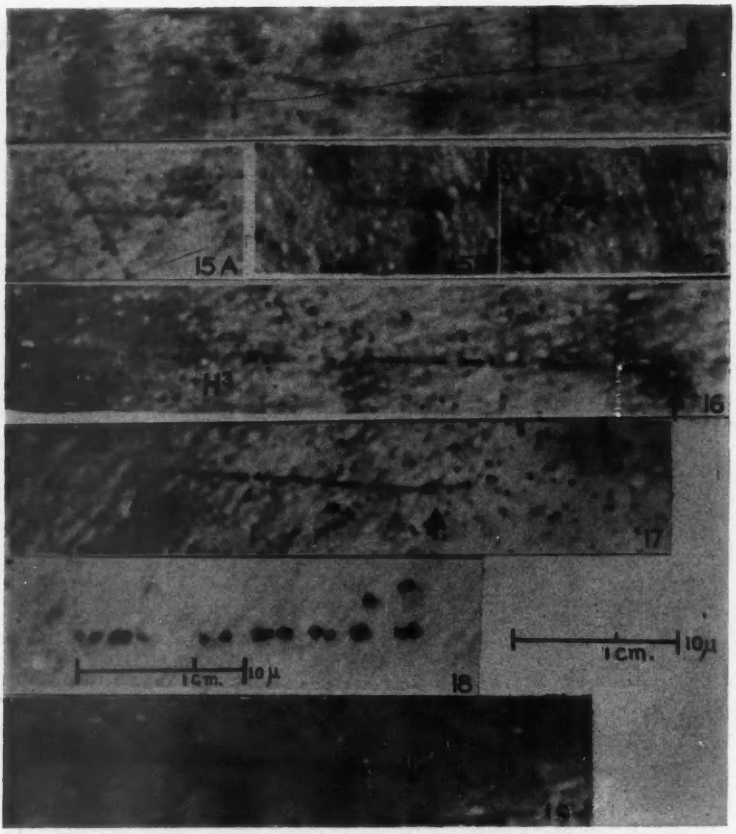

FIG. 14. *End of proton track in Emulsion II containing lithium chloride.*

FIGS. 15*A, B, C. Proton tracks of range 1.06 cm. air and energy 0.62 Mev. from reaction* N^{14} *(n, p)* C^{14} *in Emulsion II containing lithium chloride (same plate as Fig. 14).*

FIG. 16. *α and* H^3*-tracks from reaction* Li^6 *(n, α)* H^3 *in Emulsion II containing lithium chloride (same plate as Figs. 14, 15A-C). Differential sensitivity has been obtained.*

FIG. 17. *Track of α-ray from uranium in Emulsion II.*

FIG. 18. *Track of α-ray from uranium in Eastman α-emulsion.*

FIG. 19. *Tracks of a pair of fission fragments in Emulsion II. An α-ray track can be seen.*

PLATE III

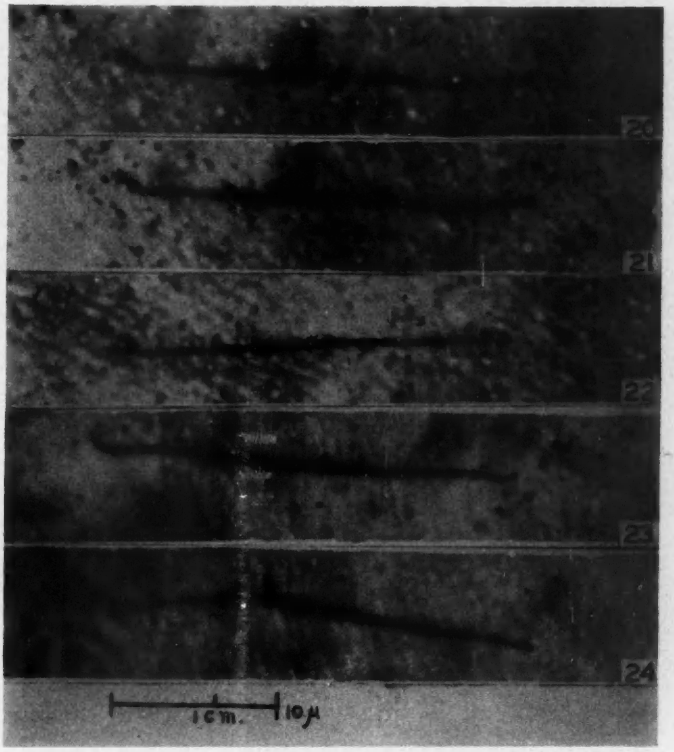

FIGS. 20, 21. *Tracks of a pair of fission fragments in Emulsion II, two focusings.*
FIGS. 22, 23, 24. *Tracks of pairs of fission fragments in Emulsion II.*

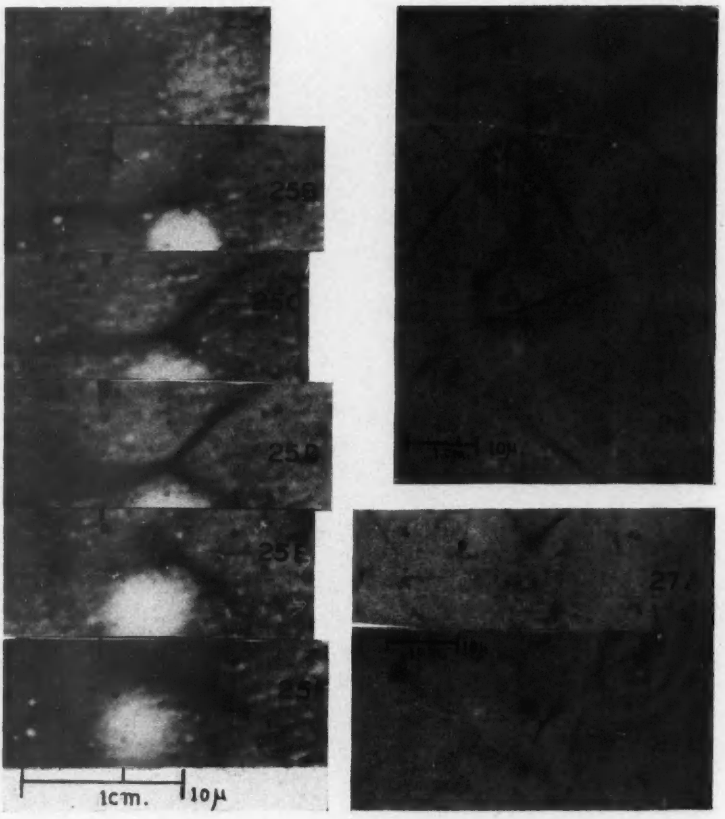

FIGS. 25*A-F*. *Tracks of fission fragments, three branches of comparable appearance, six focusings.*

FIG. 26. *Tracks of pairs of fission fragments in Eastman 548 emulsion.*

FIGS. 27*A, B*. *Tracks of fission fragments and α-rays dipping into emulsion from uranium disk lying on it; Emulsion X2 or X4 centrifuged.*

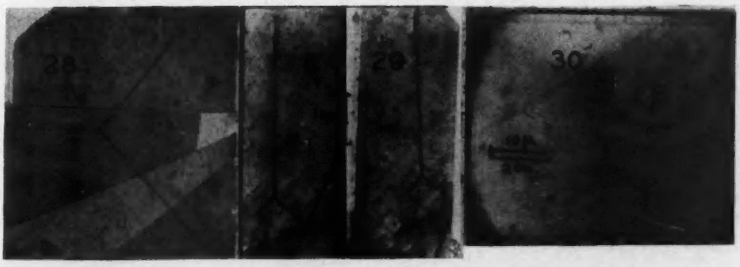

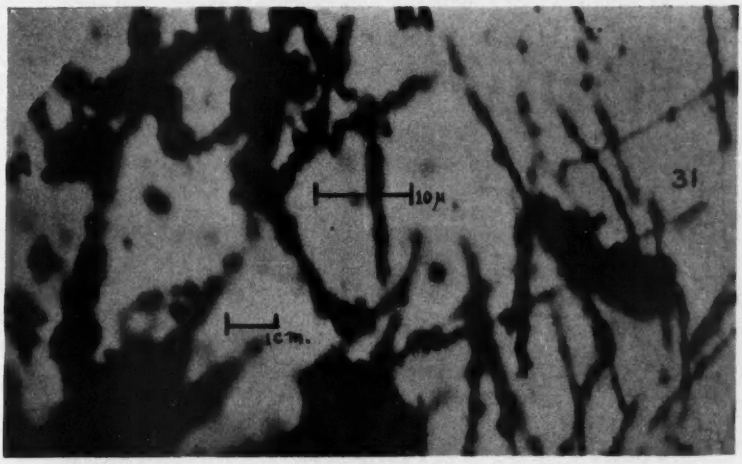

FIGS. 28, 29. *Forked tracks caused by proton–proton collisions in Emulsion I.*

FIG. 30. *Track attributed to an electron in Emulsion I. At the top a proton track is out of focus.*

FIG. 31. *α-ray tracks in Emulsion X4 centrifuged. Development has spread from tracks and fog grains to produce the club-like appearance and clumps of various sizes.*

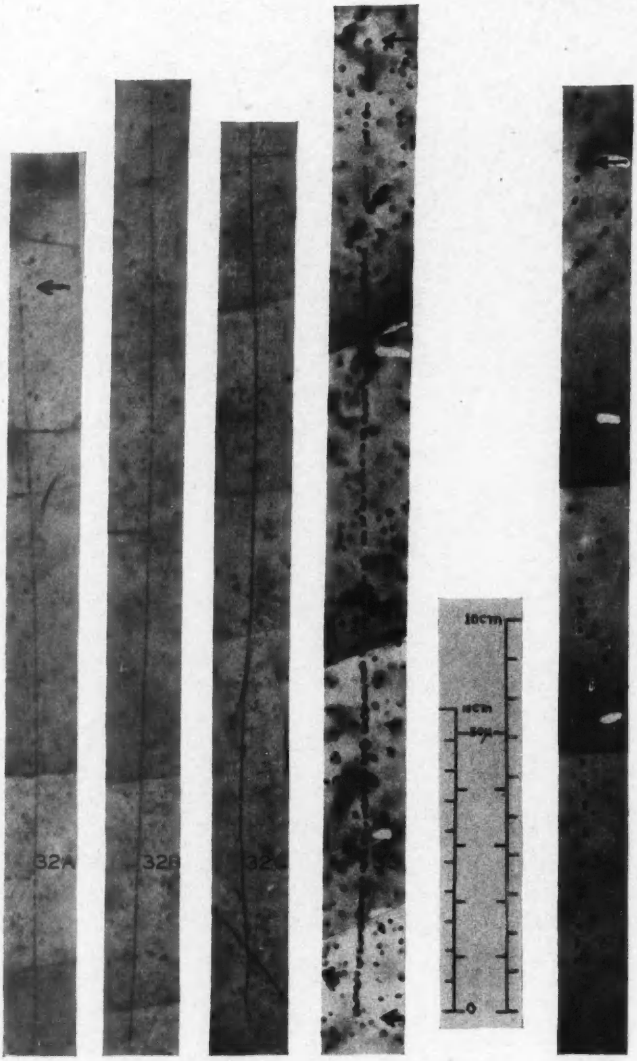

FIGS. 32A-C. *Proton track of range 85 cm. air and initial energy 8.9 Mev. begins on Fig. 32A and ends on Fig. 32C; Emulsion III centrifuged.*

FIG. 33. *Proton track of range 30 cm. air in centrifuged Eastman emulsion.*

FIG. 34. *Proton track of range 25 cm. air in Eastman α-emulsion.*

the low power, heavy water pile of the Chalk River Laboratory, and Dr. H. M. Cave and his collaborators in charge of the high tension set in Ottawa. Their assistance is gratefully acknowledged.

Miss E. O'Brien, Miss E. Mooney, and Mr. G. Gauron have assisted in preparing emulsions at various times.

The author is grateful to Dr. Marietta Blau, Dr. C. F. Powell, Dr. D. L. Livesey, and Mr. D. H. Wilkinson for private information.

The Ciba Company of Montreal has kindly given several of the dyes used in this work.

References

1. BAKER, T. T. Photographic emulsion technique. American Photographic Publishing Company, Boston. 1941.
2. BERG, W. F. Trans. Faraday Soc. 39 : 115-134. 1943.
3. BLAU, M. J. phys. radium, 5 : 61-66. 1934.
4. BLAU, M. and WAMBACHER, H. Z. wiss. Phot. 31 : 243-250. 1933.
5. BØGGILD, J. K., BROSTRØM, K. J., and LAURITSEN, T. Kgl. Danske Videnskab. Selskab. Math.-fys. Medd. 18 (4) : 1-32. 1940.
6. BORST, L. B. and FLOYD, J. J. Bull. Am. Phys. Soc. 21 (3) : 13. 1946.
7. CARROLL, B. H. J. Chem. Education, 8 : 2341-2367. 1931.
8. EGGERT, J. and NODDACK, W. Z. Physik, 43 : 222-229. 1927.
9. GURNEY, R. W. and MOTT, N. F. Proc. Roy. Soc. London, A, 164 : 151-167. 1938.
10. JDANOV, A. J. phys. radium, 6 : 233-241. 1935.
11. KINOSHITA, S. Proc. Roy. Soc. London, A, 83 : 432-453. 1910.
12. LIVINGSTON, M. S. and BETHE, H. A. Rev. Modern Phys. 9 : 245-390. 1937.
13. MEES, C. E. K. Theory of the photographic process. The Macmillan Company, New York. 1944.
14. MYSSOWSKY, L. and JDANOFF, A. Nature, 143 : 794-795. 1939.
15. MYSSOWSKY, L. and TSCHISHOW, P. Z. Physik, 44 : 408-420. 1927.
16. NEBLETTE, C. B. Photography, its principles and practice. 4th ed. D. Van Nostrand Company, Inc., New York. 1942.
17. PERFILOV, N. A. Compt. rend. acad. sci. U.R.S.S. 47 : 623-626. 1945.
18. POWELL, C. F. Proc. Roy. Soc. London, A, 181 : 344-359. 1943.
19. POWELL, C. F., OCCHIALINI, G. P. S., LIVESEY, D. L., and CHILTON, L. V. J. Sci. Instruments, 23 : 102-106. 1946.
20. REINGANUM, M. Physik. Z. 12 : 1076-1077. 1911.
21. SHAPIRO, M. M. Rev. Modern Phys. 13 : 58-71. 1941.
22. SHEPPARD, S. E. *Cited in* Theory and application of colloidal behaviour. Vol. 2. *Edited by* R. H. Bogue. McGraw-Hill Book Company, New York. 1924.
23. SHEPPARD, S. E., LAMBERT, R. H., and SWINEHART, D. J. Chem. Phys. 13 : 372-377. 1945.
24. WALL, E. J. Photographic emulsions, their preparation and coating on glass, celluloid and paper, experimentally and on the large scale. American Photographic Publishing Company, Boston. 1929.
25. WAMBACHER, H. Sitzber. Akad. Wiss. Wien, Math.-naturw. Klasse, 140 (Abt. IIa) : 271-291. 1931.
26. WEBB, J. H. J. Applied Phys. 11 : 18-34. 1940.
27. WILKINS, T. R. J. Applied Phys. 11 : 35-45. 1940.
28. WILKINSON, D. H. Private communication.
29. YOE, J. H. and SARVER, L. A. Organic analytical reagents. John Wiley & Sons, Inc., New York. 1941.

A METHOD FOR COMPUTING TRANSFORMATIONS IN RADIOACTIVE SERIES[1]

By W. H. Watson[2]

Abstract

A direct computational procedure is given for finding the coefficients of the exponential terms in the expressions for the time dependence of the amounts of the various products in a given radioactive series. The method is based on the partition of a matrix which can be written down directly from the diagram of the series. After the explanation of simple applications, an example involving double branching with 10 members of the series is considered in order to exhibit the generality and directness of the method.

Introduction

The laws of radioactive transformation are linear differential equations. If they are treated by operator methods, the problem of finding the changes in time of the amounts of the various products requires the solution of linear algebraic equations and the interpretation of the operators in series of exponential functions of the time. When more than a few products are involved, the labour of computation is exceedingly tedious. The present note shows how the coefficients of the exponential terms in the expressions for the amounts of the various products can be obtained by a direct computational procedure using matrix representation to manage the algebra.

First we write down the matrix (C) which transforms the column vector, whose elements are the masses at time t arranged in suitable order, into the column vector composed of the corresponding initial masses. One can easily see after consideration of the few examples exhibited below how this matrix may be written down immediately from a diagram of the sequence of transformations in the particular series to be treated. Next we have to compute the reciprocal matrix (U): rules are given here for writing it down *directly from the diagram of the series.*

We now split U into a sum of matrices each of which contains one exponential function of the time as a factor. Again rules are given for finding the elements of these partial matrices in terms of the various half-lives involved in the series. It is then possible to derive by matrix multiplication the explicit time dependence of the masses of any or all of the products. This, of course, requires only simple multiplication and addition. The advantages of this method are that the errors caused by approximation can be immediately assessed, and that the general result for a particular series is best left in matrix form.

[1] *Manuscript received February 11, 1947.*

Contribution from Atomic Energy Project, Chalk River Laboratory, Ont. Issued as N.R.C. No. 1564.

[2] *Head of Theoretical Physics Branch.*

We shall deal first with a series in which no branching occurs, then we shall treat $\triangle$-branching and $\diamond$-branching.

In principle the method is applicable to the growth of fission products in a reacting pile and to their subsequent decay when power is shut off. Obviously the method will apply to any system of first order linear differential equations representable by a matrix of the same general form as that imposed by the laws of radioactive transformation.

1. Series Without Branching

Suppose the series of products named in order by the subscripts $1, 2, \ldots, r, \ldots n$. Let the rth member have decay constant λ_r, half-life T_r; let the amount of it at time t be x_r, and let a_r be the amount at $t = 0$. In operational form (1, 2) the equations governing decay are

$$(p + \lambda_r)x_r = a_r + \lambda_{r-1}x_{r-1} \qquad (r = 1, 2 \ldots n,\ \lambda_0 = 0). \tag{1}$$

This set of equations may be represented in matrix form thus:

$$\begin{pmatrix} p+\lambda_1 & 0 & 0 & 0 & \cdots \\ -\lambda_1 & p+\lambda_2 & 0 & 0 & \cdots \\ 0 & -\lambda_2 & p+\lambda_3 & 0 & \cdots \\ 0 & 0 & -\lambda_3 & p+\lambda_4 & \cdots \\ - & - & - & - & - \\ & & & & (p+\lambda_n) \end{pmatrix} \begin{pmatrix} x_1 \\ x_2 \\ x_3 \\ x_4 \\ - \\ x_n \end{pmatrix} = \begin{pmatrix} a_1 \\ a_2 \\ a_3 \\ a_4 \\ - \\ a_n \end{pmatrix} \tag{2}$$

or

$$C(x) = (a).$$

The inverse transformation is

$$(x) = U(a).$$

If we write

$$q_r = \frac{1}{p + \lambda_r} \tag{3}$$

and

$$s_r = \frac{\lambda_r}{p + \lambda_r} \tag{4}$$

we find for U the form

$$U = \begin{pmatrix} q_1 & 0 & 0 & 0 & . & . & . \\ s_1q_2 & q_2 & 0 & 0 & . & . & . \\ s_1s_2q_3 & s_2q_3 & q_3 & 0 & . & . & . \\ s_1s_2s_3q_4 & s_2s_3q_4 & s_3q_4 & q_4 & . & . & . \\ - & - & - & - & - & & \\ - & - & - & - & & & q_n \end{pmatrix} \tag{5}$$

Now the operator $s_1s_2s_3q_4$, for example, is

$$\frac{\lambda_1\lambda_2\lambda_3}{(p+\lambda_1)(p+\lambda_2)(p+\lambda_3)(p+\lambda_4)}, \text{ leading to the function}$$

$$\frac{\lambda_1\lambda_2\lambda_3 e^{-\lambda_1 t}}{(\lambda_2-\lambda_1)(\lambda_3-\lambda_1)(\lambda_4-\lambda_1)} + 3 \text{ like terms}$$

$$= \frac{T_4T_1^2}{(T_1-T_2)(T_1-T_3)(T_1-T_4)}\left(\frac{1}{2}\right)^{t/T_1} + 3 \text{ like terms.}$$

Accordingly we may split the matrix U as follows

$$U = \left(\frac{1}{2}\right)^{t/T_1} u_1 + \left(\frac{1}{2}\right)^{t/T_2} u_2 + \left(\frac{1}{2}\right)^{t/T_3} u_3 + \ldots\ldots \qquad (6)$$

where

$$u_1 = \begin{pmatrix} 1 & 0 & 0 & 0 \\ \frac{T_2}{T_1-T_2} & 0 & 0 & 0 \\ \frac{T_3T_1}{(T_1-T_2)(T_1-T_3)} & 0 & 0 & 0 \\ - & - & - & - \end{pmatrix}$$

$$u_2 = \begin{pmatrix} 0 & 0 & 0 & 0 \\ \frac{T_2}{T_2-T_1} & 1 & 0 & 0 \\ \frac{T_2T_3}{(T_2-T_1)(T_2-T_3)} & \frac{T_3}{T_2-T_3} & 0 & 0 \\ - & - & 0 & - \end{pmatrix}$$

$$u_3 = \begin{pmatrix} 0 & 0 & 0 & 0 \\ 0 & 0 & 0 & 0 \\ \frac{T_3^2}{(T_3-T_1)(T_3-T_2)} & \frac{T_3}{T_3-T_2} & 1 & 0 \\ - & - & - & - \end{pmatrix}$$

and so on.

Rule. (i) To find the matrix u_k, put equal to zero all the elements in U which do not contain q_k or s_k.

(ii) Replace s_m by $\frac{T_k}{T_k-T_m}$ and q_m by $\frac{T_mT_k}{T_k-T_m}$.

(iii) Omit q_k and replace s_k by $\frac{1}{T_k}$.

Ex. In u_3

$$s_1s_2q_3 \rightarrow \frac{T_3}{T_3 - T_1} \cdot \frac{T_3}{T_3 - T_2} = \frac{T_3^2}{(T_3 - T_2)(T_3 - T_1)}$$

$$s_1s_2s_3q_4 \rightarrow \frac{1}{T_3} \cdot \frac{T_3}{T_3 - T_2} \cdot \frac{T_3}{T_3 - T_1} \cdot \frac{T_3T_4}{T_3 - T_4}$$

$$= \frac{T_4T_3^2}{(T_3 - T_1)(T_3 - T_2)(T_3 - T_4)} .$$

In this way we may read off the coefficients of the various powers of $\frac{1}{2}$, for we have only to multiply the given column vector (a) by the appropriate u_k, to obtain the contributions to (x) which vary as $\left(\frac{1}{2}\right)^{t/T_k}$.

2. Branching

We consider first the introduction of a $\triangle$-branch connecting the rth and $(r+1)$th products in the series. This is represented in Fig. 1. We denote the intermediate product by (αr), α being the fraction of r atoms disintegrating which go to the branch product; β is the complementary fraction $(\alpha + \beta = 1)$ disintegrating to the product $(r+1)$ directly.

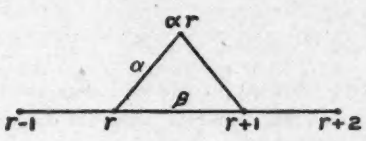

FIG. 1

The relevant equations to be considered are:

$$\begin{aligned}(p + \lambda_r)x_r &= a_r + \lambda_{r-1}x_{r-1} \\ (p + \lambda_{ar})x_{ar} &= a_{ar} + \alpha\lambda_r x_r \\ (p + \lambda_{r+1})x_{r+1} &= a_{r+1} + \lambda_{ar}x_{ar} + \beta\lambda_r x_r .\end{aligned} \tag{7}$$

Thus the matrix operator C and Equation (2) are modified as follows:

$$\begin{pmatrix} \dots & \dots & \dots & \dots & \dots & \dots & \dots \\ \dots & p+\lambda_{r-1} & 0 & 0 & 0 & 0 & \dots \\ \dots & -\lambda_{r-1} & p+\lambda_r & 0 & 0 & 0 & \dots \\ \dots & 0 & -\alpha\lambda_r & p+\lambda_{ar} & 0 & 0 & \dots \\ \dots & 0 & -\beta\lambda_r & -\lambda_{ar} & p+\lambda_{r+1} & 0 & \dots \\ \dots & 0 & 0 & 0 & -\lambda_{r+1} & p+\lambda_{r+2} & \dots \\ \dots & \dots & \dots & \dots & \dots & \dots & \dots \end{pmatrix} \begin{pmatrix} \dots \\ x_{r-1} \\ x_r \\ x_{ar} \\ x_{r+1} \\ \dots \\ \dots \end{pmatrix} = \begin{pmatrix} \dots \\ a_{r-1} \\ a_r \\ a_{ar} \\ a_{r+1} \\ \dots \\ \dots \end{pmatrix} \tag{8}$$

The introduction of the off-diagonal element $-\beta\lambda_r$ still leaves the determinant of the matrix C equal to the product of its principal diagonal elements.

To compute the reciprocal matrix, consider the following.

$$B = \begin{pmatrix} a_1 & 0 & 0 & 0 & 0 \\ -a_2 & b_1 & 0 & 0 & 0 \\ 0 & -b_2 & c_1 & 0 & 0 \\ 0 & -b_3 & -c_2 & d_1 & 0 \\ 0 & 0 & 0 & -d_2 & e_1 \end{pmatrix}$$

It is not difficult to show that if $\triangle$ denotes the framed determinant in B, then the reciprocal of B is

$$\begin{pmatrix} \frac{1}{a_1} & 0 & 0 & 0 & 0 \\ \frac{a_2}{a_1b_1} & \frac{1}{b_1} & 0 & 0 & 0 \\ \frac{a_2b_2}{a_1b_1c_1} & \frac{b_2}{b_1c_1} & \frac{1}{c_1} & 0 & 0 \\ \frac{a_2\triangle}{a_1b_1c_1d_1} & \frac{\triangle}{b_1c_1d_1} & \frac{c_2}{c_1d_1} & \frac{1}{d_1} & 0 \\ \frac{a_2\triangle d_2}{a_1b_1c_1d_1e_1} & \frac{\triangle d_2}{b_1c_1d_1e_1} & \frac{c_2d_2}{c_1d_1e_1} & \frac{d_2}{d_1e_1} & \frac{1}{e_1} \end{pmatrix}.$$

In terms of the s and q notation introduced in Equation (4), the part of the reciprocal matrix U extending from its principal diagonal to the left and corresponding to (8) for $\triangle$-branching is

$$\begin{array}{ccccc} q_{r-1} & & & & \\ s_{r-1}q_r & q_r & & & \\ s_{r-1}\alpha s_r q_{ar} & \alpha s_r q_{ar} & q_{ar} & & \\ s_{r-1}s_r(\alpha s_{ar}+\beta)q_{r+1} & s_r(\alpha s_{ar}+\beta)q_{r+1} & s_{ar}q_{r+1} & q_{r+1} & \\ s_{r-1}s_r(\alpha s_{ar}+\beta)s_{r+1}q_{r+2} & s_r(\alpha s_{ar}+\beta)s_{r+1}q_{r+2} & s_{ar}s_{r+1}q_{r+2} & s_{r+1}q_{r+2} & q_{r+2} \end{array} \qquad (9)$$

The rules for translating the q's and s's and splitting U into partial matrices apply in the way already indicated when there was no branching.

The rules for constructing U, the reciprocal of C are evident.

1. Replace the principal diagonal elements of C by their reciprocals, i.e., insert q_k in the kth place in the diagonal.

2. All elements to the right of the principal diagonal are zero. It is unnecessary, therefore, to write them down.

3. On the left, build up each row from the principal diagonal. Each step to the left in the matrix corresponds to the transition from the member of the series named by the index of the column from which we start to that named by the adjacent column on its left. When these two members are related as daughter and parent multiply the element of U on the right by the s for the element on the left when there is no branching. If the two members are not related in this way write zero for the corresponding element of U.

When the column of U corresponds to a point of branching the element to be written down represents the complete series of transitions between the point of branching and the member represented by the principal diagonal element on the same row. For instance in (9) above in the second column and fourth row we find the element $s_r(\alpha s_{\alpha r} + \beta)q_{r+1}$. So the procedure is to write down a q-factor for the series member naming the row of the matrix and an s-factor for each step when simple and when the branching occurs the obvious linear combination of s-factors in the proportion of the branching ratio.

Thus we can write down U by inspection from the diagram of the series once we have decided how to number the members of the series.

For the convenience of the reader we shall treat ◇-branching explicitly (see Fig. 2).

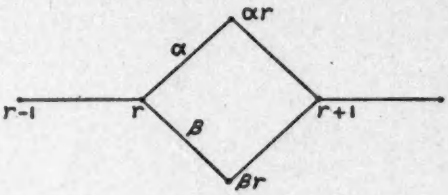

FIG. 2

In operational form the equations governing decay are

$$\begin{aligned}
(p + \lambda_r)x_r &= a_r + \lambda_{r-1}x_{r-1} \\
(p + \lambda_{\alpha r})x_{\alpha r} &= a_{\alpha r} + \alpha\lambda_r x_r \\
(p + \lambda_{\beta r})x_{\beta r} &= a_{\beta r} + \beta\lambda_r x_r \\
(p + \lambda_{r+1})x_{r+1} &= a_{r+1} + \lambda_{\alpha r}x_{\alpha r} + \lambda_{\beta r}x_{\beta r}\,.
\end{aligned} \tag{10}$$

The relevant part of the matrix C is

$$\begin{array}{ccccc}
-\lambda_{r-1} & p + \lambda_r & 0 & 0 & 0 \\
0 & -\alpha\lambda_r & p + \lambda_{\alpha r} & 0 & 0 \\
0 & -\beta\lambda_r & 0 & p + \lambda_{\beta r} & 0 \\
0 & 0 & -\lambda_{\alpha r} & -\lambda_{\beta r} & p + \lambda_{r+1} \\
0 & 0 & 0 & 0 & -\lambda_{r+1}
\end{array} \tag{11}$$

To check the computing of the reciprocal matrix by the rules given above, consider

$$\begin{pmatrix} a_1 & 0 & 0 & 0 & 0 & 0 \\ -a_2 & b_1 & 0 & 0 & 0 & 0 \\ 0 & -b_2 & c_1 & 0 & 0 & 0 \\ 0 & -b_3 & 0 & d_1 & 0 & 0 \\ 0 & 0 & -c_2 & -d_2 & e_1 & 0 \\ 0 & 0 & 0 & 0 & -e_2 & f_1 \end{pmatrix} = C.$$

Let

$$\Delta = -\begin{vmatrix} b_2 & c_1 & 0 \\ -b_3 & 0 & d_1 \\ 0 & -c_2 & d_2 \end{vmatrix}$$

Compute U, the reciprocal of C following the rules of matrix theory. The result is

$$U = \begin{pmatrix} \frac{1}{a_1} & 0 & 0 & 0 & 0 & 0 \\ \frac{a_2}{a_1b_1} & \frac{1}{b_1} & 0 & 0 & 0 & 0 \\ \frac{a_2b_2}{a_1b_1c_1} & \frac{b_2}{b_1c_1} & \frac{1}{c_1} & 0 & 0 & 0 \\ \frac{a_2b_3}{a_1b_1c_1} & \frac{b_3}{b_1d_1} & 0 & \frac{1}{d_1} & 0 & 0 \\ \frac{a_2\Delta}{a_1b_1c_1d_1e_1} & \frac{\Delta}{b_1c_1d_1e_1} & \frac{c_2}{c_1e_1} & \frac{d_2}{d_1e_1} & \frac{1}{e_1} & 0 \\ \frac{a_2\Delta e_2}{a_1b_1c_1d_1e_1f_1} & \frac{\Delta e_2}{b_1c_1d_1e_1f_1} & \frac{c_2e_2}{c_1e_1f_1} & \frac{d_2e_2}{d_1e_1f_1} & \frac{e_2}{e_1f_1} & \frac{1}{f_1} \end{pmatrix}$$

Apply this result to matrix (11) to find

$$\begin{array}{cccccccc} q_{r-1} & & & & & & & \\ s_{r-1}q_r & & q_r & & & & & \\ s_{r-1}\alpha s_r q_{ar} & & \alpha s_r q_{ar} & & q_{ar} & & & \\ s_{r-1}\beta s_r q_{\beta r} & & \beta s_r q_{\beta r} & & 0 & q_{\beta r} & & \\ s_{r-1}s_r(\alpha s_{ar}+\beta s_{\beta r})q_{r+1} & & s_r(\alpha s_{ar}+\beta s_{\beta r})q_{r+1} & & s_{ar}q_{r+1} & s_{\beta r}q_{r+1} & q_{r+1} & \\ - & - & - & - & - & - & s_{r+1}q_{r+2} & q_{r+2}\,. \end{array}$$

This is the result which could have been written down directly from Fig. 2.

q_1									
s_1q_2	q_2								
$s_1\alpha s_2q_3$	αs_2q_3	q_3							
$s_1\alpha s_2\gamma s_3q_4$	$\alpha s_2\gamma s_3q_4$	γs_3q_4	q_4						
$s_1\alpha s_2\delta s_5q_5$	$\alpha s_2\delta s_5q_5$	δs_5q_5	0	q_5					
$s_1\alpha s_2s_3(\gamma s_4 + \delta s_5)q_6$	$s_2\alpha s_3(\gamma s_4 + \delta s_5)q_6$	$s_3(\gamma s_4 + \delta s_5)q_6$	s_4q_6	s_5q_6	q_6				
$s_1\beta s_2q_7$	βs_2q_7	0	0	0	0	q_7			
$s_1\beta s_2s_7q_8$	$\beta s_2s_7q_8$	0	0	0	0	s_7q_8	q_8		
A	B	$s_3(\gamma s_4 + \delta s_5)s_6q_9$	$s_4s_6q_9$	$s_5s_6q_9$	s_6q_9	$s_7s_8q_9$	s_8q_9	q_9	
C	D	$s_3(\gamma s_4 + \delta s_5)s_6s_9q_{10}$	$s_4s_6s_9q_{10}$	$s_5s_6s_9q_{10}$	$s_6s_9q_{10}$	$s_7s_8s_9q_{10}$	$s_8s_9q_{10}$	s_9q_{10}	q_{10},

where

$$A = s_1s_2[\alpha s_3(\gamma s_4 + \delta s_5)s_6 + \beta s_7s_8]q_9, \qquad B = s_2\alpha s_3(\gamma s_4 + \delta s_5)s_6q_9,$$

$$C = s_1s_2[\alpha s_3(\gamma s_4 + \delta s_5)s_6 + \beta s_7s_8]s_9q_{10}, \qquad D = s_2\alpha s_3(\gamma s_4 + \delta s_5)s_6s_9q_{10}.$$

As a further example to show the directness of the method we shall choose the quite complicated series shown in Fig. 3 and write down U.

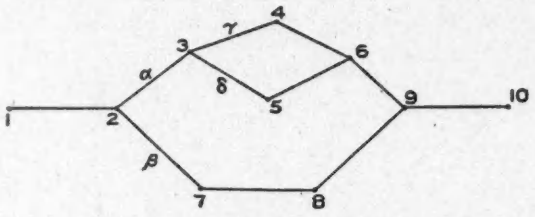

FIG. 3

The result is shown on p. 259.

It remains to remark that in carrying out the numerical computation of the partial matrices u_k we should take advantage of the recurrence of common factors and economize in the number of elementary operations of multiplication. This can be done by evaluating the s_m and q_m for a particular k and following the complete matrix U as a guide, after noting the elements to be put equal to zero in accordance with the rule given above.

References

1. BERG, C. J. Heaviside's operational calculus as applied to engineering and physics. 2nd ed. McGraw-Hill Book Co., Inc., New York. 1936.
2. CARSLAW, H. S. and JAEGER, J. C. Operational methods in applied mathematics. Oxford University Press, New York. 1941.

RATIO OF NEUTRON ABSORPTION CROSS-SECTIONS OF BORON AND HYDROGEN[1]

By W. J. Whitehouse[2] and G. A. R. Graham[3]

Abstract

Using a Ra-α-Be source and a small boron trifluoride chamber as detector, the ratio of the neutron absorption cross-sections of boron and hydrogen, σ_B/σ_H, has been measured by the integration method in water and in aqueous solutions of boric acid. The result is

$$\sigma_B/\sigma_H = 2270$$

with a statistical error of ± 30. Subsidiary experiments have been made which fix at about 3% the upper limit of the systematic error caused by perturbation of the neutron density in the neighbourhood of the ionization chamber.

Introduction

The integration method used in this experiment is due to Frisch, Halban, and Koch (4). Using a small boron-lined chamber as detector they obtained the result $\sigma_B/\sigma_H = 1940 \pm 100$, where σ_B and σ_H are the absorption cross-sections of boron and hydrogen. Fenning, Halban, and Seligman (3) repeated the measurement using boron trifluoride chambers as detectors and found the ratio σ_B/σ_H to be 2160 ± 30. In both measurements no correction has been applied to the final result for the perturbation by the detector of the neutron density in its neighbourhood.

Kubitschek (6, 7) has carried out an extensive series of measurements using thin manganese foils as detectors and found the ratio σ_B/σ_H to be 2380 ± 70. This result has been corrected for perturbation effects by an extrapolation to infinitely thin foils.

Recently Schulz and Goldhaber (8) have obtained the value $\sigma_B/\sigma_H = 1954 \pm 24$; details of the method are not given.

In view of the diversity of results obtained in previous experiments it was decided to make still another determination of the ratio, using as detector a much smaller boron trifluoride chamber than that previously used. It was hoped, in particular, to remove the discrepancy between the results obtained with boron trifluoride chambers and with foils.

The theory of the experiment has been adequately treated in several papers (3, 4, 6, 7) and will not be reproduced in detail here. The neutron density (I) is measured in an effectively infinite bath at a number of distances (R) from a neutron source. The measurements are made first in distilled water and then in a dilute boric acid solution. (The neutron capture by oxygen is

[1] *Manuscript received in original form November 6, 1946, and, as revised, May 1, 1947.*

Contribution from the Nuclear Physics Branch, Montreal Laboratory, Atomic Energy Division of the National Research Council of Canada. Publication of this work done in 1945 has been delayed owing to security restrictions. Issued as N.R.C. No. 1573.

[2] *Physicist, United Kingdom Staff; now at the Atomic Energy Research Establishment, Harwell, England.*

[3] *Assistant Research Physicist, National Research Council of Canada; now at the University of Rochester, Rochester, N.Y.*

negligible.) If the $1/v$ law of capture is obeyed by hydrogen and boron, the ratio of the capture cross-sections is independent of the velocity of the neutrons and is given by the formula:

$$\sigma_B/\sigma_H = \frac{C_H}{C_B}\left(\frac{S_H}{S_B} - \frac{C'_H}{C_H}\right), \tag{1a}$$

where

σ_B = absorption cross-section of boron,
σ_H = absorption cross-section of hydrogen,
C_H = volume concentration of hydrogen atoms in water,
C'_H = volume concentration of hydrogen atoms in the solution,
C_B = volume concentration of boron atoms in the solution,
S_H = area under curve IR^2 vs. R for water,

and

S_B = area under curve IR^2 vs. R for the solution.

Since $C_H \simeq C'_H$ in this experiment, this formula may be written

$$\sigma_B/\sigma_H = \frac{C_H}{C_B}\left(\frac{S_H}{S_B} - 1\right). \tag{1b}$$

(The error so introduced is less than 1 part in 500.)

Scope of Present Experiments

The present experiments may be separated into the following sections:

IA. (1) Measurement in distilled water,
(2) Measurement in 1% boric acid solution,
(3) Measurement in 2% boric acid solution.

IB. (1) Measurement in distilled water,
(2) Measurement in 0.4% boric acid solution,
(3) Measurement in 3% boric acid solution.

(The measurements of Section IA were carried out using one boron trifluoride chamber, and those of Section IB with a different chamber of about the same dimensions.)

II. Comparative measurements with boron trifluoride chambers and manganese foils.

Measurements with Boron Trifluoride Chambers

A boron trifluoride chamber was chosen in preference to foils as a detector of neutrons for the principal measurement because of the advantages of very low background and the possibility of long uninterrupted counts. The chambers were constructed by Mr. N. Veall (10). They had the dimensions 0.4 cm. in diameter, 1.5 cm. long, and were filled with boron trifluoride to 1.5 atm. The chamber was mounted on a brass tube (diameter, 0.5 cm.), the opposite end of which was attached to the carriage supporting the head amplifier. The carriage rode upon two rails, which were part of a rigid steel framework. The latter also supported the source on another carriage. The source and

chamber were arranged with their centres on a horizontal line corresponding to the central axis of the tank, which was contained within the framework. For convenience the distance between the chamber and source was varied by moving the source only. The separation, chamber to source, could be read from a mirror scale attached to the framework using indicators fixed to the two carriages. The scale was first calibrated by measuring the separation with a cathetometer at several distances.

The tank containing the solutions was made of stainless steel. Its cross-section had a U-shape, and the dimensions were: length 78 cm., width 40 cm., and greatest depth 41 cm. A second tank, rectangular in shape (87 by 42 by 42 cm.) contained ordinary water, to be used for check measurements. The whole frame, bearing source and chamber, could be moved readily from one tank to the other. The conventional linear amplifier, discriminator, and scaling units were used to count the impulses from the chamber.

For intensity reasons and to eliminate the effect of 'γ-noise' two Ra-α-Be sources were used.

(*a*) A 110 mgm. source, contained in a thin brass cylinder approximately 3 cm. long and 1.3 cm. in diameter, was used for measurements up to a separation of 12 cm.

(*b*) A 600 mgm. source, contained in a thin brass cylinder approximately 3 cm. long and 2.3 cm. in diameter, was used for all measurements with separations greater than 12 cm.

The ratio of the neutron intensities of the two sources was measured and all readings adjusted to values appropriate to the smaller source (see below).

The solutions were prepared in the stainless steel tank by dissolving a weighed quantity of Baker's analytical boric acid in a measured volume of distilled water. The concentrations were determined chemically by Mr. A. C. English and Mr. A. H. Booth of the Chemistry Branch. A description of their analyses is contained in Appendix I.

The intensity I (counts per min.) was measured at various distances R (separation source – chamber in cm.). The readings are given in full in Tables I and II, together with the statistical accuracy of each count. The readings in Column 4 have all been adjusted by multiplying by the ratio of the neutron intensities of the two sources.

The results are also presented graphically in Figs. 1 and 2, where the graphs are smaller and less accurate than those under which the areas were actually measured. The constancy of the counting apparatus was checked frequently by a measurement at the closest point. A further check was made by measurements in the auxiliary tank of water each day. Some drift occurred within a few hours of switching on the electronic equipment, but subsequently no drift could be detected within the statistical accuracy of the counts (usually 1%). The apparatus ran continuously during the course of each experiment.

In certain cases the separation R was slightly different for the two sources, and to allow for this difference an adjustment to I, based on the graph of

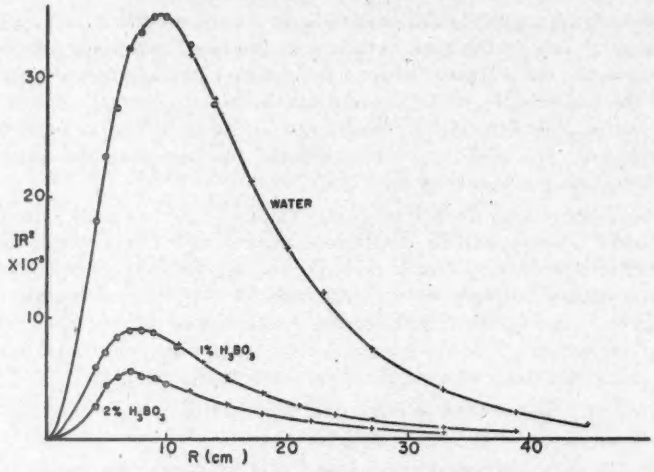

FIG. 1. *Distribution of neutron density, I, multiplied by R². Circles indicate measurements with 110 mgm. source; crosses those with 600 mgm. source.*

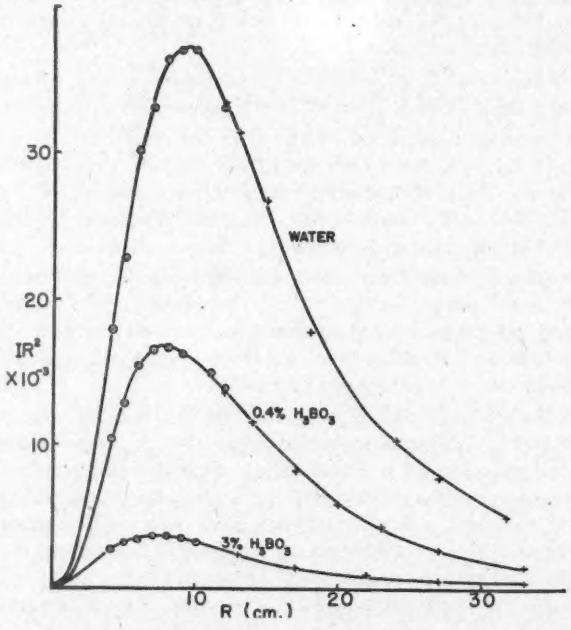

FIG. 2. *Distribution of neutron density, I, multiplied by R². Circles indicate measurements with 110 mgm. source; crosses those with 600 mgm. source.*

TABLE I

READINGS WITH BORON TRIFLUORIDE CHAMBER, TAKEN IN EXPERIMENT IA

Source	R, cm.	I, Counts/min.	I, Adjusted	$IR^2 \times 10^{-3}$	Statistical error, %
Medium: Water					
110 mgm.	4.1	1077	—	18.1	1
"	4.9	975	—	23.4	1
"	5.9	810	—	27.3	1
"	6.9	677	—	32.2	1
"	7.9	538	—	33.6	1
"	8.9	440	—	34.8	1
"	9.9	356	—	34.9	1
"	10.9	280	—	33.2	1
"	11.9	229*	—	32.5	1
"	13.9	143*	—	27.6	1
"	16.9	74.5*	—	21.4	1
600 mgm.	12.0	1203*	220.5	31.7	1
"	14.0	780*	143	28.0	1
"	17.0	400*	73.2	21.1	1
"	20.0	—	39.2	15.7	1½
"	23.0	—	22.7	12.0	1½
"	27.0	—	10	7.3	1½
"	32.9	—	3.7	4.0	3
"	38.9	—	1.46	2.2	6
"	44.9	—	0.62	1.2	13
Medium: 1% boric acid solution (10.07 gm. per litre)					
110 mgm.	4.1	492	—	5.86	1
"	4.9	297	—	7.14	1
"	5.9	239	—	8.34	1
"	6.9	185	—	8.80	1
"	7.9	142	—	8.85	1
"	8.9	110	—	8.72	1
"	10.9	64.2*	—	7.63	1
600 mgm.	11.0	345*	63.2	7.66	1
"	13.0	—	37.1	6.27	1
"	15.0	—	22.3	5.02	1
"	18.0	—	11.5	3.73	1½
"	21.0	—	6.1	2.69	1½
"	24.0	—	3.36	1.94	3
"	27.0	—	2.18	1.59	3½
"	32.9	—	0.75	0.81	5
"	38.9	—	0.34	0.51	13
Medium: 2% boric acid solution (20.2 gm. per litre)					
110 mgm.	4.1	213	—	3.58	1
"	5.0	174.5	—	4.36	1
"	6.0	137.5	—	4.95	1
"	7.0	105.5	—	5.47	1
"	8.0	80.4	—	5.14	1
"	9.0	61.7	—	5.00	1
"	10.0	45.2	—	4.52	1
600 mgm.	12.0	—	26.7	3.84	1
"	15.0	—	12.35	2.78	1½
"	18.0	—	6.14	1.98	2½
"	22.0	—	2.72	1.31	2
"	27.0	—	1.09	0.80	3½
"	33.0	—	0.40	0.44	8½

log I vs. R, has been applied to obtain the proper ratio. The readings from which the ratio of the strengths of the two sources was obtained are marked with an asterisk in Tables I and II. They are collected in Table III.

TABLE II

READINGS WITH BORON TRIFLUORIDE CHAMBER TAKEN IN EXPERIMENT IB

Source	R, cm.	I, Counts/min.	I, Adjusted	$IR^3 \times 10^{-3}$	Statistical error, %
Medium: Water					
110 mgm.	4.1	1122	—	18.9	1
"	5.0	994	—	24.8	1
"	6.0	826	—	30.1	1
"	7.0	673	—	33.0	1
"	8.0	554	—	36.4	1
"	9.0	454	—	36.8	1
"	10.0	369	—	36.9	1
"	11.0	292	—	36.3	1
"	12.0	229*	—	33.0	1
600 mgm.	12.0	1277*	232.5	33.4	1
"	13.0	—	186.5	31.4	1
"	15.0	—	118.5	26.7	1
"	19.0	—	49.0	17.7	1
"	24.0	—	18.0	10.4	1
"	27.0	—	10.5	7.7	1½
"	31.8	—	4.5	4.9	3
Medium: 0.4% boric acid solution (4.02 gm. per litre)					
110 mgm.	4.1	607	—	10.25	1
"	5.0	513	—	12.8	1
"	6.0	426	—	15.35	1
"	7.0	337	—	16.5	1
"	8.0	260	—	16.6	1
"	9.0	201	—	16.25	1
"	11.0	123	—	14.9	1
"	12.0	96*	—	13.8	1
600 mgm.	12.0	515*	93.8	13.5	1
"	14.0	—	58.9	11.55	1
"	17.0	—	28.5	8.25	1
"	20.0	—	14.7	5.9	1½
"	23.0	—	8.2	4.33	2
"	27.0	—	3.82	2.7	2½
"	33.0	—	1.47	1.6	3
Medium: 3% boric acid solution (30.17 gm. per litre)					
110 mgm.	4.1	159	—	2.67	1
"	5.0	126.5	—	3.16	1
"	6.0	95.9	—	3.49	1
"	7.0	76.0	—	3.72	1
"	8.0	58.6	—	3.75	1
"	9.0	43.8	—	3.55	1
"	10.0	32.9	—	3.29	1
600 mgm.	13.0	—	14.6	2.47	1
"	17.0	—	5.66	1.63	1
"	22.0	—	1.98	0.96	2
"	27.0	—	0.84	0.61	3
"	33.0	—	0.41	0.45	4½

TABLE III

RATIO OF INTENSITIES OF THE TWO SOURCES

Medium	110 mgm. source			600 mgm. source		Ratio $\frac{\text{110 mgm. source}}{\text{600 mgm. source}}$
	R, cm.	I, Counts/min.	I, Adjusted	R, cm.	I, Counts/min.	
H_2O	11.9	229	224	12.0	1203	0.186
H_2O	13.9	143	140	14.0	780	0.180
H_2O	16.9	74.5	72.8	17.0	400	0.182
1% H_3BO_3	10.9	64.2	61.7	11.0	345	0.179
H_2O	12.0	229	229	12.0	1277	0.179
0.4% H_3BO_3	12.0	96	96	12.0	515	0.186
						0.182 ± 0.0012 (s.d.)

The error to be attributed to the measured ratio σ_B/σ_H in each case was determined from the individual errors. Let the percentage errors in the separate quantities be as follows: ϵ in σ_B/σ_H, α_1 in S_H, α_2 in S_B, γ_1 in C_H, and γ_2 in C_B. The following formula was used to combine the errors:

$$\epsilon^2 = \gamma_1^2 + \gamma_2^2 + \left(\frac{S_H}{S_H - S_B}\right)^2 (\alpha_1^2 + \alpha_2^2) . \qquad (2)$$

The errors in the concentrations are given in Appendix I. However, since a small amount of evaporation and replacement of water occurred during the course of each experiment, an accuracy of only ±0.5% is claimed in the concentration, although the chemical analysis is more accurate than this.

In estimating the error to be attributed to the area under each density distribution curve several factors must be considered.

(*a*) Since all the important points on the curves have a statistical accuracy of 1%, the error in the area will be much less on this account. The error in R is negligible, cathetometer measurements indicating an accuracy of ±0.05 cm. Since the boron trifluoride chamber has a small cross-sectional area, the measured separation, R, from the centre of chamber to centre of source may be used without correction. The use of two sources may also introduce a small error of the order of ½%, but this affects each area equally and does not contribute fully to the final result. We have allowed an error of 1% in the area in each case for all the above factors including any possible drift of the counting apparatus.

(*b*) Secondly, the exponential nature of the curve for $R > 20$ cm. approximately, was investigated fully only in the case of the first water curve, for which the relaxation length is 10.1 cm. In the other cases the relaxation lengths agree within 5% with this value in the portions of the curves measured. In each case an extrapolation has been made beyond the last measured point using this value of the relaxation length.

The error in the area under the tail of the curve has been estimated taking 5% error in the relaxation length together with the statistical error of the last measured point on the curve.

(*c*) Lastly, since we were unable to measure at separations less than $R = 4.1$ cm. because of 'γ noise', the portion of the curve near the origin has been drawn on the basis of previous experience. This introduces an additional error for which we have allowed arbitrarily.

In Table IV, Columns (*a*), (*b*), and (*c*) give the percentage errors attributed to the causes discussed in the similarly lettered paragraphs above. The total error* α in the area, given by

$$\alpha^2 = a^2 + b^2 + c^2, \tag{3}$$

is entered in Column 5. The error in the corresponding value of σ_B/σ_H is given in the last column.

TABLE IV

ERRORS IN DETERMINATION OF σ_B/σ_H

Curve	Percentage errors in areas				ϵ, %
	Drift, etc. (*a*)	Tail (*b*)	Portion near origin (*c*)	Total α	
1st H_2O	1	0	0	1	—
1% H_3BO_3	1	0.72	0	1.25	2.2
2% H_3BO_3	1	0.8	0.5	1.35	2.1
2nd H_2O	1	0.6	0	1.20	—
0.4% H_3BO_3	1	0.7	0	1.20	2.8
3% H_3BO_3	1	0.8	1	1.7	2.3

The final results calculated on the basis of Equation (1*b*) are contained in Table V.

TABLE V

Expt.	Solution	C_H, gm-atoms/litre	C_B, gm-atoms/litre	S_H arbitrary	S_B units	σ_B/σ_H
IA	H_2O	111	0	60.72	—	—
	1% H_3BO_3	111	0.1628	—	14.11	2250 ± 50
	2% H_3BO_3	111	0.327	—	7.99	2240 ± 45
IB	H_2O	111	0	64.03	—	—
	0.4% H_3BO_3	111	0.0650	—	26.95	2350 ± 65
	3% H_3BO_3	111	0.488	—	5.81	2280 ± 50

* *The error α stands for α_1 or α_2, as defined above.*

Taking the weighted mean we arrive at the result:

$$\sigma_B/\sigma_H = 2270 \pm 30.$$

It must be emphasized that this result is not corrected for perturbation effects due to the detector.

Comparative Measurements with Boron Trifluoride Chamber and Manganese Foils

In the experiments to be described here the ratio of the readings of the boron chamber and of an 'ideal' detector is measured in water and in a 1% boric acid solution. If there were no perturbation of the neutron density owing to the absorption by, and the finite size of, the boron chamber, we would expect this ratio to be independent of the medium. Further, since both detectors obey the $1/v$ law of capture we would expect the ratio also to be independent of the velocity distribution of the neutrons, i.e., in this case, of the distance from the source.

Manganese foils can be considered as 'ideal' detectors only after two conditions are fulfilled. (1) The foils must be so thin that there is no disturbance of the neutron density in the neighbourhood, or else a correction for this disturbance must be applied. (2) A correction must be made for the resonance absorption of manganese. The first condition is met in these experiments by choosing very thin foils. Activation measurements are consequently limited to points of high neutron density. The correction for resonance activity is described later. It introduces a factor of the order of 3% in a 1% boric acid solution, and would become serious in the stronger solutions. The activation measurements have therefore been restricted to water and a 1% boric acid solution. The small statistical errors and good agreement of the results in Table V show that the perturbation by the boron chamber does not vary significantly from one solution to another.

Two foils of manganese alloy were used, each 2 by 1.6 cm. and having a mass of 0.02 gm. per cm.^{2} Calculations based on a formula given by Skyrme (9) show that these foils produce negligible perturbation of the neutron density in the aqueous media. The foils were mounted upon bakelite plates of thickness 0.38 mm., which had machined edges, and could be accurately held in position near the Geiger–Müller counter by a spring mechanism. During the irradiation in the liquids the detectors were held in frames of beryllium–copper wire of diameter 0.51 mm. In a subsidiary experiment it was shown that the bakelite plates caused no perturbation of the neutron density in the aqueous media. The foils were covered with a thin layer of cellulose cement to prevent oxidation.

All counts were made to a statistical accuracy of about 1%. (Actually 7500 particles was the smallest number counted.) Thus the statistical error in the comparison between the boron trifluoride chamber and the foil is about 2%, and to this must be added an error of the order of 1% due to possible differences in position.

Owing to the small size of the manganese foils, their activities acquired when shielded by cadmium were too small for measurement. Instead, Kubitschek's experimental results (6, 7) for the cadmium difference were used in the calculation of our resonance correction.

The correction for resonance absorption in manganese requires an estimate, experimental or otherwise, of the percentage of neutrons having energies above the cadmium cut-off, which exist in the whole space surrounding the source. A measurement, made in paraffin oil, with a boron trifluoride chamber under cadmium, gave this quantity as 0.93% (2). Since the scattering and absorption of neutrons, both in water and paraffin oil, are mainly due to hydrogen, the same percentage may be used for water.

If the scattering and capture mean free paths are compared with each other both in water and a 1% boric acid solution, for neutrons at various energies above the cadmium cut-off, it is found that the capture mean free path is the greater. Even at the cadmium cut-off the scattering mean free path in water is about 0.5 cm., while the capture mean free path in a 1% boric acid solution is about 10 cm. Neutrons are therefore removed from the energy region above the cadmium limit almost exclusively by scattering. It is reasonable therefore to assume that the actual *number* of neutrons having energies above the cadmium limit in the space surrounding a given source is almost the same in dilute boric acid solutions as in water.

The total *number* of neutrons in the medium is $Q\tau$, where Q is the number of neutrons per second emitted by the source, and τ is the mean lifetime of the neutrons in the medium concerned. It follows, therefore, that the *percentage* of neutrons with energies above the cadmium limit in the boron solution is $0.93\ \tau_H/\tau_B$, where τ_H and τ_B are the mean lifetimes of neutrons in water and the boric acid solution respectively. This value is entered under Method I in Column 4 of Table VI. A more detailed calculation is not easy to make with accuracy, owing to the uncertain nature of the available constants, particularly the variation of the scattering cross-section of hydrogen in water with the energy of the neutrons.

An alternative method of estimating the percentage of neutrons above the cadmium limit is as follows. Let P be the probability that a neutron escapes capture during the slowing-down process to the energy of the cadmium cut-off in the boric acid solution. The number QP of neutrons per second reach the cadmium limit, and may be regarded as a source of slow neutrons. Hence the number of slow neutrons is $QP\tau$, and the percentage below the cadmium cut-off is $100P$. The probability P was calculated from Equation (2) of Appendix II. The results obtained by this method are shown in Column 5 of Table VI. The agreement between the two different methods is satisfactory (Columns 4 and 5).

Kubitschek (7) gives a graph of the neutron distribution (IR^2) measured in water by a manganese foil under cadmium. The area under this curve is not a correct measure of the total number of neutrons with energies above

TABLE VI

Medium	Molar fraction of boron	τ, sec.	Percentage of neutrons above cadmium limit	
			Calculated by Method I	Calculated by Equation (2) of Appendix II
Water	—	219×10^{-6}	0.93	0.90
1% H_3BO_3	1.455×10^{-2}	51×10^{-6}	4.00	3.88

the cadmium limit, but is an overestimate owing to the extra sensitivity of the manganese foil for neutrons of resonance energy. In fact the area under this curve is 1.7% of the area obtained when the C-group of neutrons is considered, whereas it should be about 0.9% (Table VI). We may artificially divide the neutrons absorbed by a manganese foil in water into the following three groups. (1) A fraction t is absorbed with energies below the cadmium cut-off according to the $1/v$ law. (2) A fraction f is assumed to be absorbed with energies above the cadmium cut-off according to the $1/v$ law. (3) A fraction r is assumed to be absorbed in the resonance band. We have now the following approximate relations between t, f, and r:

$$\frac{f}{t+f} = \frac{0.93}{100}; \qquad \frac{f+r}{t} = \frac{1.7}{100}; \qquad f+t+r = 1; \tag{4}$$

whence

$$t = 0.984, \quad f = 0.009, \quad r = 0.007, \quad \frac{r}{f+r} = 0.44. \tag{5}$$

We shall now assume that the fractions f and r, which refer to the population of neutrons, can also be applied to each reading of the manganese foil, no matter what its distance from the source may be. This amounts to an assumption that the spatial distribution of epithermal neutrons of all energies is the same, i.e., that the amount by which the cadmium-enclosed foil overestimates the neutron density is independent of position. Within the very wide limits of accuracy sufficient in applying this correction, the assumption is permissible. (See, for example, the curves of the distribution of neutrons of several energies in water around a point source, obtained by Amaldi and Fermi (1).)

It is now possible to correct the reading of a manganese foil to that of an ideal detector, simply by subtracting the fraction r from its reading. This is done in Table VII. The figures in the first three columns were obtained by Kubitschek (7). Both Kubitschek's and our notation are given in the headings to this table.

The results of comparative experiments with manganese foils and the boron trifluoride chamber are given in Table VIII, where the counts for the boron trifluoride chamber are in the same units as in Tables I and II. (The readings in Tables I and II and VIII do not agree exactly owing to readjustment of the

apparatus between experiments.) The counts given by the foils are in arbitrary units, being expressed in terms of a standard β-ray source. The resonance correction has been explained above.

TABLE VII

Distance from source	Intensity measured with bare Mn foil	Intensity measured by Mn foil under Cd	r	Resonance Correction
$\sqrt{r^2}$	A_{sat}	A_{res}		
R, cm.	$t+f+r$	$f+r$		$r/(t+f+r)$
2.19	21620	798	350	0.016
4.10	17650	478	210	0.012
6.06	12600	286	126	0.010
8.05	8361	142	62	0.0074
10.04	5320	72	32	0.0060
12.03	3340	55	24	0.0072
10.18	36010	554	244	0.0068
10.18	35780	550	242	0.0068
10.18	35680	550	242	0.0068
20.09	3954	48	21	0.0053
20.09	3945	47.7	21	0.0053
20.09	4026	47.7	21	0.0052

R, cm.	5.8	7	12
$r/(t+f+r)$ interpolated	0.010	0.008	0.0055

TABLE VIII

Distance from source, cm.	Medium	Count I_{Ch} with BF_3 chamber	Count with Mn foils					$\frac{I_{Ch}}{I_{Mn}}$	$K = \frac{(I_{Ch}/I_{Mn})B}{(I_{Ch}/I_{Mn})H_2O}$
			First foil	Second foil	Mean $t+f+r$	r	$t+f$		
12	Water	1240	531	525	528	3	525	2.36	1.03
	1% H_3BO_3	267	110	115	113	3	110	2.43	
5.8	Water	835	340	347	344	3	341	2.45	1.03
	1% H_3BO_3	250	102	102	102	3	99	2.53	
12	Water	1220	513	506	510	3	507	2.41	1.03
	1% H_3BO_3	272	114	112	113	3	110	2.47	
7	Water	665	274	269	272	2	270	2.46	0.975
	1% H_3BO_3	187	78.7	80.8	79.7	2	79.9	2.40	

From the last column it is seen that the mean of the ratio K, of I_{Ch}/I_{Mn} in boric acid solution to I_{Ch}/I_{Mn} in water, is not significantly different from unity.

The accuracy of these experiments is only sufficient to show that the perturbation error, if it exists, is less than $\pm 3\%$. Greater accuracy could have been obtained only by a long series of experiments which would have been very largely a duplication of Kubitschek's work (7). We do not consider it justifiable to make any modification to our result for σ_B/σ_H on the basis of the results shown in Table VIII.

Conclusion

The result of the integration experiment with the boron trifluoride chamber,

$$\sigma_B/\sigma_H = 2270,$$

has a statistical error of approximately 1%. The systematic error that might exist because of perturbation by the boron trifluoride chamber of the neutron density has been shown to be less than 3% if it exists. It is, therefore, not felt justifiable to correct the ratio given above on this account.

Within the errors of measurement this result is in agreement with Kubitschek's (7), and it is felt that the former discrepancy between measurements with boron trifluoride chambers and with foils has been removed.

In view of the difficulties inherent in the method used in the experiment, it is considered improbable that, in a reasonable time, the method would yield a value more accurate than either of the above results.

APPENDIX I

Analyses of Boric Acid Solutions

By A. H. Booth and A. C. English

Standard solutions of Analar boric acid were made up at the concentrations of the samples to be analysed so that in no case was the difference greater than 1%. Standard and sample were then estimated by the titration of the boric acid, in the presence of excess glycerine, by sodium hydroxide to the phenolphthalein end-point. The same pipette was used for both and the same burette over the same range. Quantities of glycerine and phenolphthalein added were constant and the end-point was taken by comparing the pink colour in 100 ml. Nessler tubes.

Using this technique, the absolute value obtained is dependent solely on the graduated flask, the weighing of the boric acid and its quality.

The average deviation of single titrations was less than 0.05 ml. in 40 ml. and the errors given are obtained by combining titration figures for standard and sample in the most unfavourable manner.

The results were: $(0.402 \pm 0.001)\%$ for 0.4% solution, $(1.007 \pm 0.002)\%$ for 1% solution, $(2.020 \pm 0.005)\%$ for 2% solution, and $(3.017 \pm 0.007)\%$ for 3% solution.

APPENDIX II

Calculation of the Probability that a Neutron Escapes Capture During the Slowing-down Process

The following formulae are essentially the same as those used by Kubitschek (6, 7) and are derived from the work of Wigner (11).

The probability P that a neutron escapes capture during the process of slowing-down from an initial energy E_I to the energy E_{Cd} of the cadmium cut-off in a boric acid solution may be written as follows:

$$P = \exp\left\{ -\int_{E_{Cd}}^{E_I} \frac{\sigma_B(E)C_B + \sigma_H(E)C_H}{\sigma_S C_H} \frac{dE}{\xi E} \right\}, \tag{1}$$

where $\sigma_B(E)$ and $\sigma_H(E)$ are the absorption cross-sections of boron and hydrogen, respectively, at energy E, σ_S the scattering cross-section of hydrogen, C_B and C_H the concentrations of boron and hydrogen respectively, and ξ the average logarithmic energy loss for neutron collisions with hydrogen. The effect of the oxygen has been neglected.

Writing $\sigma(E) = \sigma(kT)\sqrt{E_{kT}/E}$ for the absorption cross-sections of boron and hydrogen, and assuming that σ_S and ξ are constant, we obtain the approximate formula:

$$P = \exp\left\{ -\frac{2}{\xi\sigma_S}\sqrt{\frac{E_{kT}}{E_{Cd}}}\left[\sigma_B(kT)\frac{C_B}{C_H} + \sigma_H(kT)\right]\right\}. \tag{2}$$

This formula is used to calculate the percentage of neutrons in the solution that have energies below that of the cadmium cut-off. The following numerical values, partly taken from Goldsmith's tables (5), were used in the calculations:

$E_{kT} = 0.025$ ev., $\quad E_{Cd} = 0.3$ ev.

$\sigma_B(kT) = 705 \times 10^{-24}$ cm.^{2} per atom,

$\sigma_H(kT) = 0.31 \times 10^{-24}$ cm.^{2} per atom,

$\xi = 1$,

$\sigma_S = 20 \times 10^{-24}$ cm.^{2} per atom.

The last is an approximate average value for neutrons with energies greater than 0.3 ev.

References

1. AMALDI, E. and FERMI, E. Phys. Rev. 50 : 899-928. 1936.
2. ELLIOTT, L. G. Private communication.
3. FENNING, F. W., HALBAN, H. v., JR., and SELIGMAN, H. Unpublished report, Br-135. The ratio between absorption cross-sections of boron and hydrogen. British Atomic Energy Project. 1943.
4. FRISCH, O. R., HALBAN, H. v., JR., and KOCH, J. Kgl. Danske Videnskab. Selskab. Math.-fys. Medd. 15 (10) : 1-37. 1938.
5. GOLDSMITH, H. H. Unpublished report, CL-697. A critical survey of neutron cross-sections. Manhattan District Project. 1944.
6. KUBITSCHEK, H. Unpublished report, CP-972. Absorption cross-section ratio of boron and hydrogen. Manhattan District Project. 1943.

7. KUBITSCHEK, H. Unpublished report, CP-1824. Absorption cross-section ratio of boron to hydrogen. Manhattan District Project. 1944.
8. SCHULZ, L. G. and GOLDHABER, M. Phys. Rev. 67 : 202. 1945.
9. SKYRME, T. H. R. Unpublished report, MS-91. Reduction in neutron density caused by an absorbing disc. British Atomic Energy Project. 1944.
10. VEALL, N. Unpublished report, MP-60. On the construction of small boron chambers. National Research Council of Canada. 1944.
11. WIGNER, E. P. Unpublished report, C-1. Discussion of the homogeneous and lattice arrangements for power plants. Manhattan District Project. 1942.

A THEOREM ON NEUTRON MULTIPLICATION[1]

BY G. PLACZEK[2] AND G. VOLKOFF[3]

Abstract

The asymptotic behaviour of the neutron distribution due to a point source in an infinite homogeneous medium in which a convergent chain reaction (multiplication constant $k<1$) takes place is investigated without special assumptions about the properties of the medium and the mechanism of neutron diffusion. It is shown under very general assumptions that at large distances r from the point source the neutron distribution always has the form

$$\frac{A}{r}\exp(-\mu r)\,.$$

General expressions for the constants μ and A of this asymptotic form of the distribution are given for any $k<1$ in terms of the Fourier transform of the spatial distribution of primary fission neutrons. These expressions reduce to particularly simple form for $(1-k)<<1$. The exact expression for the neutron distribution throughout the medium is given in integral form. Four special frequently occurring cases are discussed as illustrations of the general result.

1. Introduction

This paper reports work done at the Montreal Laboratory, National Research Council of Canada, in 1943 and early 1944. An investigation is made of the behaviour far from a source of the neutron distribution in an infinite homogeneous medium in which a convergent chain reaction (multiplication factor $k<1$) takes place.

The discussion is restricted to the simplest case of a plane source of neutrons at $z = 0$ since once the neutron distribution is known for this case the point source neutron distribution in an infinite medium may be obtained from it in the usual manner by differentiation. The neutron distribution in an infinite medium corresponding to any other arbitrary source distribution may then be expressed in terms of the point source distribution.

The problem of finding the neutron distribution due to a plane source in an infinite multiplying medium is formulated in Section 2 in terms of an inhomogeneous integral equation. In Section 3 an elementary method of finding the approximate solution for $(1-k)<<1$ is given. In Section 4 the exact solution for any $k<1$ is obtained in integral form, and its asymptotic expression is shown to be of the form $C\exp(-\mu|z|)$ at distances $|z|$ from the plane source large compared to a characteristic length M (defined below in Section 2) for the diffusion of neutrons of a single generation. The theorem proved in Section 4 is that this exponential form of the asymptotic solution is *independent* of detailed assumptions about the nature of the medium and of

[1] *Manuscript received February 17, 1947.*

Contribution from the Division of Atomic Energy, National Research Council of Canada, Chalk River, Ont. Issued as N.R.C. No. 1576.

[2] *Formerly with the Montreal Laboratory, National Research Council; now with the Research Laboratory, General Electric Company, Schenectady, New York.*

[3] *Formerly with the Montreal and Chalk River Laboratories of the National Research Council; now Professor of Physics, University of British Columbia, Vancouver, B.C.*

the process of neutron diffusion. The value of the ratio of the relaxation length $1/\mu$ of this asymptotic solution to the characteristic length M referred to above depends, for a general $k<1$, not only on the value of k but also on the mechanism of diffusion of a single generation of neutrons, e.g., on the nature of the slowing down mechanism. However, as $k \to 1$ this ratio approaches $(1-k)^{-\frac{1}{2}}$ *independently* of the mechanism assumed. Likewise the value of C as $k \to 1$ is found to approach

$$C = \frac{Qs}{2M\sqrt{1-k}}, \tag{1.1}$$

(where Q is the source strength and s is a constant defined in Section 2) independently of the nature of the diffusion mechanism assumed, although the dependence of C on k for general values of $k<1$ is affected by the diffusion mechanism.

In Section 5 four special cases based on specific models of the diffusion of a single generation of neutrons are discussed. Explicit expressions for the constants in the asymptotic form of the solution of the integral equation in these four cases are given as illustrations of the general theorem.

2. Formulation of the Problem

We define $G(|z|)dz$ to be the number of *primary* fission neutrons of all energies created (as the result of direct absorption of source neutrons only) between z and $z+dz$ per neutron emitted by a plane source of neutrons placed at $z = 0$ in the multiplying medium. $G(|z|)$ will depend on the properties of the multiplying medium with respect to the diffusion, capture, relative fission probability, and neutron yield for neutrons of various energies, and also on the form of the energy distribution of source neutrons (see Appendix). Let $G_s(|z|)$ be the particular expression for $G(|z|)$ corresponding to a source of some specified neutron energy spectrum in a given medium. Similarly let $G_f(|z|)$ be the expression for $G(|z|)$ corresponding to a fission source in the same medium. The use made below of a single function $G_f(|z|)$ for fission sources involves the assumption that the form of the energy spectrum of fission neutrons is independent of the energy of the neutron which causes fission. This is the only restrictive assumption on the nature of the multiplication process required to set up the problem.

The integral of $G(|z|)$ over all z gives the total number of primary fission neutrons per source neutron which may in general depend on the energy spectrum of the source. In particular the quantity

$$\int_{-\infty}^{+\infty} G_s(|z|)\, dz = s \tag{2.1}$$

for source neutrons may be different from

$$\int_{-\infty}^{+\infty} G_f(|z|)\, dz = k \tag{2.2}$$

for a fission source. The latter quantity k is defined as the multiplication factor.

We introduce for mathematical convenience

$$F(|z|) = \frac{1}{k} G_f(|z|) , \tag{2.3}$$

which is normalized to unity:

$$\int_{-\infty}^{+\infty} F(|z|)\, dz = 1 . \tag{2.4}$$

We use $F(|z|)$ to define* a characteristic length M (usually called a migration length) by means of

$$M^2 = \int_{-\infty}^{+\infty} \frac{z^2}{2} F(|z|) dz . \tag{2.5}$$

M is therefore a measure of the distance a neutron on the average travels away from a plane source of fission neutrons before being captured to give rise to k primary fission neutrons.

We consider now the physical problem of a given plane source of strength Q introduced into an infinite multiplying medium and wish to determine the resulting neutron distribution. If we describe the neutron distribution by specifying the number $f(z)dz$ of fission neutrons to which it gives rise per unit time between z and $z+dz$ then $f(z)$ must satisfy the simple inhomogeneous integral equation

$$f(z) = Q\, G_s(|z|) + k \int_{-\infty}^{+\infty} f(z')dz'\, F(|z - z'|) , \tag{2.6}$$

since fission neutrons created at a rate $f(z)dz$ in the interval between z and $z+dz$ are due partly to the given source of strength Q at the origin (first term on the right) and partly to fission sources distributed throughout the infinite medium with a density $f(z')$ (second term on the right).

If some other property of the neutron distribution were chosen to describe it, e.g., the number of fissions, or the number of neutron captures taking place per unit volume per unit time, then additional restrictive assumptions would have to be made in order to obtain a simple integral equation analogous to (2.6). Thus if the number of fissions per unit volume per unit time is taken as the variable describing the neutron distribution, then not only the *form* of the energy distribution but also the *average number* ν of neutrons emitted in a fission process must be assumed to be independent of the energy of the neutrons causing fission (see Appendix). We therefore retain the rate of creation of fission neutrons $f(z)$ as the variable describing the neutron distribution, and shall have $f(z)$ in mind when speaking for the sake of brevity simply of neutron distribution.

* *The inclusion of the factor 2 in this definition for the sake of mathematical convenience later is in accord with general usage.*

An integral property of $f(z)$ follows immediately from integrating (2.6) over all z and applying (2.1) and (2.4):

$$\int_{-\infty}^{+\infty} f(z)dz = \frac{Qs}{1-k} \,. \tag{2.7}$$

This may also be obtained by summing the number of fission neutrons of all generations to which Q source neutrons give rise, viz., $Qs + Qsk + Qsk^2 + Qsk^3 + \ldots$

3. Elementary Method of Obtaining the Approximate Solution of the Integral Equation for $(1-k)<<1$

If $(1-k)<<1$ then many generations of neutrons will contribute to $f(z)$, and it seems plausible that $f(z)$ will vary much more slowly with z than $F(|z|)$ which describes a single neutron generation. It may be expected that this will be true even in the neighbourhood of the given source at the origin since for $(1-k)<<1$ the effect of the given source will be swamped by that of the secondary sources of fission neutrons.

This difference in the rate of variation of $f(z)$ and $F(|z|)$ enables us to replace (2.6) approximately by a differential equation. We invert the convolution in (2.6) by introducing a new variable $u = z - z'$, and expand $f(z-u)$ in a Taylor series about z. In place of (2.6) we obtain:

$$\begin{aligned} f(z) &= Q\,G_s(|z|) + k\int_{-\infty}^{+\infty} du\, F(|u|)\Big[f(z) - uf'(z) + \\ &\qquad \frac{u^2}{2}f''(z) - \frac{u^3}{3!}f'''(z) + \frac{u^4}{4!}f^{iv}(z)\,..\Big] \\ &= Q\,G_s(|z|) + k\Big[f(z) + M^2 f''(z) + \frac{m_4}{4!}f^{iv}(z) + \ldots\ldots\Big], \end{aligned} \tag{3.1}$$

where

$$m_4 = \int_{-\infty}^{+\infty} u^4\, F(|u|)\, du \,. \tag{3.2}$$

The odd moments of $F(|u|)$ are all zero. In view of our assumption, that $f(z-u)$ changes but little over the region in which $F(|u|)$ differs appreciably from zero, the successive terms in the square brackets of (3.1) must fall off rapidly, so that by keeping only the first few terms of the expansion we can approximately replace the integral equation (2.6) by a differential equation of low order. The boundary conditions on the solution of this differential equation are:

$$\begin{aligned} &f(|z|)\to 0 \text{ for } |z|\to\infty, \text{ and } \left[\frac{d^{2n+1}f(z)}{dz^{2n+1}}\right]_{z=0} \\ &\qquad = Q\left[\frac{d^{2n+1}G_s(z)}{dz^{2n+1}}\right]_{z=0} \quad (n = 0, 1, 2, \ldots) \,. \end{aligned} \tag{3.3}$$

The second part of (3.3) is obtained by differentiating (2.6) an odd number of times, setting $z = 0$, and noting that the resulting integrand is odd.

If we keep only the first two terms in the brackets of (3.1) and consistently let $k \to 1$ we obtain the second order differential equation:

$$f''(z) - \frac{1-k}{M^2} f(z) = -\frac{Q\, G_s(|z|)}{M^2} . \tag{3.4}$$

The solution of (3.4) vanishing at infinity is

$$f(z) = C e^{-\sqrt{1-k}\frac{|z|}{M}} + S(|z|) , \tag{3.5}$$

where

$$S(z) = -\frac{Q}{M\sqrt{1-k}} \int_{|z|}^{\infty} \sinh\left[\sqrt{1-k}\,\frac{(z'-|z|)}{M}\right] G_s(|z'|)dz' \tag{3.6}$$

is the particular integral of (3.4) which falls off with increasing $|z|$ at a rate determined by $G_s(|z|)$ and represents the deviation of $f(z)$ from the asymptotic exponential solution in the neighbourhood of the given source at the origin.

Since (3.6) falls off with increasing z at a rate comparable with that of $G_s(|z|)$ and hence of $F(|z|)$, it can at best represent only an order of magnitude estimate* of the actual deviation near the source of the solution of the integral equation (2.6) from its asymptotic exponential form. The reason for this is that although the expansion of (3.1) converges rapidly for the main slowly varying exponential part of $f(z)$ it may converge only slowly, or not at all, for the small correction term $S(|z|)$ which may vary as fast, or faster than $F(|z|)$. Therefore to determine C in (3.5) it is not safe to use $f'(0) = Q\,G_s'(0)$ from (3.3), since we depend then on the accurate knowledge of $S'(0)$. It is preferable to determine C by applying (2.7) to (3.5) and neglecting** $\int_{-\infty}^{+\infty} S(|z|)dz$ in comparison with $Qs/(1-k)$. This gives

$$C = \frac{Qs}{2M\sqrt{1-k}} . \tag{3.7}$$

Since for $(1-k) \ll 1$ $S(0)$ is smaller† than C by a factor $\sqrt{1-k}$ and $S(|z|)$ falls off faster than the exponential of (3.5), we may neglect $S(|z|)$ everywhere and the approximate solution of (2.6) valid everywhere is

$$f(z) = C \exp(-\mu\,|z|) , \tag{3.8}$$

with C given by (3.7) and $\mu = \sqrt{1-k}/M$.

* *The simple example of case I in Section 5 below shows that for $\gamma < 1$ (3.6) may even have the wrong sign.*

** *The order of magnitude of $\int_{-\infty}^{+\infty} S(|z|)dz$ is $2M_s\, S(0) \approx QsM_s^2/M^2 \approx Qs$, where M_s is the characteristic length associated with $S(|z|)$ or $G_s(|z|)$.*

† *From (3.6) the order of magnitude of $S(0)$ is $QsM_s/2M^2 \approx Qs/2M$.*

The point source solution $\rho(r)$ is obtained from the plane source solution $f(z)$ as follows (see reference (2)):

$$\rho(r) = -\frac{1}{2\pi r}\frac{df(r)}{dr} = -\frac{C}{2\pi r}\frac{d}{dr}\exp(-\mu r) = A\frac{\exp(-\mu r)}{r}, \quad (3.9)$$

where

$$A = \frac{C\mu}{2\pi}. \quad (3.10)$$

The value of the exponent μ in (3.8) and (3.9), but not of the coefficient C or A in front, may be somewhat improved by retaining three terms in the second square brackets of (3.1) to give a fourth order differential equation:

$$\frac{m_4}{4!}f^{(iv)}(z) + M^2 f''(z) - \frac{1-k}{k}f(z) = -\frac{Q}{k}G(z). \quad (3.11)$$

Using the trial solution (3.8) for the complementary function we find that μ must satisfy

$$\frac{m_4}{4!}\mu^4 + M^2\mu^2 - \frac{1-k}{k} = 0, \quad (3.12)$$

which gives for the smallest root μ

$$\mu = \frac{1}{M}\sqrt{\frac{\sqrt{1+\frac{1-k}{k}\frac{m_4}{3!\,M^4}}-1}{\frac{2m_4}{4!\,M^4}}}$$
$$= \frac{\sqrt{1-k}}{M}\left[1+\frac{1}{2}\left(1-\frac{m_4}{4!\,M^4}\right)(1-k)+0\{(1-k)^2\}\right]. \quad (3.13)$$

4. Solution of Integral Equation by Fourier Transforms. Asymptotic Behaviour of the Solution

Let $\phi(\zeta)$, $\Phi(\zeta)$, and $\Gamma_s(\zeta)$ be respectively the Fourier transforms of $f(z)$, $F(|z|)$, and $G_s(|z|)$ defined by

$$\phi(\zeta) = \int_{-\infty}^{+\infty} f(z)\,e^{i\zeta z}dz; \quad \Phi(\zeta) = \int_{-\infty}^{+\infty} F(|z|)\,e^{i\zeta z}dz;$$
$$\Gamma_s(\zeta) = \int_{-\infty}^{+\infty} G_s(|z|)\,e^{i\zeta z}dz. \quad (4.1)$$

Multiplying (2.6) by $e^{i\zeta z}$, integrating over all z, and applying the convolution theorem to the integral on the right-hand side we obtain:

$$\phi(\zeta) = Q\Gamma_s(\zeta) + k\phi(\zeta)\Phi(\zeta). \quad (4.2)$$

Solving for $\phi(\zeta)$ we get

$$\phi(\zeta) = Q\frac{\Gamma_s(\zeta)}{1-k\Phi(\zeta)}, \quad (4.3)$$

which on inversion gives:

$$f(z) = \frac{Q}{2\pi}\int_{-\infty}^{+\infty}\frac{\Gamma_s(\zeta)e^{-i\zeta z}d\zeta}{1-k\Phi(\zeta)}. \quad (4.4)$$

In order to determine the asymptotic behaviour of $f(z)$ for large $|z|$ we now investigate the poles of the integrand of (4.4) which lie at the roots of

$$\Phi(\zeta) = \frac{1}{k}, \tag{4.5}$$

and at the poles of $\Gamma_s(\zeta)$ which are not at the same time poles of $\Phi(\zeta)$.

From their physical nature $F(|z|)$ and $G_s(|z|)$ are positive and even. We also assume that both $F(|z|)$ and $G_s(|z|)$ fall off at least exponentially at large $|z|$ so that $F(|z|)e^{\eta z}$ and $G_s(|z|)e^{\eta z}$ are quadratically integrable in the whole interval $-\infty<z<\infty$ for $|\eta|<\eta_f$ and $|\eta|<\eta_s$ respectively, where η_f and η_s are positive quantities characteristic of $F(|z|)$ and $G_s(|z|)$. Considered as a function of the complex variable $\zeta = \xi + i\eta$, $\Phi(\zeta)$ defined by (4.1) has the following properties.

(*a*) $\Phi(\zeta)$ is holomorphic in the strip $|I(\zeta)|<\eta_f$,

(*b*) $\Phi(\zeta) = \Phi(-\zeta)$, $\overline{\Phi(\zeta)} = \Phi(\bar{\zeta})$, (4.6)

which show that $\Phi(\zeta)$ is real along both the real and the imaginary axes in the ζ plane.

(*c*) $\Phi(0) = 1$, $\Phi''(0) = -2M^2$, $\Phi^{(2n+1)}(0) = 0$, (4.7)

the first two relations following from (2.4) and (2.6), the last from the fact that $F(|z|)$ is even.

(*d*) $$\frac{d}{d\eta}\Phi(i\eta) = 2\int_0^\infty F(|z|)z \sinh \eta z\, dz > 0 \text{ for } 0 < \eta < \eta_f, \tag{4.8}$$

which shows that $\Phi(\zeta)$ increases monotonically from 1 to ∞ as ζ goes from 0 to $i\eta_f$ (or from 0 to $-i\eta_f$) along the imaginary axis.

(*e*) For $\xi \neq 0$, and $0 \leqslant \eta < \eta_f$

$$R\,\Phi(\xi + i\eta) = \int_{-\infty}^{+\infty} F(|z|)e^{-\eta z}\cos \xi z\, dz < \int_{-\infty}^{+\infty} F(|z|)e^{-\eta z}dz = R\,\Phi(0 + i\eta). \tag{4.9}$$

In order for ζ to be a root of (4.5) it must simultaneously satisfy the two conditions

$$R\,\Phi(\zeta) = \frac{1}{k} > 1 \qquad I\,\Phi(\zeta) = 0. \tag{4.10}$$

The second of these conditions is satisfied along all points of the imaginary axis in virtue of (4.6). Because of (4.8) the first condition will certainly be satisfied at a pair of points $\zeta = \pm i\mu$ with $0<\mu<\eta_f$. Since $\Phi'(i\mu) \neq 0$ these will be simple roots of (4.5). Expanding $\phi(i\mu)$ in powers of μ we may rewrite (4.5) in the form

$$\frac{1-k}{k} = M^2\mu^2 + \frac{m_4}{4!}\mu^4 + \ldots\ldots, \tag{4.11}$$

which we recognize to be the same as (3.12). We see that as $k \to 1$ the smallest root μ of (4.11) is such that

$$\zeta = \pm i\mu \to \pm i \frac{\sqrt{1-k}}{M} \tag{4.12}$$

independently of the exact form of $F(|z|)$ *and* $\Phi(\zeta)$.

If (4.5) has any roots other than $\zeta = \pm i\mu$ their imaginary parts must be larger than μ. This may be seen from the fact that the first of conditions (4.10) cannot be satisfied for $|\eta| < \mu$ or for $|\eta| = \mu$, $\xi \neq 0$ because of (4.8) and (4.9).

The singularities of $\Gamma_s(\zeta)$ must have imaginary parts not smaller than η_s which for $1-k$ sufficiently small will always be greater than μ (otherwise when the multiplication is not sufficiently strong even the asymptotic behaviour of $f(z)$ will be governed by the neutrons coming from the given source). The integrand of (4.4) consequently has simple poles at $\zeta = \pm i\mu$, and all its other singularities, if any, lie further away from the real axis in the ζ plane and are situated symmetrically with respect to both the real and the imaginary axes. Let η_1 be the magnitude of the imaginary part of the next singularity of the integrand. For $z > 0$ we shift the path of integration in (4.4) from the real axis to the line $I(\zeta) = -\eta_1$ (or to the line $I(\zeta) = +\eta_1$, for $z < 0$), and obtain the asymptotic expression for large $|z|$:

$$f_{as}(z) = Ce^{-\mu|z|} + 0(e^{-\eta_1|z|}), \tag{4.13}$$

where μ is defined as the positive real root of

$$\Phi(i\mu) = \frac{1}{k} \tag{4.14}$$

and

$$C = \frac{Q}{k} \frac{\Gamma_s(i\mu)}{\dfrac{d\Phi(i\mu)}{d\mu}} = \frac{Q}{k} \frac{\displaystyle\int_0^\infty G_s(|z|) \cosh \mu z \, dz}{\displaystyle\int_0^\infty F(|z|)\, z \sinh \mu z \, dz}. \tag{4.15}$$

For $k \to 1$ (4.14) reduces to (4.12) and (4.15) reduces to

$$C \to Q \frac{\Gamma_s(0) + 0(k-1)^2}{\dfrac{d}{d\mu}\left[\Phi(0) - \dfrac{\mu^2}{2}\Phi''(0)\right]} \to \frac{Qs}{2M^2\mu} \to \frac{Qs}{2M\sqrt{1-k}}, \tag{4.16}$$

where s is defined by (2.1). Thus the μ and C of (4.13) reduce for $k \to 1$ to those of (3.7) independently of the nature of $F(|z|)$. For k appreciably less than unity (4.14) and (4.15) give the *exact* expressions for both the inverse relaxation length μ and the coefficient C of the asymptotic form (4.13) of $f(z)$.

The asymptotic solution for a *point* source of primary neutrons may again be determined from the plane source case with the aid of (3.9) where A is now given by:

$$A = \frac{C\mu}{2\pi} = \frac{Q}{2\pi k} \frac{\mu\Gamma_s(i\mu)}{\dfrac{d\Phi(i\mu)}{d\mu}}. \tag{4.17}$$

If the energy spectrum of the given source is taken to be the same as that of a fission source, so that

$$G_s(|z|) = G_f(|z|) = k\,F(|z|)\,, \tag{4.18}$$

then $\Gamma_s(\zeta)$ in (4.2) to (4.4) should be replaced by $k\,\Phi(\zeta)$, and $\Gamma_s(i\mu)$ in (4.15) to (4.17) should be replaced by $k\Phi(i\mu) = 1$ in virtue of (4.14).

Let us denote $\phi(\zeta)$ and $f(z)$ in the special case (4.18), respectively, by:

$$\phi_0(\zeta) = Q\,\frac{k\,\Phi(\zeta)}{1 - k\,\Phi(\zeta)}\,, \tag{4.19}$$

and

$$f_0(z) = \frac{Q}{2\pi}\int_{-\infty}^{+\infty}\frac{k\,\Phi(\zeta)e^{-i\zeta z}}{1 - k\Phi(\zeta)}\,d\zeta\,. \tag{4.20}$$

Then in the general case $G_s(|z|) \neq G_f(|z|)$ we have:

$$\phi(\zeta) = \frac{Q\Gamma_s(\zeta)}{1 - k\,\Phi(\zeta)} = Q\Gamma_s(\zeta)\left[1 - \frac{k\,\Phi(\zeta)}{1 - k\,\Phi(\zeta)}\right]$$
$$= Q\Gamma_s(\zeta) + \Gamma_s(\zeta)\phi_0(\zeta)\,. \tag{4.21}$$

Inverting (4.21) and applying the convolution theorem we have:

$$f(z) = Q\,G_s(|z|) + \int_{-\infty}^{+\infty} G_s(|z'|)\,f_0(z - z')\,dz'\,. \tag{4.22}$$

Thus $f(z)$ may be obtained either from (4.4) in terms of $\Gamma_s(\zeta)$ and $\Phi(\zeta)$, or from (4.22) in terms of $G_s(|z|)$ and $f_0(z)$.

5. Discussion of Special Cases

Four special cases are discussed below in which the distribution $G_f(|z|)$ of primary fission neutrons is in each case given by a particular model of neutron diffusion. The characteristic length M defined by (2.5) is used as the unit of length throughout this section.

In the first three cases the complete exact solution $f_0(z)$ corresponding to $G_s(|z|) = G_f(|z|)$ is found explicitly, so that the asymptotic term

$$f_{0as}(z) = C_0\exp(-\mu|z|) \tag{5.1}$$

may be compared directly with the other more rapidly decreasing terms. In the fourth case the asymptotic term is given explicitly, but only the order of the next term is indicated. Table I summarizes the constants μ and C_0 of (5.1) for the four cases. The value of μ remains unchanged in the more general case $G_s(|z|) \neq G_f(|z|)$, while the value of C may be obtained by multiplying C_0 by $\Gamma_s(i\mu)$. $f(z)$ may be obtained from $f_0(z)$ and $G_s(|z|)$ with the aid of (4.22), or directly from (4.4).

Case I. *Elementary Treatment of the One Velocity Problem*

$$F(|z|) = \frac{G_f(|z|)}{k} = \frac{1}{2}\exp(-|z|)\,. \tag{5.2}$$

The migration length chosen throughout this section as the unit of length in this case reduces to the *diffusion length* (see reference (2) for definition). The Fourier transform of (5.2) is

$$\Phi(\zeta) = \frac{1}{1+\zeta^2}\,. \tag{5.3}$$

From (4.19)

$$\phi_0(\zeta) = Q\,\frac{k}{\zeta^2 + 1 - k} \tag{5.4}$$

and from (4.20) by contour integration:

$$f_0(z) = \frac{Qk}{2\sqrt{1-k}}\exp\left[-\sqrt{1-k}\,|z|\right]. \tag{5.5}$$

The *complete* solution is in this case given everywhere by the single exponential term (5.5) which is simply (5.2) with the unit of length rescaled by a factor $\sqrt{1-k}$. The integrated value of $f_0(z)$ over all z is $Qk/(1-k)$ which is the same as (2.7) with $s = k$.

A simple example of $G_s(|z|) \neq G_f(|z|)$ may be considered by taking

$$G_s(|z|) = s\,\frac{\gamma}{2}\exp(-\gamma|z|) \quad \text{with } \gamma \neq 1,\ s \neq k\,. \tag{5.6}$$

The Fourier transform of (5.6) is:

$$\Gamma_s(\zeta) = \frac{s}{1+\left(\frac{\zeta}{\gamma}\right)^2}. \tag{5.7}$$

This leads to:

$$f(z) = \frac{Qk}{2\sqrt{1-k}}\,\frac{s\gamma^2}{\gamma^2-(1-k)}$$
$$\left[\exp\left(-\sqrt{1-k}\,|z|\right) - \frac{\sqrt{1-k}(1-\gamma^2)}{k\gamma}\exp(-\gamma|z|)\right]. \tag{5.8}$$

In agreement with the results of Section 3 we can see that for $(1-k)<<1$ the ratio of the second term to the first term of (5.8) near the given source ($z = 0$) is of order $\sqrt{1-k}$, and the second term falls off more rapidly than the first as long as $\sqrt{1-k} < \gamma$. The second term of (5.8) represents the exact expression for the deviation of $f(z)$ near the source from its asymptotic form, and the expression to which (3.6) reduces in this case differs from it in the value of the coefficient of $\exp(-\gamma|z|)$ for reasons outlined in Section 3. The coefficient of $\exp(-\sqrt{1-k}\,|z|)$ in (5.8) differs from that in (5.5) by the factor $\Gamma_s(i\mu)$ in accordance with (4.17).

Case II. *Exact Treatment of the One Velocity Problem with Isotropic Scattering*

$$F(|z|) = \frac{\alpha}{\sqrt{3\,\alpha}}\left[\frac{(1-\nu^2)\nu}{(1-\alpha)(\nu^2-\alpha)}\,e^{-\frac{\nu|z|}{\sqrt{3\alpha}}} + \frac{1}{2}\int_1^\infty \frac{e^{-\eta\frac{|z|}{\sqrt{3\alpha}}}\,d\eta}{\eta\left(1-\frac{1-\alpha}{\eta}\operatorname{arth}\frac{1}{\eta}\right)^2+\frac{\pi^2(1-\alpha)^2}{4\eta}}\right], \tag{5.9}$$

where $\alpha = l/l_c$ is the ratio of the total mean free path l to the capture mean free path l_c, ν is the positive real root of the transcendental equation*

$$\frac{1}{1-\alpha} = \frac{\operatorname{arth}\nu}{\nu}. \tag{5.10}$$

The unit of length is the *migration length* $l/\sqrt{3\alpha}$ which becomes the diffusion length of Case I for $\alpha\to 0$. As $\alpha\to 0$ the first term of (5.9) reduces to (5.2) and the second term vanishes so that this case reduces to the preceding one. The Fourier transform of (5.9) is (see reference (1) for derivation of (5.9) and (5.11)):

$$\Phi(\zeta) = \frac{\alpha \operatorname{art}\left[\zeta\sqrt{3\alpha}\right]}{\zeta\sqrt{3\alpha}-(1-\alpha)\operatorname{art}\left[\zeta\sqrt{3\alpha}\right]}. \tag{5.11}$$

From (4.19)

$$\phi_0(\zeta) = Q\,\frac{k\,\alpha \operatorname{art}\left[\zeta\sqrt{3\alpha}\right]}{\zeta\sqrt{3\alpha}-(1-\alpha')\operatorname{art}\left[\zeta\sqrt{3\alpha}\right]} \tag{5.12}$$

with

$$\alpha' = \alpha(1-k). \tag{5.13}$$

This differs from (5.11) only by having the extra factor Qk in the numerator, and α' in place of α in one term of the denominator. Employing the procedure of reference (1) to invert (5.12) we obtain an expression analogous to (5.9), viz.

$$f_0(z) = \frac{Qk\alpha}{\sqrt{3\alpha}}\left[\frac{(1-\nu'^2)\nu'}{(1-\alpha')(\nu'^2-\alpha')}\,e^{-\frac{\nu'|z|}{\sqrt{3\alpha}}} + \frac{1}{2}\int_1^\infty \frac{e^{-\frac{\eta|z|}{\sqrt{3\alpha}}}\,d\eta}{\eta\left(1-\frac{1-\alpha'}{\eta}\operatorname{arth}\frac{1}{\eta}\right)^2+\frac{\pi^2(1-\alpha')^2}{4\eta}}\right], \tag{5.14}$$

where ν' is the root of (5.10) with α replaced by α'. Although the *form* of (5.9) is preserved in (5.14), the *relative importance* of the two terms is altered.

* *We use the abbreviated notation* $\operatorname{arth} x \equiv \operatorname{arctanh} x$ *and* $\operatorname{art} x \equiv \arctan x$ *throughout this paper.*

The second term of (5.14), describing the influence of the neutrons coming directly from the given source, is affected relatively little by a change in α' as $k \to 1$, while the coefficient of the first term contains the factor $\nu'/(\nu'^2 - \alpha')$ which increases like $(1-k)^{-\frac{1}{2}}$ as $k \to 1$.

Case III. *Elementary Treatment of Multiplication Preceded by Slowing-down*

$$F(|z|) = \frac{1}{\sqrt{4\pi}} e^{-\frac{z^2}{4}}. \tag{5.15}$$

This corresponds to the physical model in which the fission neutron spectrum is represented by a single neutron energy E_0, and the neutrons are assumed to be captured as soon as they are slowed down to an energy $E_1 < E_0$. The age–velocity slowing-down theory (see reference (2)) is used to describe the slowing-down process, and the *slowing-down* length (to which the migration length is equivalent in this case) is used as the unit of length. The Fourier transform of (5.15) is

$$\Phi(\zeta) = e^{-\zeta^2}. \tag{5.16}$$

From (4.19)

$$\phi_0(\zeta) = Q \frac{k}{e^{\zeta^2} - k}. \tag{5.17}$$

The denominator of (5.17) has zeros at

$$\zeta_n = \pm \xi_n \pm i\eta_n, \ (n = 0, 1, 2, \ldots..) \tag{5.18}$$

where

$$\xi_n = \frac{n\pi}{\sqrt{\frac{\ln\frac{1}{k}}{2} + \sqrt{\left(\frac{\ln\frac{1}{k}}{2}\right)^2 + n^2\pi^2}}} \to \pm\sqrt{n\pi} \text{ for } n >> \frac{\ln\frac{1}{k}}{2\pi} \tag{5.19}$$

$$\eta_n = \sqrt{\frac{\ln\frac{1}{k}}{2} + \sqrt{\left(\frac{\ln\frac{1}{k}}{2}\right)^2 + n^2\pi^2}} \to \pm\sqrt{n\pi} \text{ for } n >> \frac{\ln\frac{1}{k}}{2\pi}. \tag{5.20}$$

Contour integration then gives:

$$f_0(z) = Q\left[\frac{e^{-|z|\sqrt{\ln\frac{1}{k}}}}{2\sqrt{\ln\frac{1}{k}}} + \sum_{n=1}^{\infty} \frac{e^{-\eta_n|z|}}{4\sqrt{\left(\ln\frac{1}{k}\right)^2 + 4n^2\pi^2}} \sin\left\{\tan^{-1}\left(\frac{\eta_n^2}{n\pi}\right) - \frac{n\pi}{\eta_n}|z|\right\}\right]. \tag{5.21}$$

Here the Gaussian form of (5.15) is not at all preserved in (5.21).

TABLE I

VALUES OF μ, C_0 AND A_0 IN $f_{0,os}(z) = C_0 \exp(-\mu|z|)$ AND $\rho_{0os}(r) = \frac{A_0}{r}\exp(-\mu r)$.
THE MIGRATION LENGTH M IS TAKEN AS THE UNIT OF LENGTH

Case	$\Phi(\zeta)$	μ Defined by $\Phi(i\mu) = \frac{1}{k}$	$\frac{C_0}{Q} = \frac{1}{k\frac{d\Phi(i\mu)}{d\mu}} = \frac{2\pi A_0}{\mu Q}$
I	$\frac{1}{1+\zeta^2}$	$\sqrt{1-k}$	$\frac{k}{2\sqrt{1-k}}$
II	$\frac{\alpha \operatorname{art}\zeta\sqrt{3\alpha}}{[\zeta\sqrt{3\alpha}] - (1-\alpha)\operatorname{art}[\zeta\sqrt{3\alpha}]}$	Positive real root of: $\frac{1}{1-\alpha(1-k)} = \frac{\operatorname{arth}[\mu\sqrt{3\alpha}]}{\mu\sqrt{3\alpha}}$	$\frac{k\alpha}{\sqrt{3\alpha}}\frac{(1-\nu'^2)\,\nu'}{[1-\alpha(1-k)]\,[\nu'^2-\alpha(1-k)]}$ with $\nu' = \mu\sqrt{3\alpha}$
III	$e^{-\zeta^2}$	$\sqrt{\ln\frac{1}{k}}$	$\frac{1}{2\sqrt{\ln\frac{1}{k}}}$
IV	$\frac{e^{-\delta\zeta^2}}{1+\zeta^2(1-\delta)}$	Positive real root of: $1-\mu^2(1-\delta) = k\,e^{\delta\mu^2}$	$\frac{1}{2\mu\left[\frac{1-\mu^2\delta(1-\delta)}{1-\mu^2(1-\delta)}\right]}$
All cases $(1-k)<<1$		$\sqrt{1-k}$	$\frac{1}{2\sqrt{1-k}}$

For $G_s(|z|) \neq G_f(|z|)$, C and A may be obtained from C_0 and A_0 by multiplying them by $\Gamma_s(i\mu)$.

Case IV. *Elementary Treatment of Multiplication Preceded by Slowing-down Which is Followed by Diffusion at Constant Energy*

This is an extension of Case III corresponding to the assumption that a neutron need not be immediately captured on reaching the energy E_1, but that it may diffuse for some time without further loss of energy. If δ denotes the ratio of the slowing-down length to the total *migration length*, which is taken as the unit of length, then reference (2) gives:

$$F(z) = \frac{\exp\left(\frac{\delta}{1-\delta}\right)}{4\sqrt{1-\delta}}\left\{\exp\left(-\frac{z}{\sqrt{1-\delta}}\right)\left[1-\operatorname{erf}\left(\sqrt{\frac{\delta}{1-\delta}}-\frac{z}{2\sqrt{\delta}}\right)\right]+ \exp\left(\frac{z}{\sqrt{1-\delta}}\right)\left[1-\operatorname{erf}\left(\sqrt{\frac{\delta}{1-\delta}}+\frac{z}{2\sqrt{\delta}}\right)\right]\right\}, \quad (5.22)$$

where

$$\operatorname{erf} x \equiv \frac{2}{\sqrt{\pi}}\int_0^x e^{-u^2}\,du \equiv -\operatorname{erf}(-x)\,. \quad (5.23)$$

This reduces to (5.2) as $\delta \to 0$, and to (5.15) as $\delta \to 1$. The Fourier transform of (5.22) is

$$\Phi(\zeta) = \frac{\exp(-\delta\zeta^2)}{1+\zeta^2(1-\delta)}\,. \quad (5.24)$$

From (4.19)

$$\phi_0(\zeta) = Qk\,\frac{1}{[1+\zeta^2(1-\delta)]\,e^{\delta\zeta^2}-k}\,. \quad (5.25)$$

The denominator of (5.25) has a denumerable infinity of zeros which are discussed in an Appendix of reference (2). The zeros with the smallest imaginary part lie at $\pm i\mu$, where μ is the only real positive root of

$$1-\mu^2(1-\delta) = k\,e^{\delta\mu^2}\,. \quad (5.26)$$

Inversion of (5.25) gives:

$$f_{0as}(z) = \frac{Q}{2\mu\left[\frac{1-\mu^2\,\delta(1-\delta)}{1-\mu^2(1-\delta)}\right]}\exp(-\mu|z|) + 0\,[\exp(-\eta_1|z|)]\,, \quad (5.27)$$

where η_1 is the real part of the first complex root of (5.26). The form of (5.22) is again not at all preserved in (5.27).

6. Acknowledgment

We wish to express our thanks to Dr. R. E. Marshak for helpful discussions of this problem at the time the original work was done.

7. Appendix

The Nature of $G(|z|)$

The function $G(|z|)$ introduced in Section 2 may be explicitly written as:

$$G(|z|) = \int dE' \int dE''\, x_s(E')\, H(|z|, E', E'')\,\frac{c(E'')\,\nu(E'')}{\tau(E'')}\,, \quad (7.1)$$

where

$x_s(E')dE'$ = fraction of neutrons of all energies emitted by the source at $z = 0$ with energy between E' and $E'+dE'$. The integral of $x_s(E')$ over all E' is by definition unity, but the form of the dependence of $x_s(E')$ on E' may depend on the nature of the source, e.g., in the case of a fission source it may depend on the energy of the neutron causing the fission.

$H(|z|, E', E'')dz\,dE''$ = number of neutrons between z and $z+dz$ with energy between E'' and $E''+dE''$ in a steady state distribution in a non-multiplying infinite medium of the same capture and scattering properties as the multiplying medium under consideration, due to a unit plane source at $z=0$ of neutrons of energy E'. This depends on the mechanism of neutron diffusion and slowing-down, on the properties of the medium, and on the initial energy E' of the neutrons emitted by the source.

$\frac{1}{\tau(E'')}$ = capture probability per unit time of neutrons of energy E''. This depends on the composition of the medium and the neutron absorption cross-sections of the constituent nuclei.

$c(E'')$ = fraction of captures at energy E'' which lead to fission. This depends on the composition of the medium and the variation with energy of the neutron absorption cross-sections of the various components.

$\nu(E'')$ = average number of fission neutrons of all energies emitted per fission caused by a neutron of energy E''.

Thus $G(|z|)$ for a given medium will depend on the nature of the source through the form of $x_s(E')$.

Conservation of neutrons in a non-multiplying medium gives:

$$\int dz \int dE'' \frac{H(|z|, E', E'')}{\tau(E'')} = 1, \quad \text{for all } E' \ . \tag{7.2}$$

In the multiplying medium

$$\int dz\, G_f(|z|) = k = \overline{c\,\nu} = \text{average number of fission neutrons born per neutron captured in the infinite medium.}$$

The average $\overline{c\,\nu}$ of $c(E'')\,\nu\,(E'')$ with respect to the energy E'' is taken using

$$\int dE' \int dz \frac{H\,(|z|, E', E'')}{\tau(E'')}\, x_f(E') \tag{7.3}$$

as the weighting function, which is normalized to unity in virtue of (7.2) and the definition of $x_f(E')$, but the form of whose dependence on E'' might in general depend on the nature of the fission source through the form of $x_f(E')$.

Alternative Forms of the Integral Equation

Let

$\rho(z,E)dz\,dE$ = number of neutrons between z and $z+dz$ with energy between E and $E+dE$.

We account for this number of neutrons by adding together the contributions of the given source, and of the fission sources distributed throughout the medium. This gives:

$$\rho(z,E) = Q\int dE' x_s(E')\, H(|z|, E', E) + \int dz' \int dE' \int dE'' \frac{\rho(z', E')}{\tau(E')}\, c(E')\, \nu(E')\, x_{E'}(E'')\, H(|z-z'|, E'', E)\,. \quad (7.4)$$

To get a simpler integral equation we first assume that $x_{E'}(E'')$ is independent of the energy E' of the neutron which causes fission. We may then introduce into (7.4)

$$f(z) = \int dE' \frac{\rho(z', E')}{\tau(E')}\, c(E')\, \nu(E')\,, \quad (7.5)$$

which represents the total number of fission neutrons of all energies emitted per unit time per unit z at the point z. Multiplying both sides of (7.4) by

$$\frac{c(E)\,\nu(E)}{\tau(E)}\,, \quad (7.6)$$

integrating over E, and using (7.5) and (7.1) we obtain:

$$f(z) = Q\, G_s(|z|) + \int dz'\, f(z')\, G_f(|z - z'|)\,, \quad (7.7)$$

which is obtained directly as (2.6) in Section 2.

If we wanted to introduce in place of (7.5) a different function

$$g(z) = \int dE' \frac{\rho(z, E')}{\tau(E')}\, c(E')\,, \quad (7.8)$$

which represents the number of fissions per unit time per unit z, or

$$h(z) = \int dE' \frac{\rho(z, E')}{\tau(E')}\,, \quad (7.9)$$

which represents the number of captures per unit time per unit z, or

$$n(z) = \int dE'\, \rho(z, E')\,, \quad (7.10)$$

which represents the number of neutrons of all energies in a steady state per unit z, then we would have to assume in the case of (7.8) that $\nu(E')$, in

the case of (7.9) that $\nu(E')c(E')$, and in the case of (7.10) that $\nu(E')c(E')/\tau(E')$, as well as $x_{E'}(E'')$, are not functions of E' in order to obtain a simple integral equation analogous to (7.7).

References

1. PLACZEK, G. and VOLKOFF, G. M. Notes on diffusion of neutrons without change in energy. 1943. Declassified report available in multilith form from the National Research Council of Canada, Ottawa, Canada.
2. WALLACE, P. R. and LECAINE, J. Elementary approximations in the theory of neutron diffusion. 1943. Declassified report available in multilith form from the National Research Council of Canada, Ottawa, Canada.

CANADIAN JOURNAL OF RESEARCH

Notes on the Preparation of Copy

GENERAL:—Manuscripts should be typewritten, double spaced, and the **original and at least one extra copy** submitted. Style, arrangement, spelling, and abbreviations should conform to the usage of this Journal. Names of all simple compounds, rather than their formulae, should be used in the text. Greek letters or unusual signs should be written plainly or explained by marginal notes. Superscripts and subscripts must be legible and carefully placed. Manuscripts should be carefully checked before being submitted, to reduce the need for changes after the type has been set. **All pages, whether text, figures, or tables, should be numbered.**

ABSTRACT:—**An abstract of not more than about 200 words, indicating the scope of the work and the principal findings, is required.**

ILLUSTRATIONS:

(i) *Line Drawings:*—All lines should be of sufficient thickness to reproduce well. Drawings should be carefully made with India ink on white drawing paper, blue tracing linen, or co-ordinate paper **ruled in blue only**; any co-ordinate lines that are to appear in the reproduction should be ruled in black ink. Paper ruled in **green, yellow, or red should not be used** unless it is desired to have all the co-ordinate lines show. Lettering and numerals should be neatly done in India ink preferably with a stencil (**do not use typewriting**) and be of such size that they will be legible and not less than one millimetre in height when reproduced in a cut three inches wide. All experimental points should be carefully drawn with instruments. Illustrations need not be more than two or three times the size of the desired reproduction, but the ratio of height to width should conform with that of the type page. **The original drawings and one set of small but clear photographic copies are to be submitted.**

(ii) *Photographs:*—Prints should be made on glossy paper, with strong contrasts; they should be trimmed to remove all extraneous material so that essential features only are shown. Photographs should be submitted **in duplicate**; if they are to be reproduced in groups, one set should be so arranged and mounted on cardboard with rubber cement; the duplicate set should be unmounted.

(iii) *General:*—**The author's name, title of paper, and figure number should be written on the back of each illustration.** Captions should not be written on the illustrations, but typed on a separate page of the manuscript. All figures (including each figure of the plates) should be numbered consecutively from 1 up (arabic numerals). **Each figure should be referred to in the text.**

TABLES:—Titles should be given for all tables, which should be numbered in Roman numerals. Column heads should be brief and textual matter in tables confined to a minimum. **Each table should be referred to in the text.**

REFERENCES:—**These should be listed alphabetically by authors' names, numbered in that order, and placed at the end of the paper.** The form of literature citation should be that used in this Journal. **Titles of papers should not be given in references listed in Sections A, B, E, and F, but must be given in references listed in Sections C and D. All citations should be checked with the original articles.** Each citation should be referred to in the text by means of the key number; in Sections C and D the author's name and the date of publication may be included with the key number if desired.

The *Canadian Journal of Research* conforms in general with the practice outlined in the *Canadian Government Editorial Style Manual*, published by the Department of Public Printing and Stationery, Ottawa.

Reprints

Fifty reprints of each paper are supplied free. Additional reprints, if required, will be supplied according to a prescribed schedule of charges.